INAUGURAL – DISSERTATION
zur
Erlangung der Doktorwürde
der
Naturwissenschaftlich-Mathematischen Gesamtfakultät
der
Ruprecht-Karls-Universität
Heidelberg

vorgelegt von
Diplom-Mathematiker Christoph Karl Felix Weiler
aus Lübeck

Tag der mündlichen Prüfung: 2. Juni 2014

Optimum Experimental Design for the Identification of Gaussian Disorder Mobility Parameters in Charge Transport Models of Organic Semiconductors

Betreuer:
Prof. Dr. Dres. h.c. Hans Georg Bock
Dr. Stefan Körkel

Abstract

This thesis treats optimum experimental design for the parameter estimation problem of mobility parameters in charge transport models of organic semiconductors. The models consist of the van Roosbroeck system, a quasi-electrochemical potential defining equation, and the *Extended Gaussian Disorder Model* and the *Extended Correlated Disorder Model* both describing the mobility. The arising problems are very ill-conditioned. The essential points of this work are:

- The *robust* numerical solution of the model equations w.r.t. varying parameters, control parameters, boundary values and initial guesses for iterative methods.
- The computation of *exact* derivatives up to order two, which are necessary for the optimum experimental design problem. This includes derivatives of the model functions and implicitly given derivatives of the solution.

The Scharfetter-Gummel scheme is applied to the spatial discretization in one dimension, whereas in two dimensions bilinear finite elements are used. The numerical simulation of the discretized equations is done by a hybrid simulation method consisting of Gummel's method with a special, problem-adapted stabilization term, a contraction based damping strategy, and a full step Newton method in the end for quadratic convergence near the solution. These strategies are independent of the spatial discretization and are applied to the simulation of a polymer nano-chain attached to the cathode. The simulation of the one dimensional problems are used for the optimum experimental design. The derivatives are computed with *automatic differentiation* exactly up to machine precision. Therefor we use software tools for the computation of the derivatives of the model functions and solve tangential and adjoint equations of the problem for the parameters and control parameters. With optimum experimental design we plan experiments for newest organic materials, like *NRS-PPV* and α*-NPD*. The confidence region of the parameters are reduced by a factor of 100 for *NRS-PPV*.

Zusammenfassung

Diese Arbeit behandelt die optimale Versuchsplanung zur Parameterschätzung von Mobilitätsparametern in Ladungstransportmodellen von organischen Halbleitern. Die Modelle bestehen aus dem van Roosbroeck System, einer quasi-elektrochemischen Potential definierenden Gleichung und den Mobilitätsmodellen *Extended Gaussian Disorder* und *Extended Correlated Disorder*. Die auftretenden Probleme sind sehr schlecht konditioniert. Die wesentlichen Punkte dieser Arbeit sind:

- Das, gegenüber variierender Parameter, Steuerungen, Randwerte und Anfangswerte der iterativen Verfahren, *robuste* numerische Lösen der Modellgleichungen.
- Die Berechnung der, für die Versuchsplanung benötigten, *exakten* Ableitungen bis zur Ordnung zwei. Dies beinhaltet die Berechnung von Ableitungen der Modellfunktionen und der implizit gegebenen Ableitungen der Lösung.

Für die Ortsdiskretisierung wird in einer Dimension das Scharfetter-Gummel Schema verwendet, wohingegen in zwei Dimension auf bilineare finite Elemente zurückgegriffen wird. Das numerische Lösen der diskretisierten Gleichungen erfolgt durch eine hybride Simulationsmethode bestehend aus der Gummel Methode versehen mit einem speziellen, auf obige Probleme zugeschnittenen Stabilisierungsterm, einer kontraktionsbasierten Dämpfungstrategie und einem nachgeschalteten Newton Verfahren zur rapiden Konvergenz nahe der Lösung. Diese Strategien sind unabhängig von der Ortsdiskretisierung und werden auf die Simulation einer, der Kathode angelagerten, Polymer-Nano-Kette in 2D angewendet. Die 1D Probleme werden für die Versuchsplanung benützt. Die Ableitungen werden *automatischer Differentiation* exakt bis auf Maschinengenauigkeit berechnet. Dabei werden Software Tools für die Berechnung der Modellfunktionen verwendet und tangentiale, sowie adjungierte Gleichungen der Probleme für Parameter und Steuerungen gelöst. Mit der Versuchsplanung werden Experimente zu neuesten organischen Materialien, wie *NRS-PPV* und α*-NPD* geplant. Für *NRS-PPV* wird das Konfidenzgebiet der Parameter um einen Faktor 100 reduziert.

Contents

Introduction

In 1936 Destriau discovered the electroluminescence, i.e. the emission of light from a solid due to an applied voltage. Almost two decades later, the team of Bernanose found similar behavior in organic material. Those discoveries were the first steps in a development which e.g. has resulted in organic solar cells and organic light emitting devices (OLED), used in displays of modern electronic devices like mobile phones, televisions, computer monitors, and lighting. Organic light emitting devices have major advantages compared to crystalline light emitting devices (LED) namely, they can be lightweight and flexible, they have an improved brightness and power efficiency, they can be very thin and have a short response time. On the other hand, the organic material is susceptible to degradation effects which means that the material gets destroyed under repeated excitations by an electric field. The degradation of the organic material is still an open problem and its analysis and understanding is a current research topic. The degrading process of the organic material is very slow and macroscopic effects like the loss of conductivity, disturbances in the color balance only emerge after years. Therefore the simulation of the degradation process is a highly desired topic, where the time can be scaled down. A crucial element of the degradation is the charge transport taking place in the organic material. Modern state-of-the-art models for the charge transport through organic semi-conducting material are the *Extended Gaussian/Correlated Disorder Model* (EGDM/ECDM) developed by Coehoorn et al. at Eindhoven consisting of the van Roosbroeck system, a stationary system of strongly coupled, highly nonlinear partial differential equations. Our simulation methods are based on Gummel's method, a derivative-free fixed-point iteration suited for the van Roosbroeck system. We extend the method by a quasi electrochemical potential defining equation. The solution method is tuned by a corrected stabilization term corresponding to the generalized Einstein relation, which is part of the EGDM and ECDM, and by using an adaptive damping scheme which forces contracting step lengths far away from the solution.

The drawback of the models EGDM and ECDM are unknown parameters, which cannot be measured. A common technique to identify those parameter values is the parameter estimation based on an inverse process. Experiments are performed to measure the electric current at different temperatures, voltages, and device thicknesses resulting in measurement data to which models are fitted. This is done with a least squares formulation corresponding to the minimization of a Likelihood function.

Every physical measurement process is afflicted with random errors which cause uncertain parameter estimates. The parameter uncertainty is quantified by the variance-covariance matrix which contains derivatives of a measurement function w.r.t. the parameters. Optimum experimental design is the minimization of a functional of the variance-covariance matrix over control parameters constrained by the model equations and possibly other control constrains. With the new control parameters, additional experiments are performed extracting more information out of the system. We solve the optimum experimental design problems with the sequential quadratic programming method on a reduced system.

Results of the thesis

In this work we develop robust numerical solution methods for simulating the charge transport in organic materials modeled by the EGDM and the ECDM w.r.t. varying parameters, control parameters, boundary values and initial guesses for the iterative methods. We use an adaptive approach based on Gummel's method including stabilization and damping techniques. In optimum experimental design mixed second order derivatives are required. To avoid accumulated numerical errors, we compute the derivatives with *automatic differentiation* efficiently and accurately. In the late 1990s Körkel developed the software package *VPLAN*, which offers interfaces to a variety of software tools, like *ADIFOR* for automatic differentiation, *PARFIT* for parameter estimation, and *SNOPT* for solving optimum experimental design problems. For the numerical computation of our solution method, we have written a software package, which not only simulates the problem, but also provides the required derivatives for the parameter estimation and the optimum experimental design, i.e. up to mixed second order derivatives of the solution w.r.t. the parameters, control parameters, and both. This software has been coupled to *VPLAN* interchanging solutions of the model equations, derivative information, parameters, and control parameters. Thus sensitivity analysis, parameter estimation and optimum experimental design problems can be computed. We apply optimum experimental design to reduce the uncertainty of the EGDM and ECDM parameters significantly.

Thesis overview

The chapters are arranged as follows. We first develop the van Roosbroeck system from basic physical equations as the basis of our semiconductor model in chapter 1. We extend the model to the EGDM and ECDM respectively to model the charge

transport in organic semiconductors. At the end we discuss the questions of existence, uniqueness and stability of the obtained system. In chapter 2, we discretize the spatial derivatives and show that our problem is very ill-conditioned. We present our alternative solution method, which consists of an extended Gummel method provided with a contraction based damping strategy and a full step Newton method to achieve quadratic convergence close to the solution. Finally we apply our method to a 2D problem and show that the solution method can solve 2D problems as well. Simulation results of a self-assembled nano-chain attached to the cathode are presented. An overview of the parameter estimation considered for the optimum experimental design is given in chapter 3. We derive the optimization problem from basic statistical concepts, show how to compute the variance-covariance matrix and define the linearized confidence region. We also formulate the Gauss-Newton method for solving parameter estimation problems. Chapter 4 finally treats the optimum experimental design problem. We assemble basic optimization results to guarantee the solvability and present an SQP method on the reduced problem to solve the constrained optimization problem. Optimum experimental design results are presented for the organic materials NRS-PPV and α-NPD. At the end, we discuss robust optimum experimental design and a sequential experimental design ansatz for the example of NRS-PPV with EGDM.

1 Organic semiconductor modeling

In this chapter we derive the models that are considered in this thesis starting from the involved physics for the thermally assisted transport of electrons through disordered organic media under the influence of an applied external field. We consider the Extended Gaussian Disorder Model (EGDM), cf. Pasveer et al. [75] for modeling large polymers and the Extended Correlated Disorder Model (ECDM), see Bouhassoune et al. [20] for modeling smaller molecules. The basis of the models is the stationary van Roosbroeck system, a set of coupled stationary partial differential equations for the electric potential and the electron charge density. The system gained great success by modeling the charge transport through crystalline semiconductors. Models for the "hopping" transport of electrons through organic material is well described by the master equation. Solving the master equation can be very slow, cf. the 3D simulations of Holst et al. [87]. A different approach is to fit the previously mentioned models to solutions of the master equation and thus find a nonlinear mobility dependent on the temperature, organic material parameters, the electric potential, and the electron charge density.

We start with a section about the physics and equations describing the charge transport of electrons through semi-conducting materials in general and move on to a section about altered models, which match the properties of organic materials. The equations are normalized by scaling with typical quantities. In the end we give a brief overview of the theory proving existence, uniqueness, and stability results of similar systems.

1.1 Physics of semiconductor devices

We define a semiconductor following Ashcroft [4]:
Definition 1.1.1. *Semiconductors* are solids, that are insulators at zero temperature T. Their energy gap E_g is so small, that thermal excitation of electrons is leading to measurable conductivity below the melting point. With the conduction level E_C and the valence level E_V, the energy gap is defined by $E_g := E_C - E_V$.

In the presence of an applied external field E in V/m and a carrier density gradient, i.e. Fick's law, the electric current density is given by a sum of *drift* and *diffusion* current

$$j = -e\,(\mu n E + D\,\nabla n), \tag{1.1}$$

in A/m^2, with the carrier density n in m^{-3}, the mobility μ in $m^2/(Vs)$, the diffusion coefficient D in m^2/s, and the elementary charge e in As. By convenience, we will always take e as a positive number. With the space variable x in m the units match, which can be seen by

$$\frac{A}{m^2} = As\left(\frac{m^2}{Vs}\frac{1}{m^3}\frac{V}{m} + \frac{m^2}{s}\frac{1}{m^4}\right).$$

In this work, we will only consider unipolar, i.e. electron-only transport layers. In the absence of hole carriers, we do not have recombination of holes and electrons and the conservation of charge carriers is described by the continuity equation

$$e\,\frac{\partial n}{\partial t} = -\nabla \cdot j.$$

In steady-state, which is our basic interest, this reduces to

$$0 = -\nabla \cdot j. \tag{1.2}$$

The electric potential ϕ, measured in V, is defined by

$$E = -\nabla\phi \qquad \text{and} \qquad \phi_{\text{cathode}} = 0, \tag{1.3}$$

with ϕ_{cathode} the boundary value of ϕ at the cathode contact. The electric potential ϕ and the carrier density n are related through Poisson's equation

$$-\Delta\,\phi = -\frac{e}{\varepsilon}n, \tag{1.4}$$

with the permittivity $\varepsilon = \varepsilon_0\varepsilon_r$ in $As/(Vm)$, the product of vacuum permittivity ε_0 and relative permittivity ε_r. Again we check, that the units match

$$\frac{1}{m^2}V = As\frac{Vm}{As}\frac{1}{m^3}.$$

The boundary condition of ϕ at the anode contact is obtained from the relation

$$\int_C E\,\mathrm{d}x = V_{\text{app}} - V_{\text{bi}},$$

where C is an arbitrary path connecting cathode and anode, V_{app} is the applied voltage and V_{bi} is the built-in voltage which is defined by the difference of the energy

levels of the adjacent metals

$$V_{\text{bi}} := E_{\text{anode}} - E_{\text{cathode}}.$$

On the other hand we have with (1.3)

$$\int_C E \, \mathrm{d}x = \phi_{\text{anode}} - \phi_{\text{cathode}} = \phi_{\text{anode}}$$

resulting in

$$\phi_{\text{anode}} = V_{\text{app}} - V_{\text{bi}}. \tag{1.5}$$

Boundary values for the continuity equation (1.2) are provided by the values of the carrier density at the electrodes n_{cathode} and n_{anode}.

1.1.1 Quasi chemical potential

According to Kittel [57], the *Fermi energy* E_F is defined as the energy of the topmost level in the ground state, i.e. $T = 0$, of a multi electron system. In the context of semiconductor physics it coincides with the terminology of the *chemical potential* η, spatially constant. In agreement with Ashcroft [4], we define a position-dependent *electrochemical potential* $\eta_e(x)$ by

$$\eta_e(x) = \eta + e\phi(x),$$

as the combination of chemical potential η and electric potential energy $e\phi(x)$. In degenerated semiconductors, which have a distribution of states in forbidden energy areas, one sometimes defines the electron *quasi chemical potential* $\tilde{\eta}(x)$, which is space dependent. Accordingly we mean with *quasi electrochemical potential* the quantity defined by

$$\tilde{\eta}_e(x) = \tilde{\eta}(x) + e\phi(x).$$

This generalization also holds for the non-degenerated case, which is why we drop the tilde in the following notation.

1.1.2 Generalized Einstein relation

Assuming no explicit space dependence of the carrier densities

$$n(x) = n(\eta_e(x)),$$

the carrier density gradient transforms to

$$\nabla n = \frac{\partial n}{\partial \eta_e}(\nabla \eta_e + e\nabla\phi).$$

If we consider the thermal equilibrium case, i.e. no current flow $j = 0$ at zero temperature $T = 0$ and $\eta(x) \equiv \eta$, we have

$$0 = -e\,(-\mu n \nabla\phi + D\,\nabla n) = -e\,\Big(-\mu n\nabla\phi + D\,\frac{\partial n}{\partial \eta_e} e\nabla\phi\Big) = \Big(\mu n - D\,\frac{\partial n}{\partial \eta_e} e\nabla\phi\Big) e\,\nabla\phi$$

and hence the *generalized Einstein relation*

$$D = \mu\,\frac{n}{e\frac{\partial n}{\partial \eta_e}}. \tag{1.6}$$

This relation is assumed to be valid for the non-equilibrium case, too. With Maxwell-Boltzmann statistics

$$n = n_i \exp\Big(-\frac{E_C - \eta}{k_B T}\Big),$$

with n_i the intrinsic density, the relation (1.6) simplifies to the classical Einstein relation

$$D = \mu\,\frac{k_B T}{e}, \tag{1.7}$$

discovered by Einstein and Smoluchowski [32] in their analysis of the Brownian motion. Here k_B is the Boltzmann constant in eV/K.

1.2 Organic mobility models

In an overview article of Bässler et al. [23] the first principles of modeling disordered semi-conducting organic materials were assembled. The charge transport is regarded as a hopping process between localized sites, which are conjugated polymer chain segments. Physically spoken, the charge transport is a thermally assisted tunneling process. On-site energies are assumed to be Gaussian distributed, due to disorder, cf.

[51],

$$\exp\Big(-\frac{E^2}{2\sigma^2}\Big). \tag{1.8}$$

Pasveer et al. [75] and Mensfoort et al. [88] presented the Extended Gaussian Disorder Model, EGDM, which proceeds on the assumption, that the on-site energies have no spatial correlation. For materials, where the energies are spatially correlated, Bouhassoune et al. [20] developed the Extended Correlated Disorder Model, ECDM. Both approaches determine the mobility from the numerical solution of the *stationary master equation* representing the hopping of charge carriers on a regular cubic lattice of sites with lattice constant a, see also [96]. The master equation is given by

$$\sum_{i\neq j}\left[W_{ij}p_i(1-p_j) - W_{ji}p_j(1-p_i)\right] = 0$$

with the probability p_i that site i is occupied by a charge, only one charge carrier can occupy one site, and assuming Miller-Abraham [67] transition rates

$$W_{ij} = \begin{cases} \nu_0 \exp[-2\alpha R_{ij} - \frac{\varepsilon_j-\varepsilon_i}{k_BT}], & \varepsilon_j \geq \varepsilon_i, \\ \nu_0 \exp[-2\alpha R_{ij}], & \varepsilon_j < \varepsilon_i, \end{cases}$$

with ν_0 an intrinsic rate, $R_{ij} := |R_j - R_i|$ the distance between site i and site j, $\alpha = 10/a$ the inverse localization length of the localized wave functions under consideration, and ε_i the on-sites energy of site i which are assumed to be Gaussian distributed with width σ. The maximal hopping is considered to be $\sqrt{3}a$.

1.2.1 Extended Gaussian disorder model – EGDM

With the solution of the master equation the velocity of the particles is calculated by

$$v = \sum_{i,j} W_{ij}p_i(1-p_j)(R_j - R_i),$$

and the mobility then is

$$\mu := \frac{v}{nEV},$$

with electric field $E = -\nabla\phi$, the system volume V, and the electron density $n = < p_i > /a^3$. The fitted functions dependent on the carrier density n and the electric potential ϕ appeared in Pasveer et al. [75] the first time. We rewrite them here, with

the extensions made in [88]. With

$$\hat{\sigma} = \frac{\sigma}{k_B T} \qquad \text{and} \qquad \delta^G(\hat{\sigma}) = 2\frac{\log(\hat{\sigma} - \hat{\sigma}^2) - \log\log 4}{\hat{\sigma}^2}$$

the mobility is given by

$$\begin{aligned}
\mu^G(\phi, n, \sigma, N_t, T) &= \mu_0\, g_0(\sigma, T)\, g_1^G(n, \sigma, N_t, T)\, g_2^G(\phi, \sigma, N_t, T), \\
g_0(\sigma, T) &= \exp\left\{-c_0\, \hat{\sigma}^2\right\} \\
g_1^G(n, \sigma, N_t, T) &= \exp\left[\frac{1}{2}(\hat{\sigma}^2 - \hat{\sigma})\left(\min\left\{\frac{2n}{N_t}, 0.2\right\}\right)^{\delta^G(\hat{\sigma})}\right], \\
g_2^G(\phi, \sigma, N_t, T) &= \exp\left\{0.44(\hat{\sigma}^{\frac{3}{2}} - 2.2)\right\}\left[\sqrt{1 + 0.8\left(\min\left\{\frac{e|\nabla\phi|}{N_t{}^{\frac{1}{3}}\sigma}, 2\right\}\right)^2} - 1\right].
\end{aligned}$$

The standard deviation of the Gaussian distribution (1.8) σ, in eV, and the site density denoted with N_t, in m^{-3}, are the main characteristic material parameters of the mobility. Their (exact) measurement is not possible, but their value most desirable, which is why a parameter estimation is applied for which we compute optimum experimental designs. Other parameters are the dimensionless factor c_0, the zero-temperature mobility μ_0 in $m^2/(Vs)$, and the boundary values ϕ_{cathode} and ϕ_{anode}.

1.2.2 Extended correlated disorder model – ECDM

In 2009 Bouhassoune et al. proposed another model, which assumes a spatial correlation of on-site energies [20]. This is the case for smaller molecules. Like for the EGDM their strategy is to fit the mobility to results of the master equation for different parameters σ, N_t and T. The mobility is separated in a high- and low-field dependent part

$$\mu^C(\phi, n, \sigma, N_t, T) = \left[\mu_{\text{low}}^C(\phi, n, \sigma, N_t, T)^{q(\hat{\sigma})} + \mu_{\text{high}}^C(\phi, n, \sigma, N_t, T)^{q(\hat{\sigma})}\right]^{\frac{1}{q(\hat{\sigma})}}$$

with

$$q(\hat{\sigma}) = \frac{2.4}{1 - \hat{\sigma}}$$

and

$$\mu^C_{\text{low}}(\phi, n, \sigma, N_t, T) = \mu_0\, c_1\, g_0(\sigma, T)\, g^C_1(n, \sigma, N_t, T)\, g^C_2(\phi, n, \sigma, N_t, T),$$
$$\mu^C_{\text{high}}(\phi, n, \sigma, N_t, T) = \frac{c_2}{E_{\text{red}}}\mu_0\left(1 - \frac{n}{N_t}\right),$$

where

$$c_1 = 10^{-9},$$
$$c_2 = 2.06 \cdot 10^{-9},$$
$$E_{\text{red}} = \frac{e N_t^{-\frac{1}{3}} E}{\sigma}.$$

For the low field we have

$$g^C_1(n, \sigma, N_t, T) = \exp\left[(0.25\hat{\sigma}^2 + 0.7\hat{\sigma})\left(2\min\left\{\frac{n}{N_t}, 0.025\right\}\right)^{\delta^C}\right],$$
$$g^C_2(\phi, n, \sigma, N_t, T) = \exp\left[h(E_{\text{red}})\left(1.05 - 1.2\left(\frac{n}{N_t}\right)^{r(\hat{\sigma})}\right)(\hat{\sigma}^{\frac{3}{2}} - 2)(\sqrt{1 + 2E_{\text{red}}} - 1)\right],$$

with

$$\delta^C = 2.3\frac{\log(0.5\hat{\sigma}^2 + 1.4\hat{\sigma}) - \log(\log(4))}{\hat{\sigma}^2},$$
$$r(\hat{\sigma}) = \frac{0.7}{\hat{\sigma}^{0.7}}.$$

The low field regime is further split into three areas regarding the function h

$$h(E_{\text{red}}) = \begin{cases} \frac{4}{3}\frac{E_{\text{red}}}{0.16}, & 0 \le E_{\text{red}} < 0.08, \\ 1 - \frac{4}{3}\left(\frac{E_{\text{red}}}{0.16} - 1\right)^2, & 0.08 \le E_{\text{red}} < 0.16, \\ 1, & 0.16 \le E_{\text{red}}. \end{cases}$$

For the ECDM, we will also consider the generalized Einstein relation, cf. (1.6).

1.2.3 Generalized Einstein relation for Gaussian disorder models

Roichman, Preezant, and Tessler [79], [77] showed that the generalized Einstein relation (1.6) holds for organic materials, too. A quasi electrochemical potential η is considered, assuming a non-degenerated semiconductor, i.e. $\eta \le 0$. The electron

density n and the quasi electrochemical potential η are related through

$$n = \frac{N_t}{\sqrt{2\pi\sigma^2}} \int_{-\infty}^{\infty} \exp\Big(-\frac{E^2}{2\sigma^2}\Big) \frac{1}{1+\exp\left(\frac{E-\eta}{k_B T}\right)} \,\mathrm{d}E. \tag{1.9}$$

The integral is a superposition of the Gaussian distribution of the energies and the Fermi-Dirac term

$$\frac{1}{1+\exp\left(\frac{E-\eta}{k_B T}\right)}.$$

The system of continuity (1.2) and Poisson's equation (1.4) is augmented by the equation (1.9).

Remark 1.2.1. The Gauss term is centered around the conductivity level E_C which is set to zero by convenience. Thus, in a non-degenerated semiconductor $\eta \leq 0$ holds. By integral transformation, this leads to

$$n \leq \frac{N_t}{\sqrt{2\pi\sigma^2}} \int_{-\infty}^{\infty} \exp\Big(-\frac{E^2}{2\sigma^2}\Big) \frac{1}{1+\exp\left(\frac{E}{k_B T}\right)} \,\mathrm{d}E = \frac{N_t}{\sqrt{\pi}} \int_{0}^{\infty} \exp\left(-E^2\right) \mathrm{d}E = \frac{N_t}{2},$$

where we used

$$\int_{-\infty}^{0} \exp\left(-E^2\right) \frac{1}{1+\exp\left(\frac{\sqrt{2}\sigma E}{k_B T}\right)} \,\mathrm{d}E = \int_{0}^{\infty} \exp\left(-E^2\right) \frac{1}{1+\exp\left(-\frac{\sqrt{2}\sigma E}{k_B T}\right)} \,\mathrm{d}E,$$

and

$$\frac{1}{1+\exp(-x)} + \frac{1}{1+\exp(x)} = \frac{\exp(x)}{\exp(x)+1} + \frac{1}{1+\exp(x)} = 1, \quad \text{for } x \in \mathbb{R}.$$

The derivative of the carrier density n w.r.t. η is derived from the relation (1.9) leading to

$$\frac{\partial n}{\partial \eta} = \frac{1}{k_B T} \frac{N_t}{\sqrt{2\pi\sigma^2}} \int_{-\infty}^{\infty} \exp\Big(-\frac{E^2}{2\sigma^2}\Big) \frac{1}{\left(1+\exp\left(\frac{E-\eta}{k_B T}\right)\right)^2} \,\mathrm{d}E.$$

The generalized Einstein relation (1.6) then reads

$$D(\phi, n, \sigma, N_t, T) = \frac{k_B T}{e} \mu(\phi, n, \sigma, N_t, T)\, g_3(n, \eta, \sigma, N_t, T)$$

with

$$g_3(n,\eta,\sigma,N_t,T) = \frac{1}{k_BT}\frac{n}{\frac{\partial n}{\partial \eta}} = \frac{\int_{-\infty}^{\infty} \exp\Big(-\frac{E^2}{2\sigma^2}\Big)\frac{1}{1+\exp\left(\frac{E-\eta}{k_BT}\right)}\,\mathrm{d}E}{\int_{-\infty}^{\infty} \exp\Big(-\frac{E^2}{2\sigma^2}\Big)\frac{1}{\left(1+\exp\left(\frac{E-\eta}{k_BT}\right)\right)^2}\,\mathrm{d}E}.$$

Mensfoort and Coehoorn [88] proposed a cutoff for this function by claiming that for $n > N_t/2$ the function is the constant value of $g_3\Big(N_t/2,\eta,\sigma,N_t,T\Big)$. In the following we will always denote the constantly extended function with g_3.

1.2.4 Boundary conditions

We consider three different kind of boundaries describing the cathode Γ_{cathode}, the anode Γ_{anode} and insulating material Γ_{n}. The index n corresponds to boundary conditions where normal derivatives are involved. It is only used as an index to avoid confusion with the charge density n. The boundary conditions that we apply can be separated into two classes, the Dirichlet-type boundary values imposed on the cathode and anode and Neumann-type boundary values imposed on insulating materials. For Poisson's equation, we already have seen the Dirichlet-type boundary values in (1.5):

$$\phi_{\text{cathode}} = 0 \qquad \text{and} \qquad \phi_{\text{anode}} = V_{\text{app}} - V_{\text{bi}}.$$

The carrier density is either prescribed directly as real numbers n_{cathode} and n_{anode}, in case of "Ohmic" boundary conditions, or indirectly computed by

$$n_{\text{electrode}} = \frac{N_t}{\sqrt{2\pi\sigma^2}}\int_{-\infty}^{\infty} \exp\Big(-\frac{E^2}{2\sigma^2}\Big)\frac{1}{1+\exp\left(\frac{E-E_{\text{electrode}}}{k_BT}\right)}\,\mathrm{d}E,$$

for given energy levels E_{cathode} and E_{anode} of the adjacent metal in the case of "thermionic" boundary conditions. For insulating material, we want the normal component of the electric current to vanish, i.e. $j_n = 0$. We achieve this by imposing the Neumann-type boundary conditions

$$\partial_n\phi = 0 \qquad \text{and} \qquad \partial_n n = 0.$$

Barrier lowering

Scott et al. [83] observed the effect of barrier lowering due to the applied electric field extending the ideas of Emtage et al. [33]. The injected electrons form a Coulomb potential at the interface and the effective potential E_{eff} is the sum of the energy barrier to the metal, the energy caused by the applied external field, and a Coulomb term

$$E_{\text{eff}} = E_{\text{cathode}} - eEx - \frac{e^2}{16\pi\varepsilon x}.$$

We assume a constant field E. In fact we use $|\nabla\phi|$ evaluated at the cathode contact for E. Hence E_{eff} has a maximum at

$$x_{\max} = \sqrt{\frac{e}{16\pi\varepsilon E}}$$

and the lowered energy barrier at the cathode is

$$\tilde{E}_{\text{cathode}} = E_{\text{cathode}} - e\sqrt{\frac{eE}{4\pi\varepsilon}}.$$

Thus the boundary condition of the electron density n at the cathode is

$$n_{\text{cathode}} = \frac{N_t}{\sqrt{2\pi\sigma^2}} \int_{-\infty}^{\infty} \exp\left(-\frac{E^2}{2\sigma^2}\right) \frac{1}{1+\exp\left(\frac{E-\tilde{E}_{\text{cathode}}}{k_B T}\right)} \,\mathrm{d}E.$$

1.3 Scaling

For the purpose of comparing the different physical quantities in the system and in anticipation of numerical simulations, we scale the equations by introducing normalized quantities. Our choice of scaled variables is similar to the existing scaling schemes for crystalline semiconductors, cf. [22].

$$\begin{aligned} x &\quad\to\quad \frac{x}{x_{\text{scal}}}, \\ \phi &\quad\to\quad \frac{\phi}{\phi_{\text{scal}}}, \\ n &\quad\to\quad \frac{n}{n_{\text{scal}}}, \end{aligned}$$

with

$$\begin{aligned} x_{\text{scal}} &= L \\ \phi_{\text{scal}} &= V_{\text{app}}, \\ n_{\text{scal}} &= \max\{n_{\text{cathode}}, n_{\text{anode}}\}, \end{aligned}$$

where L is the length of the device in nm. We found it convenient to make an exception by not taking SI units in this case. With this scaling the full model reads:

In the considered domain:

$$\begin{aligned} -\frac{\phi_{\text{scal}}}{x_{\text{scal}}^2}\ \Delta\,\phi &= -n_{\text{scal}}\ \frac{e}{\varepsilon}\,n, \\ j &= \frac{e\,n_{\text{scal}}}{x_{\text{scal}}},\ \mu(n,\phi)\left(\frac{n}{e\frac{\partial n}{\partial \eta}}\,\nabla n - \phi_{\text{scal}}\ n\nabla\phi\right), \\ 0 &= -\frac{1}{x_{\text{scal}}}\ \nabla\cdot j, \\ n &= \frac{N_t}{n_{\text{scal}}}\ \frac{1}{\sqrt{2\pi\sigma^2}}\int_{-\infty}^{\infty}\exp\Big(-\frac{E^2}{2\sigma^2}\Big)\frac{1}{1+\exp\left(\frac{E-\eta}{k_BT}\right)}\,\mathrm{d}E. \end{aligned}$$

On the boundary of the domain:

$$\begin{aligned} \phi_{|_{\Gamma_{\text{cathode}}}} &= 0 \qquad & n_{|_{\Gamma_{\text{cathode}}}} &= \frac{n_{\text{cathode}}}{n_{\text{scal}}}, \\ \phi_{|_{\Gamma_{\text{anode}}}} &= 1 \qquad & n_{|_{\Gamma_{\text{anode}}}} &= \frac{n_{\text{anode}}}{n_{\text{scal}}}, \\ \partial_n\phi_{|_{\Gamma_n}} &= 0 \qquad & \partial_n n_{|_{\Gamma_n}} &= 0. \end{aligned}$$

We abbreviate the scaling factors and the physical constants with

$$\lambda^2 = \frac{\phi_{\text{scal}}}{x_{\text{scal}}^2\,n_{\text{scal}}}\,\frac{\varepsilon}{e} \qquad \text{and} \qquad \nu = \frac{k_BT}{\phi_{\text{scal}}}. \tag{1.10}$$

The factor λ is known as the dimensionless minimal Debeye length. The chemical potential defining equation is shortly noted with

$$G(\eta) := \gamma\int_{-\infty}^{\infty} f(\eta,E)\,\mathrm{d}E, \tag{1.11}$$

where

$$\gamma = \frac{N_t}{n_{\text{scal}}} \qquad \text{and} \qquad f(\eta, E) = \frac{1}{\sqrt{2\pi\sigma^2}} \exp\Big(- \frac{E^2}{2\sigma^2} \Big) \frac{1}{1 + \exp\left(\frac{E-\eta}{k_B T}\right)}.$$

With the new notation the system of equations read in compact form

$$\begin{aligned} \lambda^2 \Delta \phi &= n, && \text{(1.12a)} \\ j &= \mu(n,\phi)\Big(\nu\, g_3(n,\eta)\, \nabla n - n \nabla \phi\Big), && \text{(1.12b)} \\ 0 &= \nabla \cdot j, && \text{(1.12c)} \\ n &= G(\eta), && \text{(1.12d)} \end{aligned}$$

with boundary conditions for ϕ and n and the mobility μ is either modeled by the EGDM μ^G or the ECDM μ^C.

1.4 Mathematical analysis

To our knowledge, no analysis concerning existence, uniqueness or stability has ever been done before to the system (1.12). However, there is a lot of work treating the classical van Roosbroeck system, i.e. (1.12a) - (1.12c), with the classical Einstein relation and assuming constant mobility, which was first stated by van Roosbroeck [90]. The first results go back to Jerome [52] and Mock [69], who analyzed existence and stability for the stationary van Roosbroeck system assuming the (classical) Einstein relation and constant diffusion and mobility. The existence proof follows the steps:

- The equations are decoupled and formulated iteratively. An overall map is formed from one iterate to the other. In the literature this map is often called *Gummel map*.
- Existence is shown for the separate equations.
- Contraction is shown of the overall map.
- Schauder's fixed point theorem is applied, see [41].

A crucial part is to choose the right function space on which the map is defined. The works of Markowich et al. [64], [61] and Kerkhoven [56] show existence results with a more applied approach. They focus on boundary conditions and realistic device geometries. We also refer to the books of Markowich et al. [62] and Mock [70] for

summary discussions. Considering the classical van Roosbroeck system with mobilities based on Fermi-Dirac statistics is analyzed in Gajewski [36]. Jerome [53] also shows existence and uniqueness for the instationary problem

$$\begin{aligned} \lambda^2 \Delta \phi &= n, \\ j &= D \nabla n - \mu n \nabla \phi, \\ 0 &= e \partial_t n + \nabla \cdot j, \end{aligned}$$

where no Einstein relation is assumed. However he only assumes diffusion and mobility to be dependent on the electric field. Díaz et al. [31] treat problems with nonlinear diffusion of the form

$$\begin{aligned} \lambda^2 \Delta \phi &= n, \\ j &= \nabla \varphi(n) - b(n) \nabla \varphi, \\ 0 &= e \partial_t n + \nabla \cdot j, \end{aligned}$$

where φ is a so-called pressure function and b is a nonlinear function. The existence of a solution of the stationary problem with a special pressure function is proved by Wu [94] by combining the two previous works.

A detailed analysis of our system with elaborated proofs goes beyond the scope of this work. However, we think, one can adapt the ideas of the previous mentioned papers to the system obtained by reducing the variable η.

1.4.1 Treatment of the chemical potential defining equation

The aim of this section is to reduce the system (1.12) by the chemical potential defining equation (1.12d) and the variable η. We start defining an auxiliary function g by

$$\begin{aligned} g: \quad \mathbb{R} &\to \mathbb{R} \\ y &\mapsto \gamma \int_{-\infty}^{\infty} f(y, E) \, \mathrm{d}E. \end{aligned}$$

Since the Fermi-Dirac term of the integrand function f is bounded

$$0 < \frac{1}{1 + \exp\left(\frac{E-y}{k_B T}\right)} < 1 \qquad \text{for all } (y, E) \in \mathbb{R}^2, \tag{1.13}$$

the convergence of the improper integral is dominated by the Gaussian integral. Moreover the convergence is uniform w.r.t. $y \in \mathbb{R}$ as one can see by

$$\begin{aligned}\left\| \int_{-E}^{E} f(\,.\,,E')\,\mathrm{d}E' - \int_{-\infty}^{\infty} f(\,.\,,E')\,\mathrm{d}E' \right\|_\infty &\leq \int_{E}^{\infty} \|f(\,.\,,E')\|_\infty\,\mathrm{d}E' + \int_{-\infty}^{-E} \|f(\,.\,,E')\|_\infty\,\mathrm{d}E' \\ &\leq \frac{1}{\sqrt{2\pi\sigma^2}}\left(\int_{E}^{\infty} \exp\Big(-\frac{E'^2}{2\sigma^2}\Big)\,\mathrm{d}E' + \int_{-\infty}^{-E} \exp\Big(-\frac{E'^2}{2\sigma^2}\Big)\,\mathrm{d}E' \right) \to 0, \qquad (E \to \infty).\end{aligned} \tag{1.14}$$

It also follows that g is differentiable, see i.a. Gerhardt [39], and its derivative is

$$g'(y) = \gamma \int_{-\infty}^{\infty} \frac{\partial f}{\partial y}(y,E)\,\mathrm{d}E$$

with

$$\frac{\partial f}{\partial y}(y,E) = \frac{1}{k_B T}\,\frac{1}{\sqrt{2\pi\sigma^2}} \exp\Big(-\frac{E^2}{2\sigma^2}\Big) \frac{\exp\left(\frac{E-\eta}{k_B T}\right)}{\left(1+\exp\left(\frac{E-\eta}{k_B T}\right)\right)^2}.$$

Moreover with similar arguments as used in (1.14) one can show that g' is continuous. Since

$$g'(y) > 0, \qquad \text{for all } y \in \mathbb{R},$$

g is strictly monotone and hence injective. On every compact interval $[\alpha,\beta] \subset (0,\gamma)$, g^{-1} is continuous and strictly monotone. Hence for a continuous function n defined on the closure of a bounded domain $\Omega \subset \mathbb{R}^d$, $d = 1,2,3$ with range in $(0,\beta)$, g^{-1} is continuous and monotone on the (compact) range of n. With the composition

$$\eta := g^{-1} \circ n$$

we have found a continuous η defined on $\overline{\Omega}$ for which holds

$$n = G(\eta).$$

We are also able to show that G is a diffeomorphism on the Banach space of continuous functions

$$\mathcal{C}(\overline{\Omega})$$

by applying a corollary of the inverse function theorem. The extension to the appropriate Sobolev spaces required for the analysis of system (1.12) can be done by

an approximation argument. We use the theory of Nemytskii operators to transfer the properties of g to G, cf. (1.11). For the space of continuously differentiable functions on an open subset X of a Banach space E with range in a Banach space F we write

$$\mathcal{C}^1(X, F).$$

The function G is formally defined by

$$\begin{aligned} G: \quad \mathcal{C}(\overline{\Omega}) &\to \mathcal{C}(\overline{\Omega}), \\ \eta &\mapsto \gamma \int_{-\infty}^{\infty} f(E, \eta)\, \mathrm{d}E. \end{aligned}$$

From Amann and Escher [2] we cite the following theorem unproved

Theorem 1.4.1. *Let T be a compact metric space, E and F Banach spaces, and X an open subset of E. For $\varphi \in \mathcal{C}^1(X, F)$ the function $\varphi^\natural$ defined by*

$$\begin{aligned} \varphi^\natural: \quad X^T &\to Y^T, \\ u &\mapsto \varphi(u(.)), \end{aligned}$$

belongs to $\mathcal{C}^1\left(\mathcal{C}(T, X), \mathcal{C}(T, F)\right)$ and

$$\left[\partial\varphi^\natural(u)h\right](t) = \varphi'(u(t))\, h(t), \qquad t \in T,$$

for $u \in \mathcal{C}(T, X)$ and $h \in \mathcal{C}(T, E)$.

In our case the spaces are $T = \overline{\Omega}$ and $X = E = F = \mathbb{R}$. We have shown earlier that $g \in \mathcal{C}^1(\mathbb{R})$ and hence it holds for the Nemytskii operator

$$G \in \mathcal{C}^1\left(\mathcal{C}(\overline{\Omega}), \mathcal{C}(\overline{\Omega})\right). \tag{1.15}$$

This is the first requirement of the corollary of the inverse function theorem we want to use, cf. [40]:

Theorem 1.4.2. *Let E, F be Banach spaces, X an open subset of E, and $f \in \mathcal{C}^1(X, F)$ injective. If $\partial f(x)$ is a topological isomorphism for all $x \in X$, i.e. linear, continuous, bijective from E to F, and with continuous inverse, then f is open and a diffeomorphism from X to $f(X)$, i.e. f^{-1} exists and is continuously differentiable from $f(X)$ to X.*

With $X = E = F = \mathcal{C}(\overline{\Omega})$ we have to show that $G\,(= f)$ is injective and that $\partial G(\eta)$ is bijective and has a continuous inverse for all η in $\mathcal{C}(\overline{\Omega})$. For $\eta \neq \eta'$, there is a $x \in \overline{\Omega}$,

such that $\eta(x) \neq \eta'(x)$. W.l.o.g $\eta(x) < \eta'(x)$ and with the strict monotonicity of g it follows, that

$$G(\eta)(x) < G(\eta')(x) \qquad \Longrightarrow \qquad G(\eta) \neq G(\eta')$$

and thus G is injective. The (Fréchet) derivative of G is defined by

$$\left[\partial G(\eta)h\right](x) = g'(\eta(x))\, h(x), \qquad x \in \overline{\Omega}.$$

This and the fact that

$$g'(\eta(x)) \neq 0, \qquad \text{for all } \eta \in \mathcal{C}(\overline{\Omega}),\ x \in \overline{\Omega}$$

leads to both injectivity:

$$\left[\partial G(\eta)h\right](x) = 0 \quad \Rightarrow \quad h(x) = 0 \qquad \text{for all } x \in \overline{\Omega},$$

and surjectivity:
For given $n \in \mathcal{C}(\overline{\Omega})$, there is a function $h \in \mathcal{C}(\overline{\Omega})$ defined by

$$h(x) := \frac{n(x)}{g'(\eta(x))}, \qquad \text{for all } x \in \overline{\Omega},$$

such that

$$\left[\partial G(\eta)h\right](x) = n(x), \qquad \text{for all } x \in \overline{\Omega}.$$

With a corollary of the open mapping theorem, see [40], it follows that $\partial G(\eta)$ has a continuous inverse.

2 Numerical simulation of organic semiconductors

The models presented in the previous chapter are very ill-conditioned as we will see in Section 2.2. This causes naive chosen methods to fail, if they are not preconditioned. Instead of preconditioning, which is a non-trivial task, we present an alternative, problem adapted method, namely an extended Gummel method with a special damping technique as the globalization strategy for Newton's method. The chapter is arranged as follows. We first discuss the Scharfetter-Gummel scheme applied to the one dimensional problem and introduce Gummel's method extended by the quasi electrochemical potential defining equation with a contraction based damping strategy. For the later purpose of optimization, we study the robustness of the solution method via sampling over a cut of the control parameter space. Finally, we present the discretization of higher dimensional problems with the finite element method. We apply the extended Gummel method with contraction based damping strategy to 2D simulations of self-assembled nano-chains attached to the cathode.

2.1 Scharfetter-Gummel discretization scheme

First of all, we have to choose a discretization scheme to approximate the infinite dimensional problem (1.12) by a finite dimensional one. Scharfetter and Gummel [80] developed an exponentially fitted difference formula, which provides a locally constant current j and an upwind stabilized solution. Therefor we choose a mesh with $N-1$ subintervals $[x_i, x_{i+1}]$, $i = 1, \ldots, N-1$ of constant size $h := (x_N - x_1)/(N-1)$, $N \in \mathbb{N}$. For solving the continuity equation, cf. (1.12c),

$$\partial_x j = 0,$$

in all inner mesh points x_i, $i = 2, \ldots, N-1$, we take central finite differences to approximate the derivative of j:

$$\partial_x j(x_i) \approx \frac{j_{i+\frac{1}{2}} - j_{i-\frac{1}{2}}}{h}.$$

The values $j_{i\pm\frac{1}{2}}$ are given by the *Scharfetter-Gummel* scheme

$$j_{i+\frac{1}{2}} = \mu\,\partial_x\phi\,\frac{n_{i+1}\exp\left(-\frac{\partial_x\phi\,h}{\nu\,g_3}\right)-n_i}{\exp\left(-\frac{\partial_x\phi\,h}{\nu\,g_3}\right)-1}, \tag{2.1a}$$

$$j_{i-\frac{1}{2}} = \mu\,\partial_x\phi\,\frac{n_i\exp\left(-\frac{\partial_x\phi\,h}{\nu\,g_3}\right)-n_{i-1}}{\exp\left(-\frac{\partial_x\phi\,h}{\nu\,g_3}\right)-1}, \tag{2.1b}$$

where n_{i+1}, n_i, and n_{i-1} are approximations to the electron density n at the points x_{i+1}, x_i, and x_{i-1} respectively. To motivate the formulas in (2.1) we assume the functions

$$j, \mu, g_3, \text{ and } \partial_x\phi$$

to be constant on the interval $(x_i, x_{i+1}]$. For an arbitrary $x \in (x_i, x_{i+1}]$ we then have with (1.12b):

$$\begin{aligned}-j\exp\left(-\frac{(x-x_i)\,\partial_x\phi}{\nu\,g_3}\right) &= \mu\,(\nu\,g_3\,\partial_x n - n\partial_x\phi)\exp\left(-\frac{(x-x_i)\,\partial_x\phi}{\nu\,g_3}\right)\\ &= \mu\,\nu\,g_3\,\partial_x\left(n\exp\left(-\frac{(x-x_i)\,\partial_x\phi}{\nu\,g_3}\right)\right).\end{aligned}$$

Remember that $\nu, g_3 > 0$. Now we integrate on both sides over $[x_i, x_i + h]$

$$-j\int_{x_i}^{x_i+h}\exp\left(-\frac{(x-x_i)\,\partial_x\phi}{\nu\,g_3}\right)\mathrm{d}x = \mu\,\nu\,g_3\left(n_{i+1}\exp\left(-\frac{h\,\partial_x\phi}{\nu\,g_3}\right)-n_i\right).$$

For the integration we extended the constant functions to the left point x_i continuously. Integration on the left hand side yields

$$j\frac{\nu\,g_3}{\mu\,\partial_x\phi}\left(\exp\left(-\frac{\partial_x\phi\,h}{\nu\,g_3}\right)-1\right) = \nu\,g_3\left(n_{i+1}\exp\left(-\frac{\partial_x\phi\,h}{\nu\,g_3}\right)-n_i\right). \tag{2.2}$$

The mobility $\mu > 0$ and for $\partial_x\phi$ we assume that it is unequal to zero, since otherwise the current is set to zero which is consistent with the formula (2.1a). We solve (2.2) for j and end up with the Scharfetter-Gummel scheme (2.1a) for the value $j_{i+\frac{1}{2}}$, if we interpret the constant j as an approximation to the current density at the point $x_{i+\frac{1}{2}} := x_i + \frac{h}{2}$. By exchanging $[x_i, x_i + h]$ with $[x_i - h, x_i]$ one obtains (2.1b) for $j_{i-\frac{1}{2}}$

analogously. In the following Lemma we show that the Scharfetter-Gummel scheme coincides asymptotically with standard finite difference formulas in convection and diffusion dominated regimes respectively.

Lemma 2.1.1. *The Scharfetter-Gummel scheme (2.1) provides asymptotically an upwind stabilization in form of one sided differences and converges to central finite differences in diffusion dominated regimes where the field $\partial_x\phi$ vanishes:*

$$\begin{aligned}
&i) \quad \frac{j_{i+\frac{1}{2}} - j_{i-\frac{1}{2}}}{h} \quad \simeq \quad \mu\,\partial_x\phi\,\frac{n_i - n_{i-1}}{h} && \text{for} \quad \partial_x\phi \to \infty \\
&ii) \quad \frac{j_{i+\frac{1}{2}} - j_{i-\frac{1}{2}}}{h} \quad \simeq \quad \mu\,\partial_x\phi\,\frac{n_{i+1} - n_i}{h} && \text{for} \quad \partial_x\phi \to -\infty \\
&iii) \quad \frac{j_{i+\frac{1}{2}} - j_{i-\frac{1}{2}}}{h} \quad \to \quad -\mu\,\nu\,g_3\,\frac{n_{i+1} - 2n_i + n_{i-1}}{h^2} && \text{for} \quad \partial_x\phi \to 0
\end{aligned}$$

Proof. *i*) We have to show that the left hand side divided by the right hand side converges to one if $\partial_x\phi \to \infty$:

$$\begin{aligned}
&\frac{j_{i+\frac{1}{2}} - j_{i-\frac{1}{2}}}{h}\left(\mu\,\partial_x\phi\,\frac{n_i - n_{i-1}}{h}\right)^{-1} \\
&= \frac{\mu\,\partial_x\phi}{h}\left(\frac{n_{i+1}\exp\left(-\frac{\partial_x\phi\,h}{\nu\,g_3}\right) - n_i}{\exp\left(-\frac{\partial_x\phi\,h}{\nu\,g_3}\right) - 1} - \frac{n_i\exp\left(-\frac{\partial_x\phi\,h}{\nu\,g_3}\right) - n_{i-1}}{\exp\left(-\frac{\partial_x\phi\,h}{\nu\,g_3}\right) - 1}\right)\frac{1}{\mu\,\partial_x\phi}\,\frac{h}{n_i - n_{i-1}} \\
&= \frac{n_{i+1}\exp\left(-\frac{\partial_x\phi\,h}{\nu\,g_3}\right) - n_i - n_i\exp\left(-\frac{\partial_x\phi\,h}{\nu\,g_3}\right) + n_{i-1}}{\left(\exp\left(-\frac{\partial_x\phi\,h}{\nu\,g_3}\right) - 1\right)(n_i - n_{i-1})} \quad \to \quad 1 \quad \text{for} \quad \partial_x\phi \to \infty.
\end{aligned}$$

The difference formula is appropriate for drift dominated regimes, because "information" from upwind only is taken.

ii) Analogously we get the second result by expanding the fraction in (2.1a) and (2.1b) by

$$\exp\left(\frac{\partial_x\phi\,h}{\nu\,g_3}\right)$$

and taking the limit $\partial_x\phi \to -\infty$ of the fraction of $\frac{j_{i+\frac{1}{2}} - j_{i-\frac{1}{2}}}{h}$ and $\mu\,\partial_x\phi\,\frac{n_{i+1} - n_i}{h}$.

iii) Here we have to use L'Hospital's rule, which gives us

$$\lim_{\partial_x\phi\to 0}\frac{\partial_x\phi}{\exp\left(-\frac{\partial_x\phi\,h}{\nu\,g_3}\right) - 1} = \lim_{\partial_x\phi\to 0}\frac{1}{-\frac{h}{\nu\,g_3}\exp\left(-\frac{\partial_x\phi\,h}{\nu\,g_3}\right)} = -\frac{\nu\,g_3}{h}$$

and hence

$$\begin{aligned} j_{i+\frac{1}{2}} &\to -\mu\,\nu\,g_3\,\frac{n_{i+1}-n_i}{h}, \\ j_{i-\frac{1}{2}} &\to -\mu\,\nu\,g_3\,\frac{n_i-n_{i-1}}{h}, \end{aligned}$$

and finally

$$\frac{j_{i+\frac{1}{2}}-j_{i-\frac{1}{2}}}{h} \to -\mu\,\nu\,g_3\,\frac{n_{i+1}-2n_i+n_{i-1}}{h^2}.$$

The resulting difference formula is appropriate for diffusion dominated regimes.

□

We are left with discretizing the derivatives acting on the electric potential ϕ, for which we take central difference formulas for first order derivatives

$$\partial_x\phi\Big(x_{i+\frac{1}{2}}\Big) \approx \frac{\phi_{i+1}-\phi_i}{2h}$$

and second order derivatives

$$\partial_x^2\phi(x_i) \approx \frac{\phi_{i+1}-2\phi_i+\phi_{i-1}}{h^2}.$$

Hence the equations from (1.12a) to (1.12c) result in

$$0 = \frac{\mu}{h}\left(\frac{\phi_{i+1}-\phi_i}{h}\,\frac{n_{i+1}\exp\Big(-\frac{\phi_{i+1}-\phi_i}{\nu\,g_3}\Big)-n_i}{\exp\Big(-\frac{\phi_{i+1}-\phi_i}{\nu\,g_3}\Big)-1} - \frac{\phi_i-\phi_{i-1}}{h}\,\frac{n_i\exp\Big(-\frac{\phi_i-\phi_{i-1}}{\nu\,g_3}\Big)-n_{i-1}}{\exp\Big(-\frac{\phi_i-\phi_{i-1}}{\nu\,g_3}\Big)-1}\right) \tag{2.3}$$

and

$$\lambda^2\,\frac{\phi_{i+1}-2\phi_i+\phi_{i-1}}{h^2} = n_i.$$

Dirichlet boundary conditions are applied through the right hand side. For Poisson's equation this means

$$\begin{aligned} \lambda^2\,\frac{\phi_{i+1}-2\phi_i+\phi_{i-1}}{h^2} &= n_i && \text{for } i=3,\dots,N-2, \\ \lambda^2\,\frac{\phi_{i+1}-2\phi_i}{h^2} &= n_i-\frac{\phi_{\text{cathode}}}{\phi_{\text{scal}}}\frac{1}{h^2} && \text{for } i=2, \\ \lambda^2\,\frac{-2\phi_i+\phi_{i-1}}{h^2} &= n_i-\frac{\phi_{\text{anode}}}{\phi_{\text{scal}}}\frac{1}{h^2} && \text{for } i=N-1. \end{aligned} \tag{2.4}$$

Analogously $n_{\text{cathode}}/n_{\text{scal}}$ and $n_{\text{anode}}/n_{\text{scal}}$ are applied through the right hand side of the discretized continuity equation (2.3).

2.1.1 Upwind conformal averaging

In our models, EGDM and ECDM respectively, the mobility μ and the diffusion enhancement factor g_3 are density dependent functions. In drift dominated regimes, one has to be careful not using information from downwind in the discretization formulas, which would result in numerical, unphysical oscillations. We adapted the idea of the Scharfetter-Gummel scheme to average the respective terms. A "smooth switch" is given by the function

$$\theta(y) = \frac{1 - \exp\left(\frac{y}{2}\right)}{1 - \exp(y)}.$$

It holds

$$\theta(y) \quad \to \quad \begin{cases} 1, & \text{for } y \to -\infty, \\ 0, & \text{for } y \to \infty. \end{cases}$$

With the argument $y = \nu\left(\phi_{i+1} - \phi_i\right)$, we average as follows

$$f\left(n_{i+\frac{1}{2}}\right) = \theta(y)\, f(n_{i+1}) + (1 - \theta(y))\, f(n_i),$$

with f equal to μ or g_3. The argument y is chosen to be similar to the one used in the Scharfetter-Gummel scheme but neglecting the additional g_3 influence here. Thus the flux is numerically stabilized. A different approach with the use of streamline-diffusion techniques is analyzed by Jiang [54].

2.1.2 Error analysis

For the Scharfetter-Gummel scheme Markowich et al. [63] analyzed error estimates for the electron density n dependent on the Debeye length λ, cf. (1.10),

$$\max_{1 \le i \le N} |n(x_i) - n_i| \le C(h^2 + \lambda|\lambda|), \tag{2.5}$$

with the analytical solution n and the approximated values at the mesh points n_i. We denote the boundary values n_{cathode} and n_{anode} with n_1 and n_N respectively. C includes upper bounds of n and ϕ and bounds of the derivatives of n and ϕ up to order three, cf. Markowich et al. [63]. For standard finite differences for the second

order derivatives, we can estimate the error of Poisson's equation as

$$\left| \frac{\phi_{i+1} - 2\phi_i + \phi_{i-1}}{h^2} - \Delta\,\phi(x_i) \right| \leq Ch^2 \qquad \text{for all } i = 2, \ldots, N-1,$$

where C includes fourth order derivatives of the analytical solution ϕ. Furthermore a unique discrete solution exists and with the help of a discrete maximum principle the error can be represented as

$$\max_{1 \leq i \leq N} |\phi(x_i) - \phi_i| \leq Ch^2, \tag{2.6}$$

where C again includes fourth order derivatives of ϕ. For the details, we refer to Grossmann and Roos [46]. We run simulations of the EGDM (with ECDM similar results are obtained) on a sequence of refined meshes with mesh size parameter $h, h/2, h/4, \ldots$. Assuming the error of an approximation u_h propagates like

$$u_h = u + O(h^p)$$

and hence

$$u_{\frac{h}{2}} = u + O\left(\frac{h^p}{2^p}\right),$$

the order of convergence rates should behave like

$$p = \log\left(\frac{h^p}{\frac{h^p}{2^p}}\right) / \log(2) \approx \log\left(\frac{u_h - u}{u_{\frac{h}{2}} - u}\right) / \log(2). \tag{2.7}$$

For the simulations we have developed a *C++* program using the *LAPACK* QR decomposition. The previous explained Scharfetter-Gummel discretization scheme and in anticipation the later introduced iterative extended Gummel method, cf. Section 2.2, have been implemented. We compute solutions on the scaled domain $(0, L/x_{\text{scal}}) = (0, 1)$, cf. the scaling in Section 1.3. As initial values we take

$$n^0(x) = (1-x)\,\frac{n_{\text{cathode}}}{n_{\text{scal}}} + x\,\frac{n_{\text{anode}}}{n_{\text{scal}}}, \qquad \phi^0(x) = x, \qquad \text{for } x \in (0,1). \tag{2.8}$$

For the discretization of G, i.e. approximating the integral, we use the trapezoidal rule on a fixed interval with enough evaluation points, that the error is not dominant. Alternatively one could follow Paasch et al. [73] considering an analytical expression for the integral. A benchmark with the commercial software *setfos 3.2*, cf. [35], has been performed ensuring that deviations of the solution are less than 1% measured in

the Euclidean norm. Our parameter setup of choice is displayed in Table 2.1. For the units we refer to Chapter 1. In Table 2.2 we show the norm of the errors and

V	L	T	μ_0	σ	N_t	E_{cathode}	E_{anode}	c_0
5	100	300	$4.5 \cdot 10^{-6}$	0.13	$2 \cdot 10^{27}$	0.0	0.0	0.29

Table 2.1: Parameter configuration

the order of convergence rates computed with the formula (2.7). The approximation values ϕ_i, n_i, and η_i, $i = 1, \ldots, N$ with included boundary values are assembled in vectors ϕ_h, n_h and $\eta_h \in \mathbb{R}^N$ respectively. The exact solution is not known, therefore we compute a reference solution $\bar{u} = (\bar{\phi}, \bar{n}, \bar{\eta})$ on a mesh with 6400 points. The orders

N	$\lVert\bar{\phi} - \phi_h\rVert_2$	p	$\lVert\bar{n} - n_h\rVert_2$	p	$\lVert\bar{\eta} - \eta_h\rVert_2$	p
50	2.324	-	7.360	-	1.827	-
100	1.791	0.37	4.253	0.79	0.817	1.15
200	1.256	0.51	2.019	1.07	0.288	1.50
400	0.745	0.75	0.677	1.57	0.083	1.79
800	0.334	1.16	0.151	2.15	0.035	1.21
1600	0.107	1.64	0.036	2.04	0.013	1.44
3200	0.025	2.09	0.010	1.82	0.003	1.99

Table 2.2: Errors and orders of convergence rates p of the approximations ϕ_h, n_h and η_h compared to reference solutions $\bar{\phi}$, $\bar{n}$ and $\bar{\eta}$ for different numbers of mesh points N.

of convergence rates of ϕ_h and n_h approach the value 2 when N gets large as expected, cf. (2.6) and (2.5). The quasi electrochemical potential is related to n through the equation (1.12d). For the error of η_h we can write

$$\lVert\eta - \eta_h\rVert_2 \approx \lVert G^{-1}(n) - G^{-1}(n_h)\rVert_2 \approx C\lVert n - n_h\rVert_2, \tag{2.9}$$

if one can show that G^{-1} is Lipschitz continuous. This could explain the decay of the order of convergence rate of η_h approaching 2. In Figure 2.1 we show the decrease of the norm of the errors of the solution components. We add a reference plot for the convergence of second order in h. Above $N = 1000$ the slopes are quite the same according to the expected asymptotical quadratic convergence of ϕ_h, n_h, and η_h, cf. (2.6), (2.5), and (2.9). We are interested in solutions which are stable and can be computed fast. In the optimization later on we have to simulate a couple of 1000

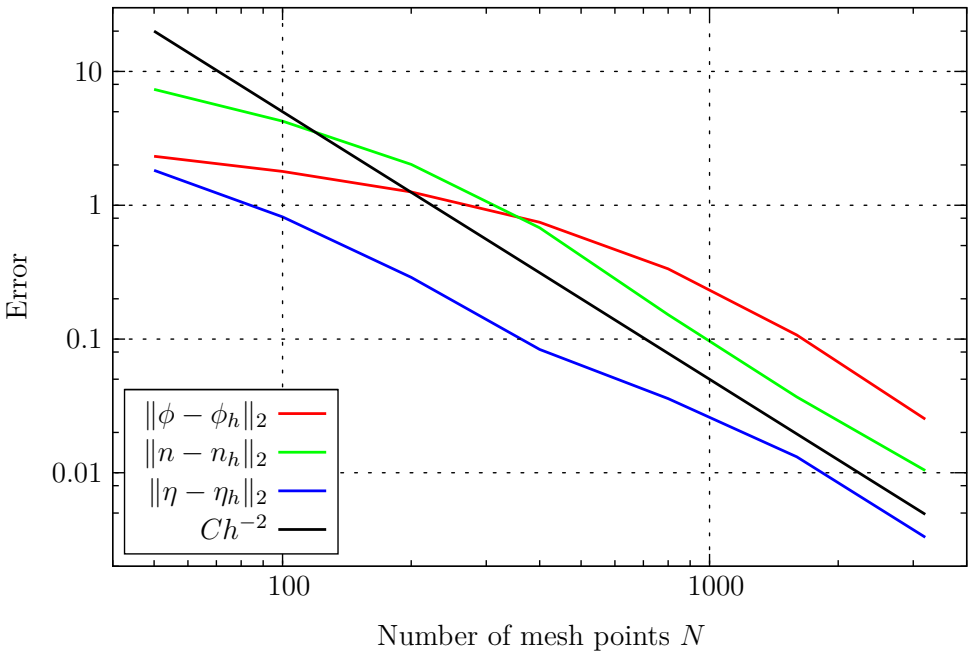

Figure 2.1: Errors of the solution and a reference function plotted against the number of mesh points.

times. For that we make a trade-off and fix from now on the number of mesh points N to 100 for all 1D computations.

2.2 Solution methods

The spatial discretization leads to a nonlinear system of equations for the vectors ϕ_h, n_h, and η_h. In this section we omit the index h because we only treat the finite dimensional problems. We rewrite the nonlinear discretized version of the system (1.12) with applied boundary conditions for the vectors ϕ, n, and $\eta \in \mathbb{R}^N$ as follows

$$\begin{aligned} A_\phi \phi &= b_\phi(n), \\ A_n(\phi, n, \eta)\, n &= b_n(\phi, n, \eta), \\ n &= G(\eta), \end{aligned} \tag{2.10}$$

where $A_\phi \in \mathbb{R}^{N\times N}$ is a constant matrix and b_ϕ a nonlinear function with values in $\mathbb{R}^N$ resulting from the finite differences (2.4). The nonlinear matrix-valued function A_n with values in $\mathbb{R}^{N\times N}$ and the nonlinear vector-valued function b_n mapping to $\mathbb{R}^N$ arise from (2.3) with the applied boundary values. The integral in G is approximated with the trapezoidal rule on a fixed interval with enough evaluation points, that the error is not dominant. The discretized version of G is also denoted with G. If nothing else is said we denote with $\|.\|$ the Euclidean norm in $\mathbb{R}^N$. We also frequently abbreviate (2.10) with

$$F(u) = 0, \tag{2.11}$$

where $u := (\phi, n, \eta) \in \mathbb{R}^{3N}$.

2.2.1 Ill-conditioned problem

According to Deuflhard [29] the *condition of a nonlinear problem* describes the amplification of the relative error, i.e. for an ill-conditioned problem like ours, small relative disturbances of the input cause huge relative errors of the output. To analyze the condition of our nonlinear problem (2.11), we fix an exemplary iterate u_k close to the solution and perform a line search along a steepest descent direction

$$p_k = -F'(u_k)^T F(u_k)$$

of the classical merit function

$$\frac{1}{2}\|F(u_k)\|^2.$$

That means we want to solve the following unconstrained optimization problem

$$\min_{\alpha} \frac{1}{2} \left\|f_{\mathrm{cl}}(\alpha)\right\|^2$$

with

$$f_{\mathrm{cl}}(\alpha) := F\left(u_k + \alpha\, p_k\right).$$

In Figure 2.2 the dependence of the objective w.r.t. α is shown for the configuration given in Table 2.1. The picture shows a very narrow valley in which acceptable values

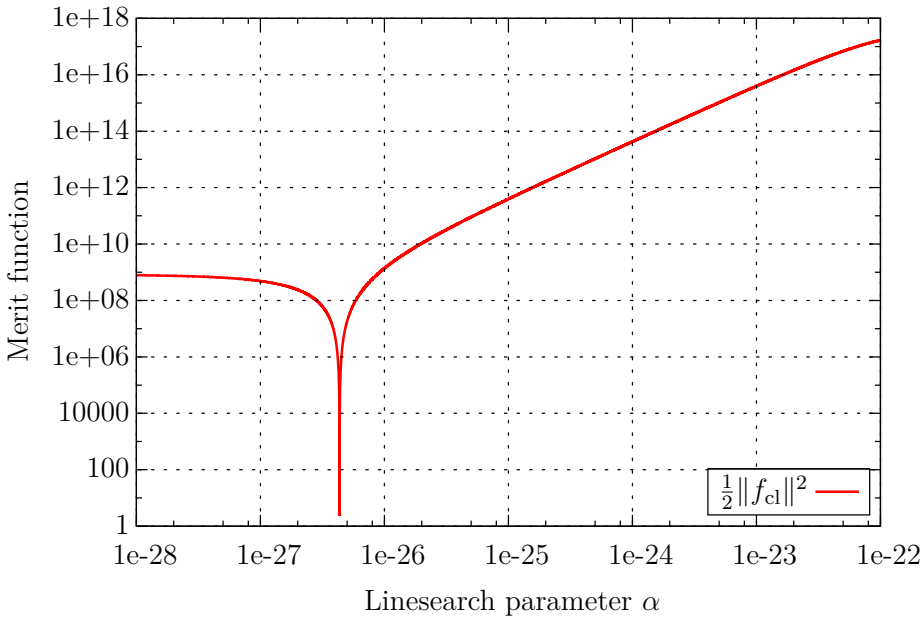

Figure 2.2: Exemplary line search valley.

for α lie, i.e. values of α which fulfill the Wolfe conditions, cf. [71]. Small disturbances on the input α leads to drastic changes in the output, here in terms of the objective function.

Remark 2.2.1. Instead of taking the EGDM similar results of the line search would have been obtained by taking the ECDM.

On the other hand, for the linearized problems of (2.11)

$$F'(u_k)\,\delta u_k = -F(u_k),$$

arising in Newton's method, cf. Section 2.2.4, we can compute the *matrix condition number* of the Jacobian $F'(u_k) \in \mathbb{R}^{3N\times 3N}$, which is defined by

$$\operatorname{cond}\left(F'(u)\right) := \left\|F'(u)\right\| \left\|F'(u)^{-1}\right\|.$$

In the case of the spectral norm $\|.\|_2$ this is

$$\operatorname{cond}\left(F'(u)\right) = \frac{|\lambda_{\max}(F'(u))|}{|\lambda_{\min}(F'(u))|}.$$

Well-conditioned problems should have a condition number around one. The condition in our case however is

$$\operatorname{cond}\left(F'(u)\right) = 5.57 \cdot 10^{15}.$$

This number shows that we have a very ill-conditioned problem. The performance and stability of algorithms are substantially determined by the condition, e.g. the convergence of iterative methods to solve systems of linear equations depends directly on the condition.

We use Gummel's method which decouples and linearizes the problem at once. We will see that the decoupling reduces the condition number drastically.

2.2.2 Classical Gummel method

For the classical van Roosbroeck system (1.12a) - (1.12c) with constant mobility and diffusion and classical Einstein relation, Gummel proposed a fixed point iteration, see [47]. In our notation for an unipolar layer, i.e. only electron transport, the algorithm is given in Algorithm 1. On the right hand side of the Poisson equation we add a stabilization term which is a common technique to improve the convergence behavior of the method, cf. Selberherr [85]. The multiplication "$*$" is to be understood pointwisely. In the continuity equation, the Matrix A_n does not depend on the states n and η, because the mobility is constant for the classical van Roosbroeck system and there is no quasi electrochemical potential, because the classical Einstein relation holds, cf. (1.7). The advantage of this decoupling algorithm is, that it transforms one nonlinear problem into two linear ones of half size. On the other side the fixed point iteration has to be contractive to guarantee convergence. First convergence results were made by Mock [68]. See the cited literature in Section 1.4 for further discussions of the contraction of Gummel's map. Other approaches to solve the van Roosbroeck system are e.g. to consider the coupled instationary equations following Pflumm et al.

Algorithm 1 Algorithm for Gummel's classical fixed point iteration.

1: Let $u^0 := (n^0, \phi^0) \in \mathbb{R}^{2N}$ be given and choose $\delta u^0 \in \mathbb{R}^{2N}$ such that $\|\delta u^0\|_2 \gg \mathrm{TOL}$ with a given error tolerance $\mathrm{TOL} > 0$. Set $i = 0$.
2: **while** $\|\delta u^i\|_2 > TOL$ **do**
3: With n^i solve

$$A_\phi\, \phi^{i+1} = b_\phi(n^i) * \left((1, \ldots, 1)^T + \frac{\phi^{i+1} - \phi^i}{\nu} \right)$$

for ϕ^{i+1}.
4: With ϕ^{i+1} solve

$$A_n(\phi^{i+1})\, n^{i+1} = b_n(\phi^{i+1})$$

for n^{i+1}.
5: Set $u^{i+1} := (n^{i+1}, \phi^{i+1})$ and $\delta u^{i+1} := u^{i+1} - u^i$.
6: $i \leftarrow i + 1$
7: **end while**

[76] or Mello [27]. A continuum approach is presented by Bonham et al. [18] and [19] for simulating single layer devices.

2.2.3 Extended Gummel method

In the case of EGDM and ECDM, where the mobility is nonlinear and the generalized Einstein relation applies, A_n also depends on the electron density n and the electrochemical potential η and we have the additional η defining equation. We extend the stabilization term of the Poisson equation by the g_3 factor [86]. The algorithm is given in Algorithm 2. With the same configuration used before, see Table 2.1, we compute the condition numbers of the Gummel subsystems obtaining the values in Table 2.3. With respect to the condition we see that Gummel's decoupling is sensible. For the classical Gummel decoupling method the effect of reducing condition numbers

$\mathrm{cond}(G'(\eta^{i+1}))$	291.22
$\mathrm{cond}(A_\phi)$	$1.07 \cdot 10^5$
$\mathrm{cond}(A_n)$	$5.08 \cdot 10^8$
$\mathrm{cond}(F'(u))$	$5.57 \cdot 10^{15}$

Table 2.3: Condition numbers of the Gummel subsystems and the Jacobian of F.

due to decoupling is analyzed in Ascher et al. [3]. A similar quasi linearization of the

Algorithm 2 Algorithm for Gummel's fixed point iteration expanded by the quasi electrochemical potential defining equation and a derivative-free linearization.

1: Let $u^0 := (n^0, \phi^0, \eta^0) \in \mathbb{R}^{3N}$ be given and choose $\delta u^0 \in \mathbb{R}^{3N}$ such that $\|\delta u^0\|_2 \gg \mathrm{TOL} > 0$ with a given error tolerance TOL. Set $i = 0$.
2: **while** $\|\delta u^i\|_2 > TOL$ **do**
3: Solve

$$n^i - G(\eta^{i+1}) = 0$$

for η^{i+1} with Newton's method started with $\eta_0^{i+1} = 0$.
4: Solve

$$A_\phi\, \phi^{i+1} = b_\phi(n^i) * \left((1, \ldots, 1)^T + \frac{\phi^{i+1} - \phi^i}{\nu\, g_3(n^i, \eta^{i+1})} \right)$$

for ϕ^{i+1}.
5: With n^i, ϕ^{i+1} and η^{i+1} solve

$$A_n(\phi^{i+1}, n^i, \eta^{i+1})\, n^{i+1} = b_n(\phi^{i+1}, n^i, \eta^{i+1}) \tag{2.12}$$

for n^{i+1}.
6: Set $u^{i+1} := (n^{i+1}, \phi^{i+1}, \eta^{i+1})$ and $\delta u^{i+1} := u^{i+1} - u^i$.
7: $i \leftarrow i + 1$
8: **end while**

continuity equation (2.12) is suggested by Gajewski [37].

Generalized Einstein relation in Poisson stabilization

We give a brief motivation for the appearance of the g_3 factor in the stabilization term of Poisson's equation in Algorithm 2. Therefor we have to mention that there are different types of variable sets in which the van Roosbroeck system can be formulated. A different choice than ours, i.e. (ϕ, n), is to use dependent variables (ϕ, v), cf. [85], where ϕ is the electric potential and v given by

$$n = v \exp\left(\frac{\phi}{\nu}\right). \tag{2.13}$$

Inserted in Gummel's method with different Gummel iteration indices for ϕ and v yields for the Poisson equation

$$\lambda^2 \Delta \phi^{i+1} = v^i \exp\left(\frac{\phi^{i+1}}{\nu}\right).$$

If we reinsert the expression (2.13) for v^i, we end up with

$$\lambda^2 \Delta \phi^{i+1} = n^i \exp\left(\frac{\phi^{i+1} - \phi^i}{\nu}\right).$$

Linearization of the exponential function and discretization leads to the stabilized Poisson equation in Algorithm 1. One can derive the expression (2.13) from the thermal equilibrium case, i.e. $j = 0$ at zero temperature $T = 0$. In case of the extended models EGDM and ECDM ν is enhanced by the factor g_3 due to the generalized Einstein relation. Hence (2.13) changes to

$$n = v \exp\left(\frac{\phi}{\nu\, g_3}\right)$$

and the resulting nonlinear Poisson equation is

$$\lambda^2 \Delta \phi^{i+1} = n^i \exp\left(\frac{\phi^{i+1} - \phi^i}{\nu\, g_3(n^i, \eta^{i+1})}\right).$$

The occurrence of the g_3 factor has positive impact on the convergence behavior especially for highly doped materials which occur in form of a scalar number C_{doping}

on the right hand side of Poisson's equation

$$\lambda^2 \, \Delta \, \phi^{i+1} = n^i \, \exp\left(\frac{\phi^{i+1} - \phi^i}{\nu \, g_3(n^i, \eta^{i+1})}\right) + C_{\text{doping}}.$$

In Figure 2.3 the results for the electron density, electric potential and quasi electrochemical potential can be seen for different choices of doping intensity. They are

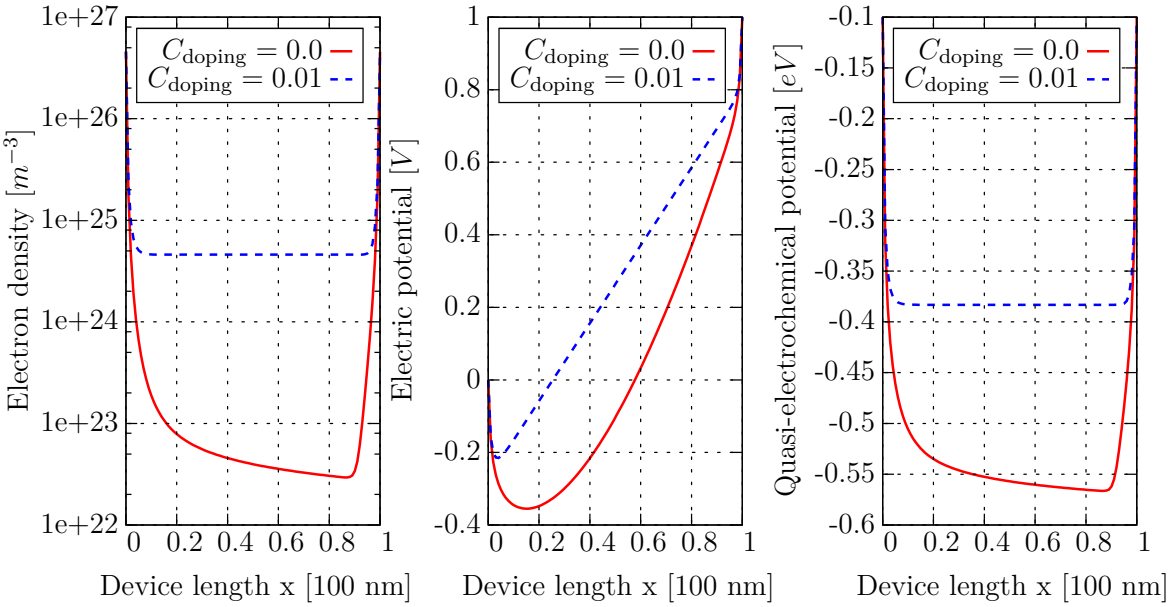

Figure 2.3: Solution components of the extended Gummel method for different doping intensities.

computed with the EGDM using the parameters given in Table 2.4, with the units declared in Chapter 1. The results are similar to the ones computed with the ECDM

V	L	T	μ_0	σ	N_t	E_{cathode}	E_{anode}	c_0
1	100	233	$4.5 \cdot 10^{-6}$	0.13	$2 \cdot 10^{27}$	0.1	0.1	0.29

Table 2.4: Parameter configuration

in Stodtmann et al. [86]. The effect on the convergence behavior is visualized in Figure 2.4, where the black lines correspond to $C_{\text{doping}} = 0.01$ and the blue lines to $C_{\text{doping}} = 0.0$. The increment of Gummel's algorithm measured in the Euclidean norm $\|\delta u^i\|_2$ is plotted against the iteration number. We observe the two nice effects, that

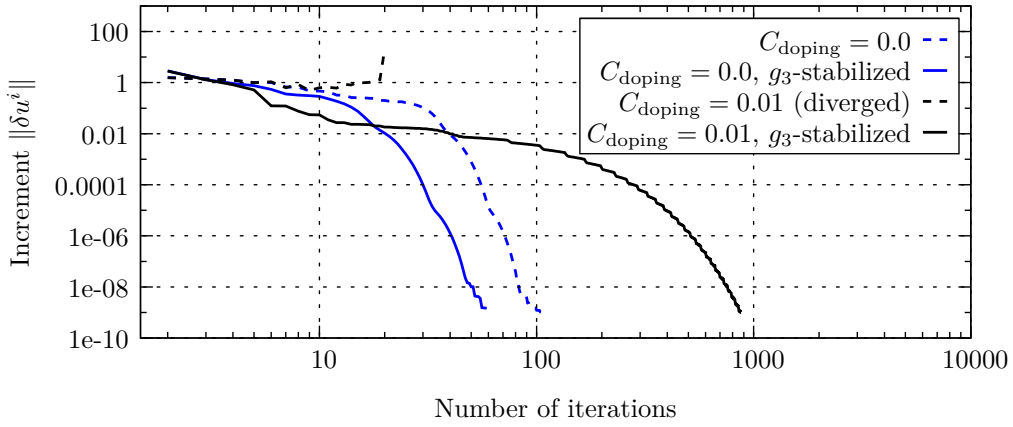

Figure 2.4: Effects of g_3 factor in Poisson stabilization on convergence behavior.

the enhanced stabilization causes

i) accelerated convergence, cf. blue lines in Figure 2.4

ii) convergence at all, cf. black lines in Figure 2.4.

This extends the method presented in Knapp et al. [58].

2.2.4 Gummel as the globalization strategy for Newton's method

When Gummel gets close to the solution, the convergence speed stays only linear for high injection profiles, cf. for example [72]. We therefore use Gummel as the globalization strategy for Newton's method. For a twice continuously differentiable mapping $F : D \to \mathbb{R}^n$ with $D \subset \mathbb{R}^m$ convex Newton-type methods compute steps

$$\delta u^i = -M(u^i)F(u^i) \tag{2.14}$$

where M is an approximation to the inverse of the Jacobian of F. For the local convergence we have the local contraction theorem of Bock [15].

Theorem 2.2.2. *Assume that for all $v, w \in D$, $\theta \in (0, 1]$ with $w - v = -M(v)F(v)$ it holds:*

- *There is an $\omega < \infty$ such that*

$$\left\| M(w) \left(F'(v + \theta(w - v)) - F'(v) \right) (w - v) \right\| \leq \omega\, \theta\, \|w - v\|^2. \tag{2.15}$$

- *There is a* $\kappa(v) \leq \kappa < 1$ *such that*

$$\|M(w)R(v)\| \leq \kappa(v)\|w - v\|$$

with the residual $R(v) := F(v) - F'(v)M(v)F(v)$.

For the initial guess v^0 *assume that*

$$\varrho_0 := \kappa + \frac{\omega}{2}\|\delta v^0\| < 1,$$

with

$$\varrho_k := \kappa + \frac{\omega}{2}\|\delta v^k\|, \qquad \delta v^k := -M(v^k)F(v^k),$$

and that $\overline{B}(v^0, \varrho_0) \subset D$.
Then the iterates $v^{k+1} = v^k + \delta v^k$ *are well defined, remain in* $B(v^0, \varrho_0)$*, and converge to a solution* $v^* \in \overline{B}(v^0, \varrho_0)$*. Moreover, the following error estimates hold*

$$\|v^{k+j} - v^*\| \leq \frac{\varrho_k^j}{1 - \varrho_k}\|\delta v^k\|$$
$$\|\delta v^{k+1}\| \leq \varrho_k\|\delta v^k\| = \kappa\|\delta v^k\| + \frac{\omega}{2}\|\delta v^k\|^2.$$

Proof. See [15]. □

For exact Newton methods with $M = (F')^{-1}$ we have quadratic convergence since $\kappa = 0$. Additionally we can make a statement about a sequence of nonlinear equations

$$F_j(u_j) = 0, \qquad j = 0, 1, \ldots$$

where F_j is the finite dimensional approximation of a partial differential equation corresponding to the jth level of an hierarchical grid, see for the details Deuflhard [30]. If ω_j are the affine covariant Lipschitz constants related to F_j, defined by (2.15), we get the asymptotical result

$$\omega_j \leq \omega + \xi_j, \quad \lim_{j\to\infty} \xi_j = 0,$$

where ω is the affine covariant Lipschitz constant of the infinite dimensional problem analogously defined to (2.15). For the proof we refer to Deuflhard [28]. Hence the local convergence of Newton's method is asymptotically grid independent. For Gummel's method this does not hold. With the configuration given in Table 2.4 the

correspondence of the number of iterations and the number of discretization points is shown in Figure 2.5. We stop Gummel's method, when $\|\delta u^i\|$ falls below 10^{-7}. Figure 2.5 confirms that Gummel's method is not grid independent. To use Gummel

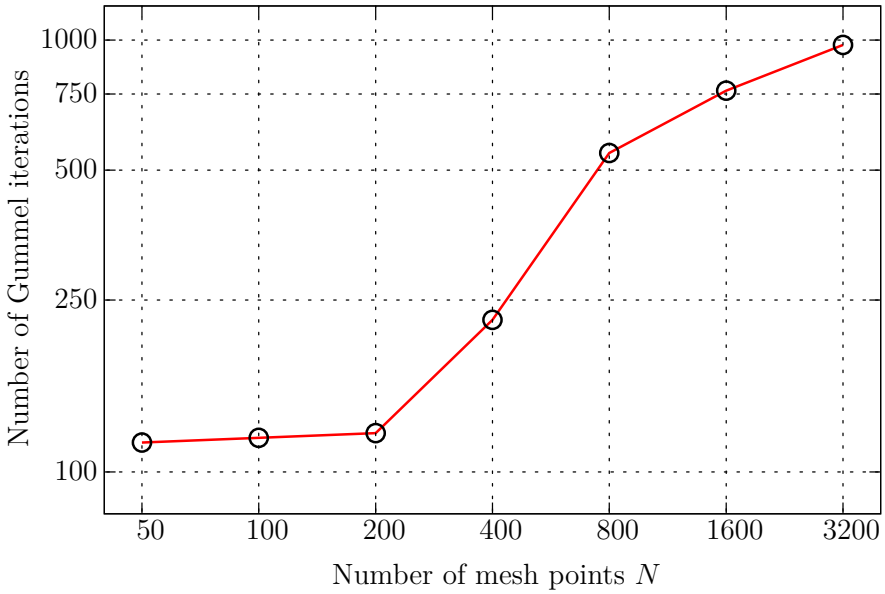

Figure 2.5: Number of iterations of Gummel's method over the number of discretization points N.

as the globalization strategy for Newton's method we have to switch at a certain point from Gummel to Newton.

Remark 2.2.3. Performing Newton steps is much more expensive than performing Gummel steps. Each Newton step is the solution of (2.11), i.e. a $3N$ times $3N$ coupled block system. Whereas Gummel solves each sub-equation of (2.11) separately, i.e. solving 3 equations of size N times N. We therefore suggest to use a sharp switching point instead of a homotopy from Gummel to Newton. We state the heuristic to perform Newton steps only within the contraction ball $\overline{B}(u^0, \varrho_0)$, cf. Theorem 2.2.2. The quadratic convergence then compensates the more expensive steps.

We are interested in solutions for a wide range of parameters and control parameters. By trial and error we have found that we can switch, if for the Gummel steps hold

$$\|\delta u^i\|_2 < 10^{-3}. \tag{2.16}$$

We claim that this switching point is independent for all parameters, control parame-

ters, and boundary values we consider in this work.

Remark 2.2.4. For damped Newton methods there are several tests like the restrictive monotonicity test (RMT), cf. [17], to approximate the affine covariant Lipschitz constant ω and hence the radius of the contraction ball ϱ_0. This directly provides a criterion when to switch to full step Newton or not. Because the steps we perform are Gummel steps and not Newton steps, we are not able to apply such tests.

Remark 2.2.5. Because of the grid dependence of Gummel's method the switching point might also depend on the number of discretization points N. However we have not noticed any influence on the switching point (2.16) in our calculations.

A comparison of Gummel's method only and Gummel as the globalization strategy for Newton's method with highly doped material is shown in Figure 2.6.

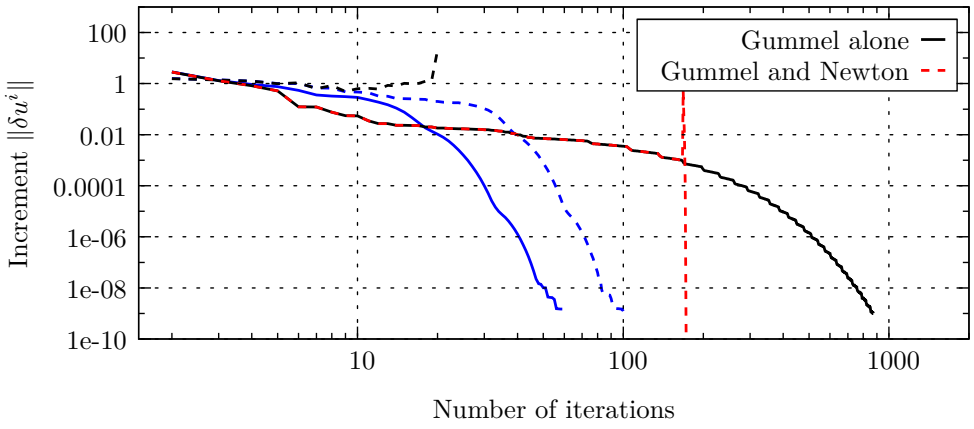

Figure 2.6: Gummel method coupled with full step Newton method.

Remark 2.2.6. We have seen in Section 2.2.1 that the matrix F' has a bad condition. For larger problems one would use iterative methods to solve the linear subproblems arising in Newton's method. The convergence behavior of iterative methods like *GMRES* strongly depends on the condition. For our comparably small problems we use direct methods to decompose the matrix. These methods are less sensitive to the condition.

As already mentioned in Remark 2.2.3 Newton steps are much more expensive than Gummel steps. However the overhead of Newton's method is justified when we compare the computational time. In Table 2.5 are displayed the computational times for performing Gummel and Newton steps starting from the switching point for a different number of mesh points.

Remark 2.2.7. When it comes to optimization, we have to perform hundreds of

simulations. The switching to Newton's method can save hours of computational time.

N	CPU time	
	Gummel	Newton
50	0.4 sec	0.05 sec
100	1.3 sec	0.24 sec
200	12.3 sec	2.1 sec
400	125 sec	22.5 sec
800	1386 sec	186 sec

Table 2.5: Computational time comparison between Gummel's and Newton's method for a different number of mesh points.

In Figure 2.7 we visualize the paths of Gummel's and Newton's method, first combined and later separated. We assembled N_G Gummel steps, which are vectors in $\mathbb{R}^{3N}$ into a matrix $Z \in \mathbb{R}^{3N \times N_G}$. Then we compute a QR decomposition with pivoting of Z yielding matrices $Q \in \mathbb{R}^{3N \times 3N}$ and $R \in \mathbb{R}^{3N \times N_G}$, where the absolute values of the diagonal entries of R are decreasing with increasing row number. For a two dimensional projection, we define the projection matrix P as the submatrix of Q

$$P := \begin{pmatrix} q_{1,1} & q_{1,2} & \cdots & q_{1,3N} \\ q_{2,1} & q_{2,2} & \cdots & q_{2,3N} \end{pmatrix}.$$

The circles and crosses in Figure 2.7 are the Gummel and Newton iterates u^i respectively, obtained by projection with P:

$$u_2^i = Pu^i \in \mathbb{R}^2.$$

The background color is achieved by sampling the two dimensional area with points $x_2 \in [-7.5, -5] \times [-2, 1]$ and mapping them to the values

$$\log \|F(P^T x_2)\|^2.$$

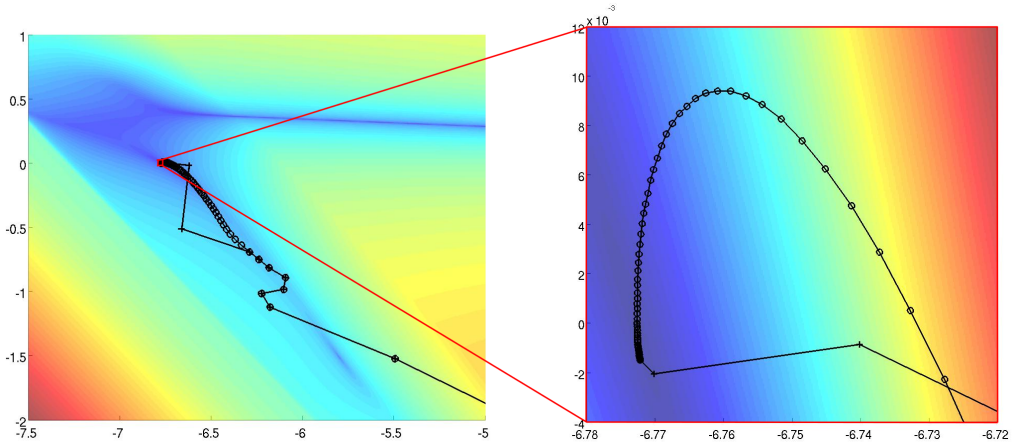

Figure 2.7: Projected Gummel and Newton paths with zoom-in close to the solution.

2.2.5 Contraction based damping strategy

Optimization algorithms are not restricted on always taking physically reasonable parameter values. However we assume, that the limit of the optimization is physically reasonable. On the other hand we allow the path, i.e. the iterates the optimization procedure produces, to lie in infeasible regions. For values lying in those regions we want that the simulation converges and that information is given back about how to proceed . In this sense, we have to robustify our method against such infeasible path methods. For example, if we take the configuration of Table 2.6, with a relatively high $\sigma = 0.21eV$, we see that neither Gummel nor Newton's method does converge, see Figure 2.8. To achieve convergence the method has to be damped. Damping

V	L	T	μ_0	σ	N_t	E_{cathode}	E_{anode}	c_0
3	100	300	$4.5 \cdot 10^{-6}$	0.21	$2 \cdot 10^{27}$	0.0	0.0	0.42

Table 2.6: Parameter configuration

means in our context to find a damping parameter α^{i+1} such that a new iterate is computed by

$$\tilde{u}^{i+1} := u^i + \alpha^{i+1}\, \delta u^{i+1}.$$

The old iterate is u^i and the old the step is calculated by

$$\delta u^{i+1} = u^{i+1} - u^i,$$

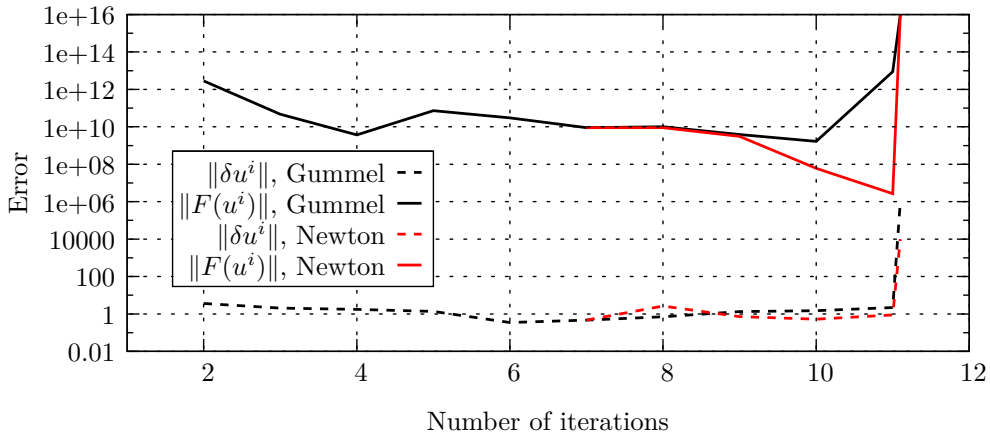

Figure 2.8: Failure of Gummel and Newton method for extreme configuration.

cf. Algorithm 2. Finding "the right" merit function and performing a line search is one possibility to get a damping parameter. But with the bad experience we have made with line searches, cf. Section 2.2.1, we rather consider a different approach. We introduce a contraction based damping strategy by adapting the idea of the restrictive monotonicity test (RMT), cf. Bock et al. [17], which does not try to minimize the classical merit function

$$\frac{1}{2}\|F\|^2$$

but rather tries to reduce the step lengths to get contracting steps. For Newton's method this leads to the *natural level function*. In our case, we just define the damping factor by

$$\alpha^{i+1} := \min\left\{\max\left\{(1-\varepsilon)\frac{\|\delta u^i\|_2}{\|\delta u^{i+1}\|_2}, \alpha_{\min}\right\}, 1\right\},$$

dependent on parameters ε and $\alpha_{\min}$. With the $\alpha_{\min}$ it is guaranteed, that the steps do not get too small and the switch in (2.16) still makes sense. In experiments we have found satisfactory values for $\alpha_{\min}$ around 10^{-4}. We observe successive behavior of Gummel's algorithm, if the steps are only slightly non-contracting. This is why we insert the parameter ε for which we suggest values around 10^{-2}. The successive damping is compared to the extreme configuration case of Figure 2.8 in Figure 2.9. In Figure 2.10 we show that our method provides converged solutions for a whole area of control parameters. A box of 100 times 100 points of temperature and length values is sampled. We set the maximum number of iterations to 660 and assign a dark red color to it. No simulation that converged reached the maximum number of iterations in Figure 2.10. So only diverged solutions correspond to the dark red pixels. One

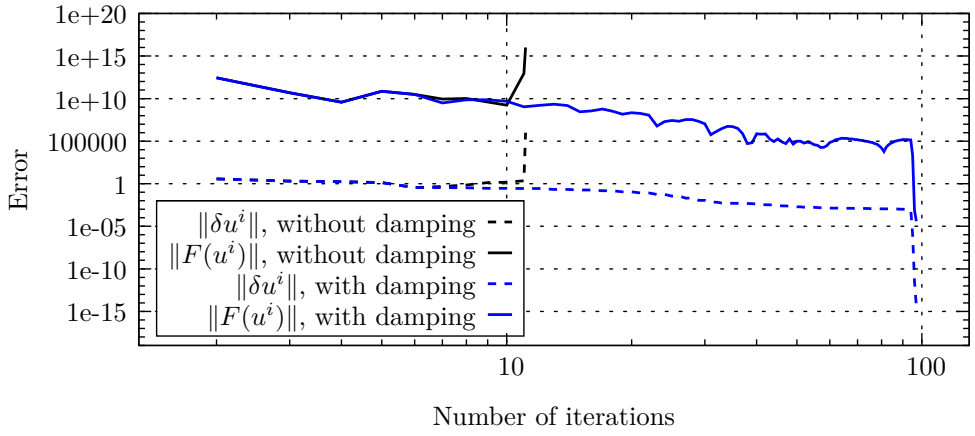

Figure 2.9: Gummel damping with switching to Newton compared Figure 2.8.

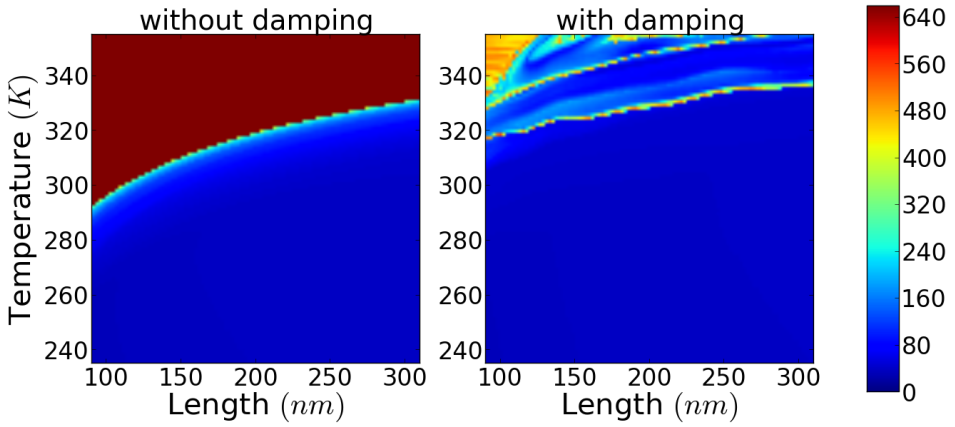

Figure 2.10: Comparison of Gummel convergence behavior for a sampled control parameter region with and without the contraction based damping strategy.

can imagine, that an optimization algorithm would follow a path through the dark red domain, where the method without damping did not converge. In this sense the solution method is robustified against infeasible path methods. Our method now is satisfactory robust for all applications under consideration.

Throughout the section we used 1D simulations, but our solution method consisting of Gummel's method with the g_3 stabilization term and the damping strategy together with Newton's method are independent of the dimension. At least up to minor changes of the heuristic damping parameters ε, $\alpha_{\min}$, and the switching point to Newton's method. The system (1.12) is already formulated for dimensions up to three and we are left with choosing an adequate discretization.

2.3 Finite element ansatz

In this section we want show how to use the simulation method presented in the previous section to simulate 2D problems based on the equations (1.12). We apply the finite element method (FEM), which is superior in complex geometries and does allow a profound mathematical analysis. We use *deal.ii*, cf. [6], a FEM library, which has gained great impact in the community of scientific computation as a research software. For an introduction to FEM calculus see e.g. Braess [21] or Grossmann [46]. We start with a regular, quadrilateral triangulation $\mathcal{T}$ of Ω consisting of elements T. We want to use isoparametric bilinear finite elements and denote the underlying polynomial space with

$$Q_1(T) = \operatorname{span}\{1, x_1, x_2, x_1x_2\}.$$

The bilinear elements have their support points in corners of the cells T. We take an H^1-conform finite element ansatz

$$\begin{aligned} V_h = \{&\varphi_h \in H^1(\Omega) : \varphi_{h|_T} \in Q_1(T), T \in \mathcal{T}, \varphi_h \text{ continuous in corners of } T \text{ and} \\ &\varphi_h = 0 \text{ on } \Gamma_{\text{cathode}} \cup \Gamma_{\text{anode}}\}. \end{aligned}$$

for the state charge density n, the electric potential ϕ and the quasi electrochemical potential η. We recall the partitioning of the boundary, cf. Section 1.2.4,

$$\partial\Omega = \Gamma_{\text{cathode}} \dot\cup \Gamma_{\text{anode}} \dot\cup \Gamma_n.$$

Only on that parts of the boundary where Dirichlet-type boundary conditions are imposed, Γ_{cathode} and Γ_{anode}, the ansatz functions φ_h are set to zero. On the part Γ_n Neumann-type boundary conditions are imposed. Our equations (1.12) in weak form lead to the problem:
Find $(\phi_h, n_h, \eta_h) \in u^\partial + V_h^3$, such that

$$\begin{aligned}
&\lambda^2 \int_\Omega \nabla\phi_h \cdot \nabla\varphi_h \,\mathrm{d}x + \int_\Omega n_h\varphi_h \,\mathrm{d}x = 0 && \text{for all } \varphi_h \in V_h \\
&\int_\Omega \mu(\phi_h, n_h)\Big(n_h\nabla\phi_h - \nu\, g_3(n_h, \eta_h)\,\nabla n_h\Big) \cdot \nabla\varphi_h \,\mathrm{d}x = 0 && \text{for all } \varphi_h \in V_h, \\
&\int_\Omega \big(n_h - G(\eta_h)\big)\,\varphi_h \,\mathrm{d}x = 0 && \text{for all } \varphi_h \in V_h.
\end{aligned} \tag{2.17}$$

u^∂ is assumed to be a function in $H^1(\Omega)$ which trace on the boundary coincides with the boundary data of ϕ and n. With N the dimension of V_h and the nodal basis $\{\varphi_h^1, \ldots, \varphi_h^N\}$ the solutions have the representation

$$\phi_h = \sum_{j=1}^N \phi_j\varphi_h^j, \qquad n_h = \sum_{j=1}^N n_j\varphi_h^j \qquad \text{and} \qquad \eta_h = \sum_{j=1}^N \eta_j\varphi_h^j.$$

We insert these representations into our system and test with all basis functions φ_h^i $i = 1, \ldots, N$. The differential operators ∇ and $\nabla\cdot$ act only on the space dependent ansatz functions φ_h^i, for which the derivatives are known exactly. Dirichlet-type boundary conditions are applied by manipulation of the system matrix and the right hand side. The degrees of freedom on the boundary are removed and the solution is set to the applied value. For homogenous Neumann-type boundary conditions nothing has to be done, because they are imposed naturally via the weak formulation in (2.17). We apply the extended Gummel method with the contraction based damping strategy as the globalization scheme for Newton's method here as well. However the equations in the Gummel steps in (2) are weakly formulated in this case.

2.3.1 Cathode attached self-assembled nano-chains – 2D simulation

We conclude this chapter with a simulation study to evince that our method can help solving 2D problems for a relevant physical example. Zhao et al. [97] showed that the molecules in organic materials can assemble nano-chains connected with H-bonds. In such fibers electrons are transported very rapidly. We want to simulate

the case, where fibers tie on the injection electrode building a spatially inhomogeneous boundary. We consider a simple mathematical model by taking the unit square $(0,1)^2$ and cut out a slit $(0,1/2]$ representing a nano-chain of molecules. Thus our domain is $\Omega = (0,1)^2 \setminus (0,1/2]$, see also Figure 2.11. In comparison to the thickness of the device,

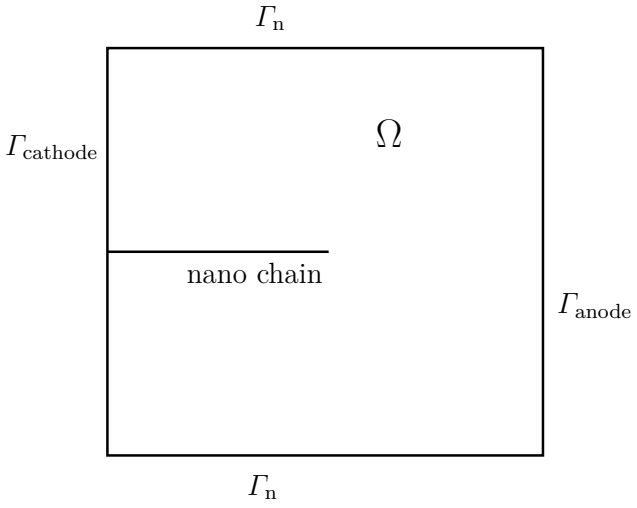

Figure 2.11: Domain and boundary description.

the molecule chain is almost infinitely thin. We therefore model it as a simple line. In 1D we have used the Scharfetter-Gummel scheme for upwind stabilization. There are extensions to 2D of the Scharfetter-Gummel scheme, cf. Selberherr [85]. Similar properties has the finite volume scheme of Bank et al. [7] and the Markowich-Zlámal finite element [65]. With the software *deal.ii* at hand which offers techniques for local grid refinement we rather stick to bilinear elements and resolve the boundary layers with locally refined grids. We start with a pre-refined grid based on the knowledge, that huge gradients occur near the electrodes (and the nano-chain here). The grid is given in Figure 2.12 and has 22750 cells corresponding to 73023 degrees of freedom for the bilinear element. On the grid appear hanging nodes, i.e. nodes on the edge of coarser cells to finer cells. To guarantee the continuity of the solution on these nodes too, constraints are added to the degrees of freedom corresponding to the hanging nodes. Similar to applying Dirichlet-type boundary conditions the constrained degrees of freedom are eliminated from the system and the appropriate values are distributed to the unconstrained degrees of freedom. We simulate with a configuration given in Table 2.7. For the linear algebra, we use the sparse direct solver of *UMFPACK*, cf. [26]. After each Gummel step, i.e. solving all three equations sequentially, we refine

V	L	T	μ_0	σ	N_t	E_{cathode}	E_{anode}	c_0
1	100	300	$22 \cdot 10^{-6}$	0.14	$2 \cdot 10^{26}$	0.0	0.0	0.42

Table 2.7: Parameter configuration

our mesh based on the new solution obtained. The refinement is done with the Kelly error indicator [55]. It approximates the error per cell by integrating over the jump of the gradient of the solution along the faces of each cell. One can see, that close to the electrodes and the nano-chain respectively, where the density has huge gradients, the mesh is strongly refined. We follow the strategy to refine a fixed fraction of the cells, namely 10%. The refined mesh is displayed in Figure 2.13 and has 228058 cells corresponding to 703164 degrees of freedom. With the Kelly error indicator we use a

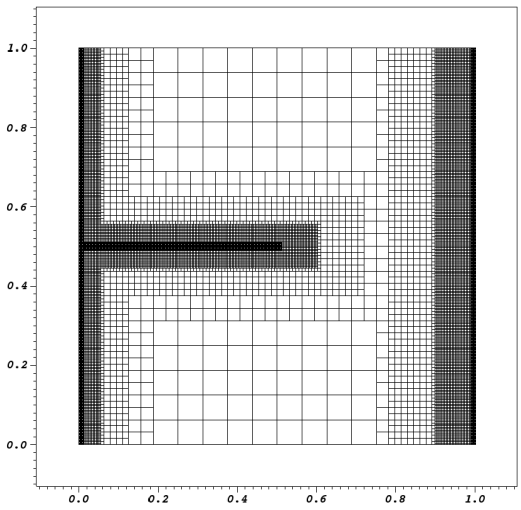

Figure 2.12: Starting grid with refined cells near the electrodes and nano-chain.

rather simple criterion for adaptive refinement. There are several works for "energy norm" based adaptive mesh refinement. See for example the surveys of Ainsworth and Oden [1], and Babuška and Strouboulis [5]. "Goal-oriented" error estimation with respect to a certain functional of interest goes back to Eriksson et al. [34]. In

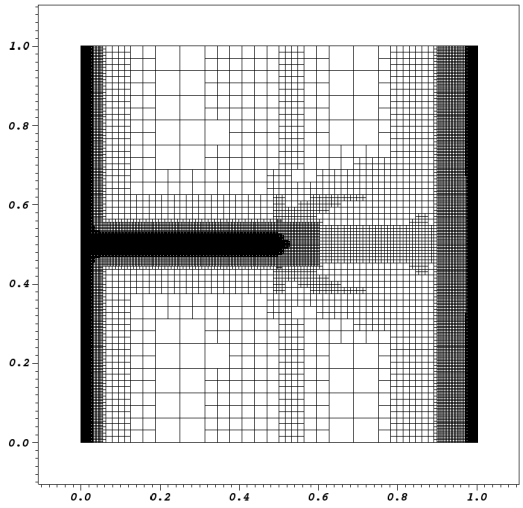

Figure 2.13: Resulting grid, adaptively refined.

our example the functional could be the current flow over the anode contact

$$\int_{\Gamma_{\text{anode}}} n \cdot j \, \mathrm{d}s.$$

Becker and Rannacher [9], [10] introduce the Dual Weighted Residual (DWR) method. We also refer to the papers of Schmich and Vexler [81] and Meidner and Vexler [66], who treat parabolic optimal control problems with adjoint based derivative computation.

The solutions for electron density n, electric potential ϕ and quasi electrochemical potential are shown in Figure 2.14. The nano-chain forms an inhomogeneity in the y-direction. The effective length of the device is reduced for electrons leaving the top of the chain at $x = (1/2, 1/2)$.

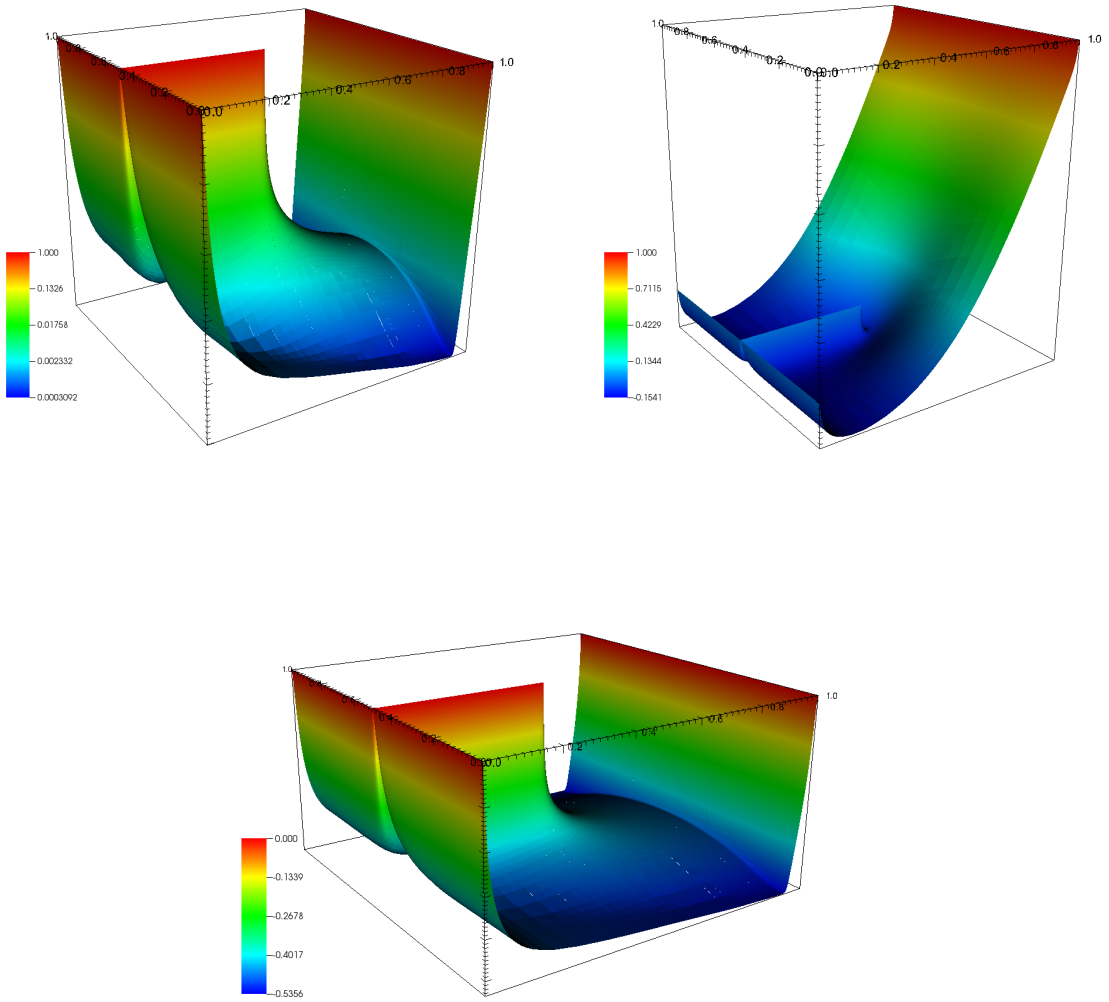

Figure 2.14: Electron density, electric potential, and quasi electrochemical potential of 2D simulation.

3 Parameter estimation

One of the most common application for model based optimization is the parameter estimation problem, also called parameter identification problem. When it comes to modeling physical processes, the underlying principles might be well understood but lack exact parameter values, which might not be measurable. One wants to determine parameters by fitting a model to measurement values. For given measurements z_i, $i = 1, \dots, M$ and model responses h_i, $i = 1, \dots, M$ that means to adjust parameters $p \in \mathbb{R}^{N_p}$ such that the distance

$$d\left((h_i(p))_{i=1}^M, (z_i)_{i=1}^M\right)$$

is minimized. In our case the functions h_i are defined by

$$h_i(p) := h(u_i(p), p)$$

where the states u_i with values in $\mathbb{R}^{3N}$ are determined by solving the model equations, cf. (2.11),

$$F_i(u_i(p), p) = 0. \tag{3.1}$$

We recall that $F_i : \mathbb{R}^{3N} \times \mathbb{R}^{N_p} \to \mathbb{R}^{3N}$, cf. the previous Chapter 2. With the index i of F we mean that the configuration, e.g. the control parameters, are the same as in the experimental setup for obtaining z_i. We consider a reduced parameter estimation problem, i.e. in each step of an optimization algorithm we solve the model equations (3.1) up to a given tolerance. If we would solve the entire optimization problem at once, we would only approximately solve the model equations. With regard to the ill-conditioning of our problems, cf. Section 2.2.1, this is not appropriate. The output of the experiments, i.e. the experimental data $z := (z_i)_{i=1}^M$ is physically spoken an observation, which is always afflicted with a measurement error. By assuming a statistical distribution of the error, the resulting parameters are random variables. To quantify the randomness, we introduce the variance-covariance matrix, which quantifies the uncertainty of the parameters, cf. the next Chapter 4. We start this chapter by giving a statistical derivation of the parameter estimation problem followed by an overview of the Gauss-Newton method for solving the computational parameter estimation problem. In this chapter we are not presenting any calculations but do use the solution method for the sequential experimental design, cf. Section 4.6.2. We also introduce automatic differentiation as the technical concept we use for the derivative

computation. The derivatives with respect to the parameters are used for optimum experimental design, too.

3.1 Statistical foundations

In this section, we derive the parameter estimation problem and show how to compute the variance-covariance matrix. For the fundamental statistical details, we refer to Seber et al. [84]. Similar approaches like our derivation are made in [91], [16], [59] and [15]. Let M measurements z_i be given and denote with $h(u_i(p^*), p^*)$, $i = 1, \ldots, M$, a measurement function h evaluated at true parameters p^*. The measurement errors

$$\varepsilon_i := z_i - h(u_i(p^*), p^*) \qquad i = 1, \ldots, M \tag{3.2}$$

are assumed to be normally distributed

$$\varepsilon_i \sim \mathcal{N}(0, s_i^2) \qquad i = 1, \ldots, M. \tag{3.3}$$

In estimation theory, one searches for an adequate estimate $\hat{p}$ for the true parameters p^*. For such an estimate, we assume that

$$\hat{p}(\varepsilon) \to p^* \qquad \text{when} \qquad \|\varepsilon\|_2 \to 0.$$

The measurement errors ε_i are concatenated to the vector $\varepsilon \in \mathbb{R}^M$. If we expand $\hat{p}(\varepsilon)$ in a Taylor series, we get

$$\hat{p}(\varepsilon) = p^* + \left.\frac{\partial p^*}{\partial \varepsilon}\right|_{\varepsilon=0} \varepsilon + O(\|\varepsilon\|^2). \tag{3.4}$$

Thus $\hat{p}$ is normally distributed up to first order, because ε is. One obtains for the mean in first order approximation

$$\mathbb{E}[\hat{p}] = p^* + \frac{\partial p^*}{\partial \varepsilon} \underbrace{\mathbb{E}[\varepsilon]}_{=0} = p^*. \tag{3.5}$$

We extend the assumption of ε_i to be distributed normally to all parameters p in a neighborhood of the true parameters p^*. The probability density function for ε_i is

$$f_p(\varepsilon_i) = \frac{1}{\sqrt{2\pi s_i^2}} \exp\left(-\frac{(z_i - h(u_i(p), p))^2}{2 s_i^2}\right) \qquad i = 1, \ldots, M.$$

For measurement realizations z_i, $i = 1, \ldots, M$, and corresponding errors $\varepsilon = (\varepsilon_1, \ldots, \varepsilon_M)$ the *likelihood function* of the parameters p is

$$L(p|\varepsilon) = \prod_{i=1}^{M} f_p(\varepsilon_i).$$

3.1.1 Parameter estimation problem

The method of maximum likelihood is to maximize the likelihood function $L(p|\varepsilon)$ over the parameters p to find the most likely parameters $\hat{p}$, given measurements ε.

$$\begin{aligned}
\hat{p} &= \operatorname{argmax}_{p \in \mathbb{R}^{N_p}} L(p|\varepsilon) \\
&= \operatorname{argmax}_{p \in \mathbb{R}^{N_p}} \log L(p|\varepsilon) \\
&= \operatorname{argmax}_{p \in \mathbb{R}^{N_p}} \log \prod_{i=1}^{M} f_p(\varepsilon_i) \\
&= \operatorname{argmax}_{p \in \mathbb{R}^{N_p}} \sum_{i=1}^{M} \log f_p(\varepsilon_i) \\
&= \operatorname{argmax}_{p \in \mathbb{R}^{N_p}} -\frac{1}{2} \sum_{i=1}^{M} \frac{(z_i - h(u_i(p), p))^2}{s_i^2} + \underbrace{\sum_{i=1}^{M} \frac{1}{\sqrt{2\pi s_i^2}}}_{\text{independent of } p} \\
&= \operatorname{argmin}_{p \in \mathbb{R}^{N_p}} \frac{1}{2} \sum_{i=1}^{M} \frac{(z_i - h(u_i(p), p))^2}{s_i^2}.
\end{aligned}$$

This is a least squares estimator, weighted with the variances s_i^2. We define the residuals

$$R(u_i(p), p, \varepsilon_i) := \frac{z_i - h(u_i(p), p)}{s_i} = \frac{\varepsilon_i + h(u_i(p^*), p^*) - h(u_i(p), p)}{s_i} \qquad i = 1, \ldots, M$$

and denote the vector of residuals with

$$R(u(p), p, \varepsilon) := \left(R(u_i(p), p, \varepsilon_i)\right)_{i=1}^{M} \tag{3.6}$$

dependent on $u(p) := (u_1(p), \ldots, u_M(p))$ and $\varepsilon = (\varepsilon_i)_{i=1}^{M}$. We rewrite the resulting unconstrained optimization problem as

$$\min_p \frac{1}{2} \left\| R(u(p), p, \varepsilon) \right\|^2, \tag{3.7}$$

For fixed parameters p the states u_i are obtained by solving the model equations

$$F_i(u_i(p), p) = 0, \quad i = 1, \dots, M.$$

The optimality conditions, namely the KKT conditions for (3.7) are

$$G(p, \varepsilon) := J(u(p), p)^T R(u(p), p, \varepsilon) = 0. \tag{3.8}$$

With the same abbreviation used in (3.6) we denote with $J(u(p), p) \in \mathbb{R}^{M \times N_p}$ the Jacobian with entries

$$J(u(p), p)_{ij} := \frac{dR}{dp_j}(u_i(p), p, \varepsilon_i) = -\frac{1}{s_i}\frac{dh}{dp_j}(u_i(p), p). \tag{3.9}$$

Assuming enough regularity we can apply the implicit function theorem to G and obtain for the true parameters $p^* = p(0)$:

$$\begin{aligned} & \frac{\partial G}{\partial p}(p^*, 0) \left.\frac{\partial p}{\partial \varepsilon}\right|_{\varepsilon=0} = -\frac{\partial G}{\partial \varepsilon}(p^*, 0) \\ \iff \quad & J^T(u(p^*), p^*) J(u(p^*), p^*) \left.\frac{\partial p}{\partial \varepsilon}\right|_{\varepsilon=0} = -J^T(u(p^*), p^*) \frac{\partial R}{\partial \varepsilon}(u(p^*), p^*, 0). \end{aligned} \tag{3.10}$$

Note, that the Jacobian J does not depend on the measurement errors ε explicitly and the residuals R vanish at $\varepsilon = 0$

$$R(u(p^*), p^*, 0) = 0.$$

We compute the variance-covariance matrix of our estimates $\hat{p}$ using (3.4) and (3.5) in first order approximation

$$\begin{aligned} C := \mathbb{E}[(\hat{p} - p^*)(\hat{p} - p^*)^T] &= \mathbb{E}\left[\left(\left.\frac{\partial p^*}{\partial \varepsilon}\right|_{\varepsilon=0} \varepsilon \right) \left(\left.\frac{\partial p^*}{\partial \varepsilon}\right|_{\varepsilon=0} \varepsilon \right)^T \right] \\ &= \left.\frac{\partial p^*}{\partial \varepsilon}\right|_{\varepsilon=0} \underbrace{\mathbb{E}[\varepsilon \varepsilon^T]}_{=\mathrm{diag}(s_i^2, i=1,\dots,M)} \left.\frac{\partial p^*}{\partial \varepsilon}\right|_{\varepsilon=0}^T \\ &= \left(J^T J\right)^{-1} J^T J \left(J^T J\right)^{-1} = \left(J^T J\right)^{-1}. \end{aligned} \tag{3.11}$$

The arguments of the Jacobian J are neglected for reasons of clarity. In the second last sept we used (3.10) and exploited that

$$\frac{\partial R_i}{\partial \varepsilon_j}(u(p^*), p^*, 0) = \delta_{ij}\frac{1}{s_i}.$$

3.1.2 Confidence region

A nonlinear confidence region for the treated case is given by

$$G_N(\alpha, p) := \{p \in \mathbb{R}^{N_p} : \|R(u(p), p, \varepsilon)\|_2^2 - \|R(u(p^*), p^*, 0)\|_2^2 \leq \gamma^2(\alpha)\},$$

where $\gamma^2(\alpha)$ is the quantile of the $\chi^2_{N_p}(1-\alpha)$-distribution with error probability α and N_p degrees of freedom. The bound is chosen in such a way, that a parameter, distributed normally, with mean p^* and variance-covariance matrix $C = \left(J^T J\right)^{-1}$ lies in the region with a probability $1-\alpha$. For the later purpose of computing the confidence regions, we also introduce the linear confidence region

$$G_L(\alpha, p) := \{p \in \mathbb{R}^{N_p} : \|R(u(p^*), p^*, 0) + J(u(p^*), p^*)(p-p^*)\|_2^2 - \|R(u(p^*), p^*, 0)\|_2^2 \leq \gamma^2(\alpha)\}.$$

With the fact that $R(u(p^*), p^*, 0)$ vanishes it follows immediately that

$$G_L(\alpha, p) = \{p \in \mathbb{R}^{N_p} : (p-p^*)^T (J^T J)(p-p^*) \leq \gamma^2(\alpha)\}. \tag{3.12}$$

Because the real parameters p^* are unknown, we compute the confidence region with the estimate returned by the parameter estimation $\hat{p}$. Useful estimates for the confidence intervals are given by the following theorem.

Theorem 3.1.1. *The linearized confidence region lies in a cuboid:*

$$G_L(\alpha, p) \subseteq [p_1 - \theta_1, p_1 + \theta_1] \times \cdots \times [p_{N_p} - \theta_{N_p}, p_{N_p} + \theta_{N_p}]$$

with

$$\theta_i := \gamma(\alpha)\sqrt{C_{ii}}, \quad i = 1, \ldots, N_p. \tag{3.13}$$

Proof. The proof can be found in Bock [15]. □

We rewrite the parameter estimation problem which we derived in this section:

$$\begin{aligned} \min_{p} \quad & \frac{1}{2} \|R(u(p), p, \varepsilon)\|_2^2, \\ \text{where} \quad & F_i(u_i(p), p) = 0, \quad i = 1, \ldots, M. \end{aligned} \tag{3.14}$$

Remark 3.1.2. We have linearized the confidence region and the objective function. The variance-covariance matrix is evaluated at the parameter estimate instead of the real parameters. For enough regularity and not too nonlinear problems, this is appropriate, according to Bock [15].

3.2 Gauss-Newton method

In this section we deal with the numerical solution of the parameter estimation problem (3.14) although we do not show computational results. We solve the least-squares problems with the *Gauss-Newton* algorithm where "Gauss" stands for solving regression problems and "Newton" for solving linearized problems. This method has the advantage that it only converges to statistically reasonable parameters, cf. κ-theory of Bock [15]. We start with an initial value for the parameters p^0 and solve in every iteration i the linearized unconstrained parameter estimation problem

$$\min_{\delta p} \|R(u(p^i), p^i, \varepsilon) + J(u(p^i), p^i)\delta p\|_2^2.$$

If $J^T J$ is positive definite, these partial problems are solvable with the solution

$$\delta p^i = -\left(J^T J\right)^{-1} J^T R(u(p^i), p^i, \varepsilon).$$

With

$$M = \left(J^T J\right)^{-1}$$

this method is a Newton-type method for solving

$$J^T R = 0,$$

cf. Section 2.2.4. The local contraction Theorem 2.2.2 guarantees local convergence with

$$\|\delta p^{k+1}\| \leq \kappa \|\delta p^k\| + \frac{\omega}{2} \|\delta p^k\|^2.$$

For a globalization of the convergence the next iterate is computed by

$$p^{i+1} = p^i + \alpha^i \delta p^i$$

with a damping parameter α^i, which can be determined by the RMT for example, see for the details Bock [15]. The iteration is stopped when e.g. $\|\delta p^i\|_2$ falls below a sufficient small error tolerance. In each step we also solve

$$F_j(u_j(p^i), p^i) = 0, \quad j = 1, \ldots, M$$

with the solution method presented in Chapter 2.

3.3 Computing the Jacobian

In this section we show how to compute the Jacobian, defined in (3.9), required for the parameter estimation problem and the later purpose of optimum experimental design. We need derivatives of the model response h and of our model equations F w.r.t. states u and parameters p

$$\partial_u h, \quad \partial_p h, \quad \partial_u F, \quad \partial_p F.$$

In anticipation of the optimum experimental design problems, where higher order order derivatives are involved, we choose automatic differentiation (AD) as the method to compute the derivatives. AD has the two main advantages compared with symbolic differentiation or using finite differences:

i) The evaluation is done efficiently, i.e. already computed expressions are not evaluated twice.

ii) No numerical truncation error occurs.

3.3.1 Automatic differentiation

We follow Griewank [44] for a brief introduction to AD. Therefor we consider a continuously differentiable function f defined on a domain $D \subset \mathbb{R}^n$

$$\begin{array}{rccc} f: & D & \to & \mathbb{R}^m \\ & x & \mapsto & y. \end{array} \tag{3.15}$$

We assume that f can be decomposed in a sequence of *elemental functions* $(\varphi_i)_{i=1,\dots,l}$. The φ_i are basic arithmetical operations like addition, subtraction, multiplication, division, or elementary function calls like exp(.), log(.), $\sqrt{.}$. According to Griewank the evaluation of f at an argument x can be represented in the general procedure given in the three-part form in Table 3.1. With $v_{j\prec i}$ we denote only those v_j which

Initialization	$v_{i-n} := x_i$	$i = 1, \dots, n$
Computation	$v_i := \varphi_i(v_{j\prec i})$	$i = 1, \dots, l$
Result	$y_{m-i} := v_{l-i}$	$i = m-1, \dots, 0$

Table 3.1: General evaluation procedure.

φ_i depend on for $i < j$. One distinguishes between the *forward mode* and the *reverse mode* for differentiating f via the elementary operations in Table 3.1. The *forward mode* is commonly used for directional derivatives like

$$\dot{y} = \frac{df}{dx}\dot{x} \tag{3.16}$$

with a tangential direction vector $\dot{x} \in \mathbb{R}^n$. The schematic differentiation of Table 3.1 is displayed in Table 3.2. For achieving further efficiency one can save effort in evaluating

Initialization	$v_{i-n} := x_i$ $\dot{v}_{i-n} := \dot{x}_i$	$i = 1, \dots, n$
Computation	$v_i := \varphi_i(v_{j\prec i})$ $\dot{v}_i := \sum_{j\prec i} \frac{\partial \varphi_i}{\partial v_j}\dot{v}_j$	$i = 1, \dots, l$
Result	$y_{m-i} := v_{l-i}$ $\dot{y}_{m-i} := \dot{v}_{l-i}$	$i = m-1, \dots, 0$

Table 3.2: Tangent recursion for the general evaluation procedure.

the derivative and the function at the same time. For the *reverse mode* final results are differentiated w.r.t. intermediate results. It is applied to derivatives given as linear combinations like

$$\overline{x} = \overline{y}\frac{df}{dx} \tag{3.17}$$

with $\overline{y} \in \mathbb{R}^m$. The *reverse mode* requires a forward sweep of the function evaluation like in Table 3.1. The intermediate results are saved and the derivative computation follows the adjoint evaluation procedure of Table 3.3.

Remark 3.3.1. From Griewank [44] we cite some results of the complexity analysis of

Initialization	$\overline{v}_i := 0$	$i = 1-n, \ldots, l-m$
	$\overline{v}_{l-i} := \overline{y}_{m-i}$	$i = 0, \ldots, m-1$
Computation	$\overline{v}_j := \overline{v}_j + \overline{v}_i \frac{\partial \varphi_i}{\partial v_j}$ for all $j \prec i$,	$i = l, \ldots, 1$
Result	$\overline{x}_i := v_{i-n}$	$i = n, \ldots, 1$

Table 3.3: Incremental adjoint recursion.

AD:

i) The evaluation of the derivative of an arbitrary elemental function is a fixed multiple of the evaluation of the elemental function itself, e.g. for the division we have:

$$\left(\frac{a}{b}\right)' = \frac{a' \cdot b - a \cdot b'}{b^2}, \tag{3.18}$$

which is five times more expensive than evaluating simply a/b.

ii) The whole complexity for the computation of f is the sum of all complexities of the elemental functions.

iii) The effort of the *forward mode* grows linearly with the number of tangential directions, i.e. $\dot{x}$ in (3.16).

iv) The effort of the *reverse mode* grows linearly with the number of the adjoint directions, i.e. $\overline{y}$ in (3.17).

We conclude, that the *forward mode* is more sensible, if the number of dependent variables, i.e. m in (3.15), is larger than the number of independent variables, i.e. n. The *reverse mode* is preferable, if n is bigger than m, although more memory consumption is required because of the forward sweep. For the computational implementation of AD there are the two possibilities:

i) *Operator overloading*, implemented in software packages like *ADOL-C* (C/C++) [45], *CppAD* (C/C++) [11], or *Algopy* (Python) [92].

ii) *Source code transformation*, used by the software packages *ADIFOR* (Fortran 77) [12] [14] [13], and *TAPENADE* (C/C++, Fortran 77, Fortran 95) [48].

3.3.2 EGDM/ECDM derivatives

For the parameter estimation problem we need to assemble the whole Jacobian, i.e. differentiating h in every unit direction of $\mathbb{R}^{N_p}$. To determine N_p parameters without

regularization one needs at least N_p measurements. With $M \geq N_p$ we conclude that in general the forward mode of automatic differentiation is appropriate for parameter estimation problems, cf. Remark 3.3.1. Coming back to our problem of a discretized stationary partial differential equation, cf. (1.12), we however observe that using the reverse mode can save effort. For parameters p we have to compute solutions u_i of (1.12) for different configurations corresponding to model responses h_i, $i = 1, \ldots, M$. Hence the complexity has to be regarded separately for every h_i. This changes the argumentation, because now N_p is equal to or greater than one and using the reverse mode is more efficient, cf. Remark 3.3.1.

Remark 3.3.2. Similar considerations are made in Schmidt [82] related to local preaccumulation of Jacobian matrices.

The application of the reverse mode on the computation the derivative of h_i w.r.t. the parameters p results in

$$\frac{dh_i}{dp} = \left(\lambda_i^T \frac{\partial F_i}{\partial p} + \frac{\partial h_i}{\partial p} \right) \qquad \text{for } i = 1, \ldots, M,$$

where $\lambda_i \in \mathbb{R}^{3N}$ are the solutions of the *adjoint equations*

$$\left(\frac{\partial F_i}{\partial u} \right)^T \lambda_i + \left(\frac{\partial h_i}{\partial u} \right)^T = 0, \tag{3.19}$$

see i.a. [50]. With F_i we denote the model equations for different configurations corresponding to h_i.

Remark 3.3.3. In the reverse mode of automatic differentiation the expression $\lambda_i^T \frac{\partial F_i}{\partial p}$ occurring in (3.3.2) is computed efficiently and not as a product of a vector with a matrix.

Remark 3.3.4. Because the equations (3.19) are linear, we do not need to solve them in every Gummel and Newton step respectively but just in the solution for one time. If one is interested in the derivatives at intermediate iterates, Gummel's and Newton's method have to be differentiated. We refer to Christianson [25] for further investigations.

The equations (3.19) have a similar shape as the linear subproblems of Newton's method, cf. (2.14),

$$F'(u^i)\, \delta u^i = -F(u^i). \tag{3.20}$$

We use direct methods to solve these subproblems, e.g. the LU decomposition

$$\left(F'(u^i) =\right) \frac{\partial F_i}{\partial u} = LU,$$

with a lower triangular matrix L and an upper triangular matrix U. Equation (3.20) transforms into the system

$$\begin{aligned} Ly &= -F(u^i), \\ U\delta u^i &= y, \end{aligned}$$

which is solved by forward and back substitution. If we save the LU decomposition in the last step of Newton's method, we can reuse it for solving the adjoint equations, too, because (3.19) transforms to the system

$$\begin{aligned} U^T y &= \left(\frac{\partial h_i}{\partial u}\right)^T, \\ L^T \lambda_i &= y. \end{aligned}$$

Since L and U are triangular matrices, L^T and U^T are triangular.

Applying the forward mode instead of the adjoint mode to calculate the derivative of h_i w.r.t. the parameters p results in

$$\frac{dh_i}{dp} = \left(\frac{\partial h_i}{\partial u}\, u_{p,i} + \frac{\partial h_i}{\partial p}\right)$$

where $u_{p,i} \in \mathbb{R}^{N \times N_p}$, $i = 1, \ldots, M$, are matrices obtained by solving the *tangential equations*

$$\frac{\partial F_i}{\partial u}\, u_{p,i} + \frac{\partial F_i}{\partial p} = 0. \tag{3.21}$$

These equations are also called variational differential equations.

4 Optimum experimental design

In the last chapter, we have introduced the variance-covariance matrix C, see (3.11), to parameterize the linearized confidence region in the parameter space. In nonlinear models, the Jacobian, see (3.9), often depends on control parameters $q \in \mathbb{R}^{N_q}$. The control parameters are quantities which can be controlled, e.g. the temperature at which the measurements are taken. By varying the control parameters, one can plan experiments whose measurement values allow a more significant estimation of the parameters. Optimum experimental design tries to find optimal control parameters which allow the most significant identification of the parameters. In principle, we follow the approaches of Lohmann [60] and Bauer et al. [8]. For the computation we use the software package *VPLAN* developed by Körkel, cf. [59], which offers interfaces to *ADIFOR* for automatic differentiation, *PARFIT* for parameter estimation and *SNOPT* for solving optimization problems with SQP methods. The strength of *VPLAN* lies in the efficient exploitation of multi-experiment structures, which is crucial for our application problems and the efficient evaluation of all required derivatives. The chapter starts with stating the optimum experimental design problem we consider in this work. We introduce an SQP method on the reduced problem as our solution method for the optimum experimental design problem. As in the chapter before we show how to compute the gradient of the objective with automatic differentiation. Numerical results are computed for the modern organic semi-conducting materials NRS-PPV and α-NPD with both the EGDM and the ECDM. We close with a robustness study w.r.t. varying parameters in a sequential experimental design for NRS-PPV.

4.1 Criteria

The objective function of the optimum experimental design problem is called "criterion". It is a function which maps the variance-covariance matrix to a scalar function. Statistically spoken, an information function ϕ is applied to the variance-covariance matrix. The classical criteria, cf. [78], are

i) A-criterion:

$$\phi_A(C) = \frac{1}{N_p} \operatorname{tr} C. \tag{4.1}$$

ii) D-criterion:

$$\phi_D(C) = \det(C)^{\frac{1}{N_p}}.$$

iii) E-criterion:

$$\phi_E(C) = \max\{\mu : \mu \text{ eigenvalue of } C\}.$$

iv) M-criterion:

$$\phi_M(C) = \max\{\sqrt{C_{ii}}, i = 1, \ldots, N_p\}.$$

A visualization of the criteria with the confidence ellipsoid can be seen in Figure 4.1.
Remark 4.1.1. The criteria are not invariant regarding possible parameter scaling. If all parameters are of comparable interest, the parameters should be scaled to the same values.

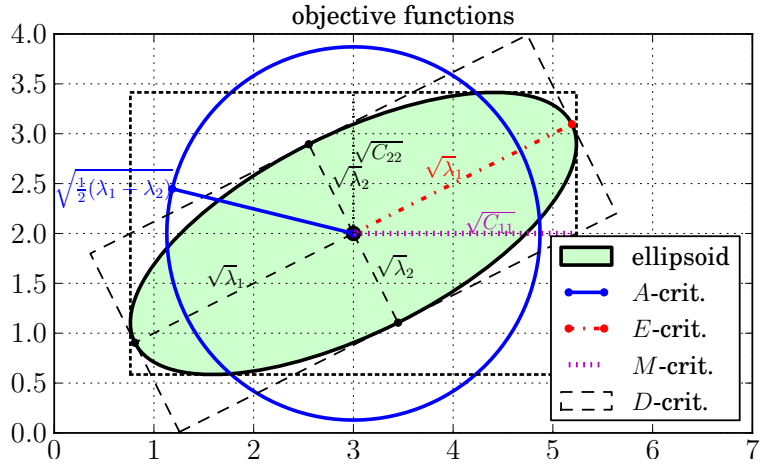

Figure 4.1: Visualization of the optimum experimental design criteria taken from Walter [91].

4.2 Optimum experimental design problem

With ϕ being any of the previous criteria, the objective has the form

$$\phi\left(C\left(\frac{dh}{dp}(u(p,q),p,q)\right)\right) = \phi\left(\lambda(p,q), u(p,q), p, q\right)$$

with the solutions λ of the adjoint equations (3.19) dependent on parameters p and control parameters q, the states u dependent on p and q. We use the same abbreviated notation as in Section 3.1.1 writing the arguments of the objective $\phi(\lambda(p,q), u(p,q), p, q)$ as

$$\lambda(p,q) := (\lambda_1(p,q), \ldots, \lambda_M(p,q)) \quad \text{and} \quad u(p,q) := (u_1(p,q), \ldots, u_M(p,q)).$$

Remark 4.2.1. For evaluating the objective function a parameter set is required. If the parameters are obtained by a parameter estimation, the objective function depends on measurement values indirectly through the estimate.

We keep the parameter dependence in mind, but neglect the argument p in the following. The optimum experimental design problem is stated as a constrained nonlinear optimization problem:

$$\begin{aligned}
\min_q \quad & \phi(\lambda(q), u(q), q) \\
\text{s.t.} \quad & c_i(q) = 0, \qquad i \in \mathcal{E}, \\
& c_i(q) \geq 0, \qquad i \in \mathcal{I}, \\
\text{where} \quad & F_j(u_j(q), q) = 0, \\
& \left(\partial_u F_j(u_j(q), q)\right)^T \lambda_j(q) + \left(\partial_u h_j(u_j(q), q)\right)^T = 0, \\
\text{for} \quad & j = 1, \ldots, M.
\end{aligned} \tag{4.2}$$

$\mathcal{E}$ is the index set of equality constraints and $\mathcal{I}$ the index set of all inequality constraints. The control constraints are of two kinds:

- Equality constraints, i.e. c_i for $i \in \mathcal{E}$: In a multi experiment setup, we want equal starting values for the control parameters, like the length of the device, to be equal in the end of the optimization. We therefor only need linear constraints.
- Inequality constraints, i.e. c_i for $i \in \mathcal{I}$: The ranges of control parameters are bounded due to physical boundaries, e.g. for high temperatures the material breaks down, or experimental doability, e.g. high costs for performing very low temperature experiments. These constraints are linear box constraints.

The dependence of the states u_j and the control parameters q is given by the model equations

$$F_j(u_j(q), q) = 0, \quad j = 1, \ldots, M.$$

Remember that we think of F_i as our discretized system of equations with

$$F_j : \mathbb{R}^{3N} \times \mathbb{R}^{N_q} \to \mathbb{R}^{3N}, \quad u_j : \mathbb{R}^{N_q} \to \mathbb{R}^{3N} \quad \text{and} \quad q \in \mathbb{R}^{N_q},$$

where N_q is the number of control parameters and N the number of discretization points.

4.3 Solving the optimum experimental design problem

We recite the most important results to guarantee the unique existence of a solution of (4.2) following the presentation of Nocedal and Wright [71] for solving constrained nonlinear optimization problem. By assuming continuously differentiable u_j and λ_j w.r.t. q our problem (4.2) can be written in the standard form of nonlinear optimization problems

$$\begin{aligned} \min_q \quad & \phi(q) \\ \text{s.t.} \quad & c_i(q) = 0, \quad i \in \mathcal{E}, \\ & c_i(q) \geq 0, \quad i \in \mathcal{I}, \end{aligned} \tag{4.3}$$

with continuously differentiable functions ϕ and c_i.

Definition 4.3.1. We define the *active set* as

$$\mathcal{A}(q) := \mathcal{E} \cup \{i \in \mathcal{I} : c_i(q) = 0\}.$$

The inequality constraint $i \in \mathcal{I}$ is said to be *active* if $c_i(q) = 0$.

To guarantee that a solution of (4.3) exists, we have to define a condition on the active constraints.

Definition 4.3.2. The linear independence constraint qualification condition (LICQ) holds, if the set

$$\{\nabla c_i(q) : i \in \mathcal{A}(q)\}$$

is linearly independent.

With the *Lagrange function* defined by

$$\mathcal{L}(q, l) = \phi(q) - \sum_{i \in \mathcal{E} \cup \mathcal{I}} l_i c_i(q)$$

with the *Lagrange multiplier* $l = (l_i)_{i \in \mathcal{E} \cup \mathcal{I}}$. We state the first-order necessary conditions.

Theorem 4.3.3. *If q^* is a local solution of (4.3), ϕ and c_i are continuously differentiable, and LICQ holds at q^* then there is a Lagrange multiplier $l^* = (l_i^*)_{i\in\mathcal{E}\cup\mathcal{I}}$ such that the following conditions are satisfied*

$$\begin{aligned} \nabla_q \mathcal{L}(q^*, l^*) &= 0, \\ c_i(q^*) &= 0, \qquad \text{for all } i \in \mathcal{E}, \\ c_i(q^*) &\geq 0, \qquad \text{for all } i \in \mathcal{I}, \\ l_i^* &\geq 0, \qquad \text{for all } i \in \mathcal{I}, \\ l_i^* c_i(q^*) &= 0, \qquad \text{for all } i \in \mathcal{E} \cup \mathcal{I}. \end{aligned} \tag{4.4}$$

The conditions (4.4) are also known as the *Karush-Kuhn-Tucker (KKT) conditions.* With the set of *feasible linear directions*

$$\mathcal{F}(q) := \{d : d^T \nabla c_i(q) = 0, \text{ for all } i \in \mathcal{E} \text{ and } d^T \nabla c_i(q) \geq 0, \text{ for all } i \in \mathcal{A}(q) \cap \mathcal{I}\}$$

and the *critical cone*

$$\mathcal{C}(q^*, l^*) := \{w \in \mathcal{F}(q^*) : \nabla c_i(q^*)^T w = 0, \text{all } i \in \mathcal{A}(q^*) \cap \mathcal{I} \text{ with } l_i^* > 0\}$$

we also give second-order sufficient conditions for twice continuously differentiable functions ϕ and c_i:

Theorem 4.3.4. *Suppose the KKT conditions (4.4) are fulfilled with q^* and l^*. If also*

$$w^T \nabla_{qq}^2 \mathcal{L}(q^*, l^*) w > 0, \quad \text{for all } w \in \mathcal{C}(q^*, l^*), w \neq 0$$

holds, then q^* is a local solution (4.3).

4.3.1 Sequential quadratic programming (SQP)

We solve problem (4.2) with an SQP method on the reduced problem, since our model equations are ill-conditioned, cf. Section 2.2.1 and the argumentation in the introduction of Chapter 3. In Algorithm 3, we give a basic overview of the numerical method. The idea is to solve problem (4.3) iteratively with a sequence of quadratic subproblems and solve the model equations and adjoint equations in every step. When the exact Hessian is taken the method is locally equivalent to Newton's method and therefore converges local quadratically. A popular approximation strategy of the Hessian is the BFGS, named after Broyden, Fletcher, Goldfarb, and Shanno, which

Algorithm 3 SQP method on the reduced problem (4.2).

1: Start with q^0, l^0, H^0. Set $k = 0$.
2: **while** convergence test is not satisfied **do**
3: Solve the model equations

$$F_j(u_j(q^k), q^k) = 0, \quad j = 1, \ldots, M,$$

for $u_j(q^k)$ and solve the adjoint equations

$$\left(\partial_u F_j(u_j(q^k), q^k)\right)^T \lambda_j(q^k) + \left(\partial_u h_j(u_j(q^k), q^k)\right)^T = 0, \quad j = 1, \ldots, M,$$

for $\lambda_j(q^k)$.
4: **if** k > 0 **then**
5: With $\nabla\phi(q^{k-1})$, $\nabla\phi(q^k)$, p^{k-1} and H^{k-1} compute an approximation H^k of the Hessian of the Lagrange function.
6: **end if**
7: Set

$$H^k \approx \nabla^2_{qq}\mathcal{L}(q^k, l^k).$$

8: Solve

$$\begin{aligned} \min_p \quad & \frac{1}{2} p^T H^k p + \nabla\phi(q^k)^T p \\ \text{s.t.} \quad & c_i(p) = 0, \qquad i \in \mathcal{E}, \\ & c_i(p) \geq 0, \qquad i \in \mathcal{I}, \end{aligned}$$

for p^k and $\tilde{l}^k$ (Lagrange multiplier).
9: Find an acceptable step size α^k and define new iterates

$$\begin{aligned} q^{k+1} &:= q^k + \alpha^k\, p^k, \\ l^{k+1} &:= l^k + \alpha^k\, (\tilde{l}^k - l^k). \end{aligned} \tag{4.5}$$

10: $k \leftarrow k + 1$
11: **end while**

is a rank two update formula with superlinearly convergence properties. We use the software package *SNOPT 7.2-9 (Jun 2008)* [43], see also [42], which implements an SQP method with a limited memory BFGS, where past iterates are neglected from time to time, together with an active set method for handling the inequality conditions. For the theory of active set methods we refer to the literature [71]. An alternative to active set methods are the interior penalty methods, which are realized, e.g. in *IPOPT* [95]. For the application of *line search* methods for the globalization, i.e. finding α^k in (4.5), we refer to the literature [71] and [38]. As a stopping criterion one can take the KKT conditions, cf. (4.4).

4.4 Derivatives

With an approximation of the Hessian of the Lagrange function, we are left with computing the gradient of the objective ϕ and the gradient of the functions appearing in the constraints c_i, $i \in \mathcal{E} \cup \mathcal{I}$ of problem (4.2). We take the formulas for the directional derivatives of ϕ from Körkel [59]. A directional derivative is defined by

$$\frac{d\phi}{dx}\delta x := \lim_{h\to 0} \frac{\phi(x + h\delta x) - \phi(x)}{h}.$$

For the criteria of the optimum experimental design problem dependent on the variance-covariance matrix $C \in \mathbb{R}^{N_p \times N_p}$ the derivatives in the direction $\delta C \in \mathbb{R}^{N_p \times N_p}$ are

i) A-criterion:

$$\begin{aligned}\frac{d\phi_A}{dC}\delta C = \frac{1}{N_p}\frac{d\,\mathrm{tr}\,C}{dC}\delta C = \frac{1}{N_p}\sum_{i,j}\frac{d\,\mathrm{tr}\,C}{dC_{ij}}\delta C_{ij} = \frac{1}{N_p}\sum_{i,j,k}\frac{dC_{kk}}{dC_{ij}}\delta C_{ij}\\ = \frac{1}{N_p}\sum_{i,j,k}\delta_{ki}\delta_{kj}\delta C_{ij} = \frac{1}{N_p}\sum_{k}\delta C_{kk} = \frac{1}{N_p}\,\mathrm{tr}\,\delta C.\end{aligned}$$

ii) D-criterion: With

$$\frac{d}{dC}\det(C)\delta C = \sum_{i,j}\det(C)(C^{-1})_{ij}\delta C_{ij}$$

we have

$$\begin{aligned}\frac{d\phi_D}{dC}\delta C &= \frac{d}{dC}\left(\det(C)\right)^{\frac{1}{N_p}}\delta C \\ &= \frac{1}{N_p}\left(\det(C)\right)^{\frac{1}{N_p}}\sum_{i,j}\left(C^{-1}\right)_{ij}\delta C_{ij}.\end{aligned}$$

iii) E-criterion: If the largest eigenvalue is single and its corresponding normalized eigenvector is denoted with z, then, cf. [59],

$$\frac{d\phi_E}{dC}\delta C = \frac{d}{dC}\max\{\mu : \mu \text{ eigenvalue of } C\}\delta C = z^T\delta C z.$$

iv) M-criterion: The problem of minimizing

$$\phi_M(C) = \max\{\sqrt{C_{ii}}, i = 1, \ldots, N_p\}$$

is transformed to the auxiliary problem

$$\begin{aligned}\min \quad & \phi_0 \\ \text{s.t.} \quad & \phi_0 \geq \sqrt{C_{ii}}, \quad i = 1, \ldots, N_p.\end{aligned}$$

The constraints are added to the inequality constraints c_i, $i \in \mathcal{I}$ in (4.2). The derivative is given by

$$\frac{d}{dC}\left(\sqrt{C_{ii}}\right)\delta C = \frac{1}{2\sqrt{C_{ii}}}\delta C.$$

For the derivative of the variance-covariance matrix itself, we need the following lemma.

Lemma 4.4.1. *For a regular matrix $A \in \mathbb{R}^{N_p \times N_p}$ and $\delta A \in \mathbb{R}^{N_p \times N_p}$ it holds*

$$\frac{dA^{-1}}{dA}\delta A = -A^{-1}\delta A A^{-1}.$$

Proof. Define $F : \mathbb{R}^{N_p \times N_p} \times \mathbb{R} \to \mathbb{R}^{N_p \times N_p}$ as

$$F(B, h) := (A + h\delta A)B - I_{N_p \times N_p}.$$

F is continuously differentiable and it holds

i) $F(A^{-1}, 0) = 0$,

ii) $\frac{\partial F}{\partial B}(A^{-1}, 0) = A$ is regular.

By applying the implicit function theorem we end up with a continuously differentiable function B with

i) $B(h) = (A + h\delta A)^{-1}$,

ii) $B'(h) = -\left(\frac{\partial F}{\partial B}(B(h), h)\right)^{-1} \frac{\partial F}{\partial h}(B(h), h) = -(A + h\delta A)^{-1}\delta A\, B(h)$.

Hence it follows

$$\frac{dA^{-1}}{dA}\delta A = \lim_{h\to 0} \frac{B(h) - B(0)}{h} = B'(0) = -A^{-1}\delta A\, A^{-1}.$$

□

With this lemma the derivative of the variance-covariance matrix

$$C = \left(J^T J\right)^{-1}$$

in the direction δJ is

$$\frac{dC}{dJ}\delta J = \frac{d(J^T J)^{-1}}{dJ}\delta J = -(J^T J)^{-1}(\delta J^T J + J^T \delta J)(J^T J)^{-1}.$$

Since the Jacobian is given by

$$J(u(q), q)_{ij} = -\frac{1}{s_i}\frac{dh}{dp_j}(u_i(q), q),$$

cf. (3.9), the gradient of the objective ϕ is assembled by the derivatives

$$\begin{aligned}\frac{d}{dq}\Big(\frac{dh_i}{dp}\Big) &= \frac{d}{dq}\left(\lambda_i^T \partial_p F_i + \partial_p h_i\right) \\ &= \sum_{j=1}^{N} \lambda_{i,j}\partial^2_{qu}F_{i,j}\, u_{q,i} + \partial^2_{pu}h\, u_{q,i} + (\lambda_{q,i})^T \partial_p F_i + \sum_{j=1}^{N} \lambda_{i,j}\partial^2_{qp}F_{i,j},\end{aligned}$$

in unit directions $\delta q = I_{N_q \times N_q}$. The occurring derivatives $u_{q,i}$ are given by the tangential equations

$$\partial_u F_i\, u_{q,i} + \partial_q F_i = 0. \tag{4.6}$$

The sensitivities of second order $\lambda_{q,i}$ are given by second order adjoint equations

$$\sum_{j=1}^{N} \lambda_j \partial^2_{uu} F_{i,j}\, u_{q,i} + \partial^2_{uu} h_i\, u_{q,i} + (\partial_u F_i)^T \lambda_{q,i} + \sum_{j=1}^{N} \lambda_j \partial^2_{qu} F_{i,j} + \partial^2_{qu} h_i = 0, \qquad (4.7)$$

with known λ_i and $u_{q,i}$.
Remark 4.4.2. Note that in (4.7) and (4.6) the matrix $\partial_u F_i$ has to be inverted. Hence only one decomposition is required when using direct methods, cf. Section 3.3.2.
Remark 4.4.3. According to Griewank [44] using the reverse mode twice for second order derivatives (not directionally), is the same as using the reverse mode followed by the forward mode as we have done here.

We compute the derivatives of the model functions

$$\partial_u h,\ \partial_p h,\ \partial_q h,\ \partial^2_{uu} h,\ \partial^2_{qu} h,\ \partial^2_{up} h,\ \partial^2_{qp} h,$$

and

$$\partial_u F,\ \partial_p F,\ \partial_q F,\ \partial^2_{uu} F,\ \partial^2_{qu} F,\ \partial^2_{up} F,\ \partial^2_{qp} F,$$

together with the derivatives of the constraints

$$\nabla c_i$$

directionally with the automatic differentiation tool ADIFOR.

4.5 Application of optimum experimental design to organic semiconductors

Experimenters, cf. [93], proceed in the following way. Devices of different lengths L are produced by evaporating the organic material on a supporter with contacts for the cathode and anode. At different temperatures T, they apply voltages V_{app} and measure the corresponding electric current j.
Definition 4.5.1. One choice of L, T and a series consisting of several applied voltages V_{app} we call one *experiment* subsequently.

To complete the measurement model, we also have to set the standard deviation of the model response j, cf. (3.3). We model the standard deviation as

$$s_i = 0.1 \cdot j_i, \qquad i = 1, \ldots, M$$

i.e. 10% of the measured current j, cf. [93]. We treat two different organic semiconducting materials:

i) A random copolymer poly[4'-(3,7-dimethyloctyloxy)-1,1'-biphenylene-2,5-vinylene] (NRS-PPV) for which Bouhassoune et al. [20] found parameters by fitting current-voltage characteristics with the EGDM and the ECDM, see Figure 4.2 and cf. [74].

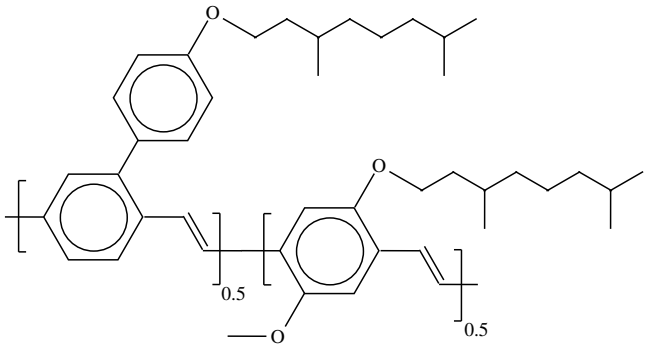

Figure 4.2: NRS-PPV, a random copolymer.

ii) Mensfoort et al. [89] studied EGDM and ECDM parameters for N,N'-bis(1-naphthyl)-N,N'-diphenyl-1,1'-biphenyl-4,4'-diamine (α-NPD), see Figure 4.3.

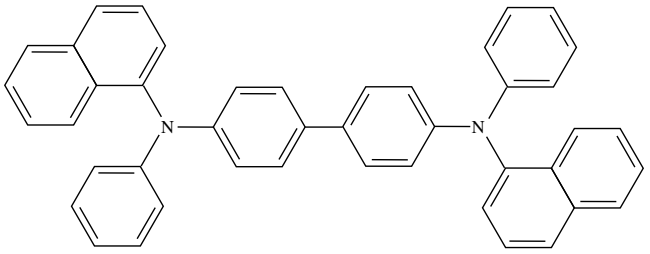

Figure 4.3: α-NPD

4.5.1 NRS-PPV

The parameters Bouhassoune et al. [20] analyzed are

$$\begin{aligned} &i)\ \text{site density } N_t, \\ &ii)\ \text{width of Gaussian distribution } \sigma, \\ &iii)\ \text{zero-temperature mobility } \mu_0, \\ &iv)\ \text{factor } c_0 \text{ occurring in the mobility enhancement term } g_0. \end{aligned} \tag{4.8}$$

They considered both the EGDM and the ECDM. We will compute optimum experimental designs for both models with the parameters they already have identified.

EGDM

Taking their parameter values for the EGDM providing a satisfactory fit of current-voltage characteristics, we take the configuration given in Table 4.1. Bouhassoune et al.

μ_0	σ	N_t	E_{cathode}	E_{anode}	c_0
$2.5 \cdot 10^{-7}$	0.14	$0.171 \cdot 10^{27}$	0.0	1.1	0.44

Table 4.1: Configuration for EGDM simulations of NRS-PPV according to Bouhassoune et al.

took one device of length $L = 560$ and measured the electric current at four different temperatures $K = 233, 252, 272$ and 298 for voltages $V_{\text{app}} = 1, 2, \ldots, 29, 30$. We have recalculated their current-voltage characteristics with our simulation program, cf. Section 2.1.2. The results are shown in Figure 4.4. We observe that taking fewer voltages but take more measurements leads to similar confidence intervals and objective value, cf. Table 4.2, where we took the voltages $V_{\text{app}} = 1, 5, 10, 20, 25, 30$ with weights $w = 5$ instead of $w = 1$. The value of the objective of the optimum experimental design problem is taken for the A-criterion, cf. (4.1). We use this criterion in all our computations. For the optimum experimental design problem, we consider two devices with lengths 500 and 600. The combination of all lengths and temperatures lead to eight experiments according to Definition 4.5.1. We scale all the parameters to one, cf. Remark 4.1.1. The optimization variables are left unscaled, because they are already the same order of magnitude. Note that the unit of L is nm and the unit of T is K, cf. Section 1.3. The whole setup is displayed in Table 4.3.

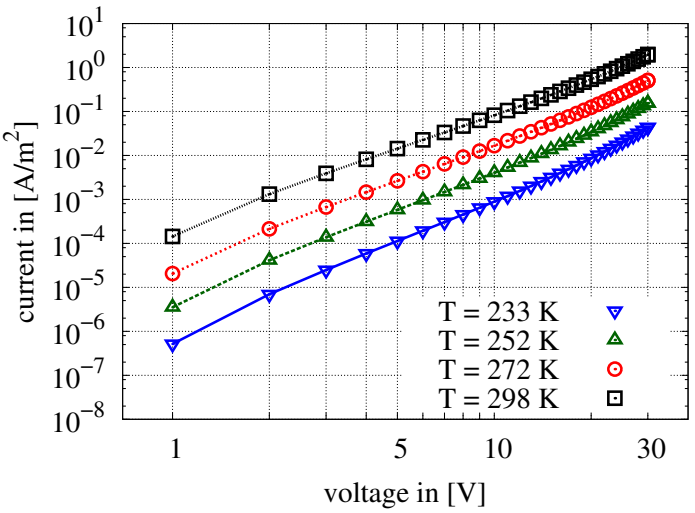

Figure 4.4: NRS-PPV current-voltage characteristics for Bouhassoune parameters computed with the EGDM.

	$M = 30$, $w = 1$	$M = 6$, $w = 5$	error
A-criterion	0.011085	0.011679	0.000593
θ_1/p_1	0.583202	0.603773	0.020571
θ_2/p_2	0.051508	0.054149	0.002641
θ_3/p_3	0.277156	0.272985	0.004171
θ_4/p_4	0.033447	0.035103	0.001656

Table 4.2: Comparison of relative radii of the confidence intervals.

We choose bounds to the lengths, temperatures, applied voltages and measurement

	length L	temperature T	voltages V_{app}	weights w
exp. 1	500	233	1,5,10,20,25,30	5,5,5,5,5,5
exp. 2	500	252	1,5,10,20,25,30	5,5,5,5,5,5
exp. 3	500	272	1,5,10,20,25,30	5,5,5,5,5,5
exp. 4	500	298	1,5,10,20,25,30	5,5,5,5,5,5
exp. 5	600	233	1,5,10,20,25,30	5,5,5,5,5,5
exp. 6	600	252	1,5,10,20,25,30	5,5,5,5,5,5
exp. 7	600	272	1,5,10,20,25,30	5,5,5,5,5,5
exp. 8	600	298	1,5,10,20,25,30	5,5,5,5,5,5

Table 4.3: Setup for the optimum experimental design with EGDM and Bouhassoune parameters.

weights according to the practicability of experiments and the validity of the model, cf. c_i, $i \in \mathcal{I}$ in (4.2),

$$\begin{aligned} 400 \leq L \leq 800, \\ 200 \leq T \leq 350, \\ 0.5 \leq V_{\text{app}} \leq 35, \\ 0 \leq w \leq 10. \end{aligned}$$

Note that these are implemented as inequality constraints, cf. (4.2). We want to end up with two devices, i.e. two lengths, for which we take measurements at different temperatures and applied voltages. We apply equality constraints to the lengths that equal initial values stay equal throughout the optimization. Another constraint is that we do not want to increase or decrease the number of measurements carried out. This can be realized by constraining the sum over all weights to be a fixed number

$$\sum_{i=1}^{6} w_i = 30.$$

In Table 4.4 we assemble the solution of the optimum experimental design problem. We cleared the voltages for which the optimal weights are zero. As constrained before, we end up with 30 measurements for each experiment and only two devices, i.e. two different lengths. For realizing the new experiments, we have to interpret the decimal numbers of weights. One possibility is to apply rounding techniques like Körkel discussed in [59]. We simply round to the next integer number, which means for experiment 5 that we take nine measurements at voltage 0.5 and one measurement at voltage 35. We observe that many parts of the solution lie at the borders. This

	length L	temperature T	voltages V_{app}	weights w
exp. 1	414.1	201.7	0.506, 0.521, 35	10,10,10
exp. 2	414.1	200	0.537, 35	10,20
exp. 3	414.1	350	0.5, 35	20,10
exp. 4	414.1	350	0.5 35	10,20
exp. 5	596.9	200	0.5, 0.511, 0.636, 35	9.044, 10, 10, 0.955
exp. 6	596.9	276.2	0.5, 1.244	20,10
exp. 7	596.9	350	0.5	30
exp. 8	596.9	350	0.5, 35	10, 20

Table 4.4: Optimum experimental design results for NRS-PPV with Bouhassoune parameters and EGDM.

is a typical behavior of optimum experimental design because it seeks for extreme cases which gain the most information. Table 4.11 shows a comparison of the relative confidence intervals of the parameters before and after the optimization. In the third column "before & after", we show the results by taking all experiments, i.e. the 30 old ones and the 30 new ones, into account. If the "old" experiments are already performed, we would insert them in a following parameter estimation to achieve a better and more validated fit. In Figure 4.7, we visualize the two dimensional

	before	after	before & after
A-criterion	0.01167	0.00010	0.00010
θ_1/p_1	0.60377	0.05752	0.05831
θ_2/p_2	0.05414	0.00421	0.00320
θ_3/p_3	0.27298	0.02815	0.02584
θ_4/p_4	0.03510	0.00268	0.00252

Table 4.5: Relative radii of the confidence intervals before and after the optimization, computed by (3.13) for the parameters (4.8).

projections of the four dimensional ellipsoid, i.e. the linearized 95%-confidence region (3.12). The projections are moved to the origin with the difference

$$\delta p_i = p_i - \hat{p}_i.$$

Remark 4.5.2. In the software *VPLAN* the computation of multiple experiments can be done in parallel with *Open MP*. On a computer with at least eight threads the computational time for evaluating the Jacobian for eight experiments is almost the

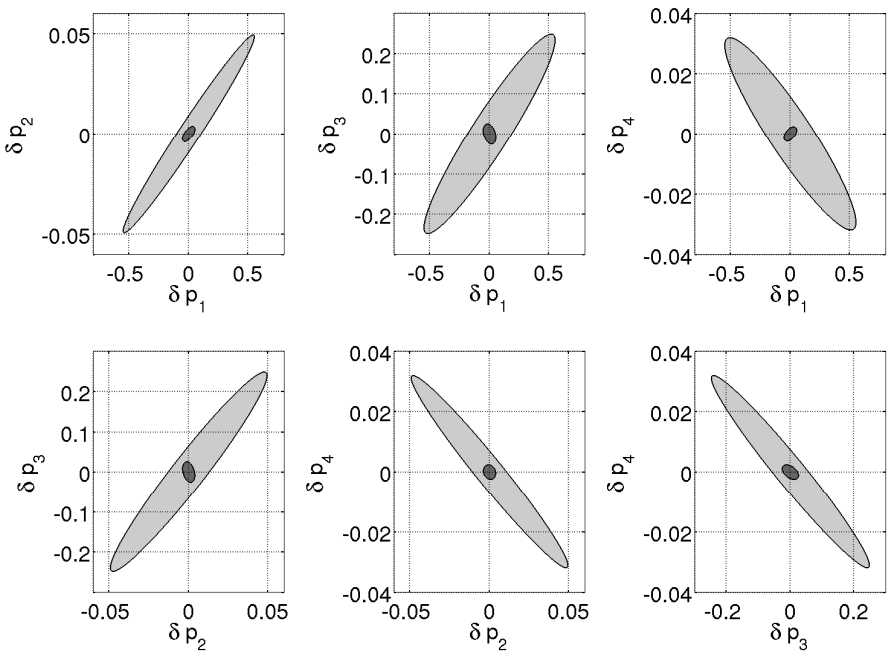

Figure 4.5: Projections of the four dimensional ellipsoid of the linearized 95%-confidence regions before (light part) and after (dark part) the optimization. Computed with EGDM for Bouhassoune parameters for NRS-PPV, cf. Table 4.1, scaled to one.

same as for one experiment.

ECDM

The ECDM parameters of Bouhassoune et al. are displayed in Table 4.6 and our recalculated current-voltage characteristics are shown in Figure 4.6. We made a

μ_0	σ	N_t	E_{cathode}	E_{anode}	c_0
$3.8 \cdot 10^{-7}$	0.18	$37.037 \cdot 10^{27}$	0.0	1.7	0.27

Table 4.6: Configuration for ECDM simulations of NRS-PPV according to Bouhassoune et al.

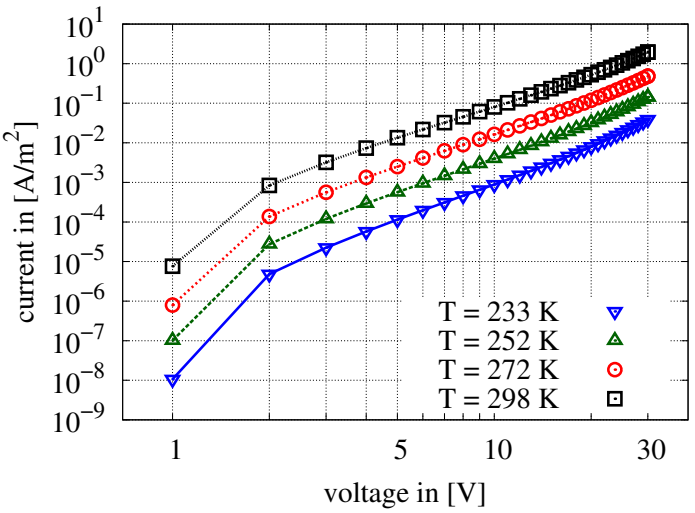

Figure 4.6: NRS-PPV current-voltage characteristics for Bouhassoune parameters computed with the ECDM.

similar study about reducing the number of voltages and increment the number of weights instead. Unlike before, we found, that this technique even decreases the objective in terms of the A-criterion, see Table 4.7, where the number $M = 10$ stands for the voltages $V_{\text{app}} = 1, 3, 6, 10, 13, 16, 20, 23, 26, 30$ and $M = 3$ stands for $V_{\text{app}} = 1, 15, 30$. The weights w are equal to $30/M$, such that each experiment comprises 30 measurement values. Again we consider the two lengths 500 and 600,

	$M = 30$, $w = 1$	$M = 10$, $w = 3$	$M = 6$, $w = 5$	$M = 3$, $w = 10$
A-criterion	0.001106	0.000797	0.000716	0.000805
θ_1/p_1	0.175812	0.144451	0.139155	0.148205
θ_2/p_2	0.010908	0.006801	0.005737	0.005564
θ_3/p_3	0.104361	0.096420	0.088017	0.092243
θ_4/p_4	0.008869	0.008005	0.007782	0.008294

Table 4.7: Comparison of relative radii of the confidence intervals.

which result in eight experiments by combination with the four lengths. We change the setup for the optimum experimental design by fixing the weights

$$w \equiv 1$$

and therefore take 30 voltages. The setup is displayed in Table 4.8. The ECDM is

	length L	temp. T	voltages V_{app}
exp. 1	500	233	1,2,...,29,30
exp. 2	500	252	1,2,...,29,30
exp. 3	500	272	1,2,...,29,30
exp. 4	500	298	1,2,...,29,30
exp. 5	600	233	1,2,...,29,30
exp. 6	600	252	1,2,...,29,30
exp. 7	600	272	1,2,...,29,30
exp. 8	600	298	1,2,...,29,30

Table 4.8: Setup for the optimum experimental design with ECDM and Bouhassoune parameters.

more restrictive w.r.t. to the control bounds. The bounds of the control parameters here are

$$\begin{aligned} 400 \leq L &\leq 800, \\ 230 \leq T &\leq 320, \\ 1 \leq V_{\text{app}} &\leq 30. \end{aligned}$$

Like in the EGDM case, we apply equality constraints that the lengths which are equal in the beginning are equal in the end of the optimization. It turns out that for the optimal control parameters the temperature constraints are all active. For each length we get out the two temperatures 230 and 320. Thus the number of experiments

reduces to four as displayed in Table 4.9. In Table 4.10, we assemble the solution

$T \diagdown L$	498.3	619.4
230	exp. 1	exp. 3
320	exp. 2	exp. 4

Table 4.9: Lengths and temperatures defining four combined experiments.

voltages for the four combined experiments. With the weights fixed to one, we end up

	voltages V_{app}
exp. 1	1 (× 15), 1.85, 2.35, 2.38, 2.42 , 2.57, 2.95, 3.09, 3.19, 3.4 (× 2), 3.59, 4.13, 10.69, 10.84, 12.14, 15.25, 24.68, 28.88, 30 (× 27)
exp. 2	1 (× 7), 2.15, 2.53, 4.6 (× 2), 6.1, 6.35, 7.29, 7.46, 7.99, 8.03, 8.7, 10.09, 11.58, 11.97, 13.21, 14.16, 15.06, 17.14, 19.63, 20.36, 23.79, 23.97, 24.61, 27.29, 29.1, 29.56, 30 (× 27)
exp. 3	1 (× 27), 1.89, 2.19, 2.57, 2.62, 2.87, 4 (× 2), 6.29, 6.82, 7.65, 8.62 (× 2), 11.75, 13.46, 14.1, 14.3, 22.71, 29.32, 30 (× 15)
exp. 4	1 (× 7), 1.1, 2.65 (× 2), 3.03, 3.9, 4.93, 5.83, 6, 6.56, 6.74, 7, 8, 8.19, 9, 9.85, 10, 11.23, 11.85, 12.48, 13.5, 13.75, 14.41, 15.31, 15.79, 16.83, 18.47, 18.02, 20.23, 20.35, 22.44, 22.71, 23.08, 25.15, 27.52, 29.62, 30 (× 18)

Table 4.10: Optimum experimental design results for NRS-PPV with Bouhassoune parameters and ECDM.

with 60 measurements in each combined experiment. Table 4.11 shows a comparison of the relative confidence intervals of the parameters before and after the optimization in this case. In Figure 4.7, we visualize the two dimensional projections, moved to the origin, of the four dimensional ellipsoid for this case. The optimization did not yield such an improvement as in the EGDM case. This is explained by the more limiting bounds. The ranges of the control parameters are more restrictive that higher sensitivities cannot be obtained and the uncertainty cannot be reduced further.

4.5.2 α-NPD

Mensfoort et al. [89], the reference work for our second study took the same parameters as Bouhassoune et al. and augmented them by the energy levels at the cathode E_{cathode}

	before	after	before & after
A-criterion	0.00110	0.00038	0.00026
θ_1/p_1	0.17581	0.09905	0.08220
θ_2/p_2	0.01090	0.00484	0.00396
θ_3/p_3	0.10436	0.06886	0.05623
θ_4/p_4	0.00886	0.00475	0.00401

Table 4.11: Relative radii of the confidence intervals before and after the optimization, computed by (3.13) for the ECDM parameters of Bouhassoune, cf. Table 4.6.

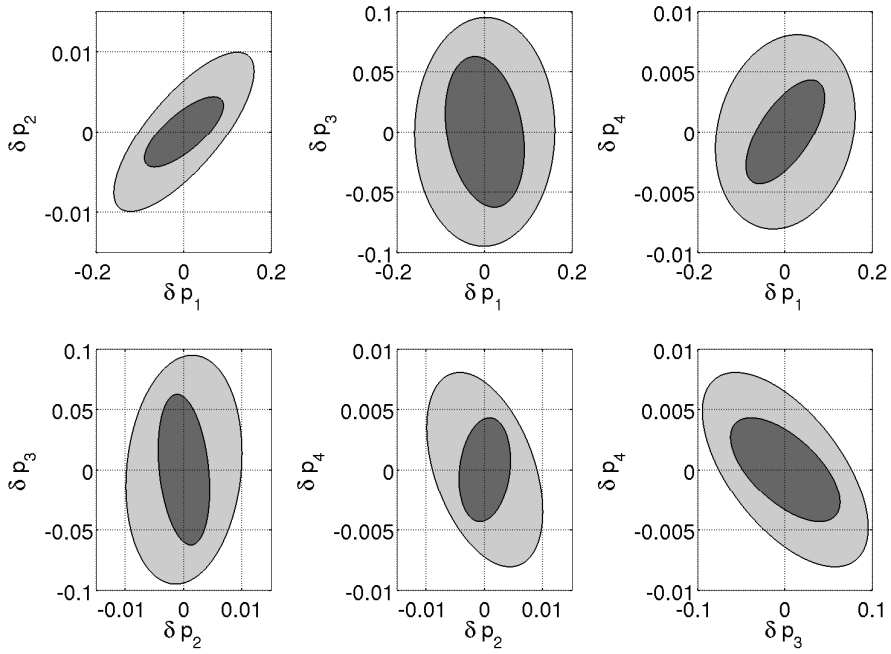

Figure 4.7: Projections of the four dimensional ellipsoid of the linearized 95%-confidence regions before (light part) and after (dark part) the optimization. Computed with ECDM for Bouhassoune parameters for NRS-PPV, cf. Table 4.6, scaled to one.

and the anode E_{anode}.

$$\begin{aligned}
&i)\ \text{site density } N_t,\\
&ii)\ \text{width of Gaussian distribution } \sigma,\\
&iii)\ \text{zero-temperature mobility } \mu_0,\\
&iv)\ \text{factor } c_0 \text{ occurring in the mobility enhancement term } g_0,\\
&v)\ \text{charge density boundary value at cathode } E_{\text{cathode}},\\
&vi)\ \text{charge density boundary value at anode } E_{\text{anode}}.
\end{aligned} \tag{4.9}$$

Again, we will compute optimum experimental designs for both the EGDM and the ECDM.

EGDM

The parameters they used are displayed in Table 4.12. They took much smaller

μ_0	σ	N_t	E_{cathode}	E_{anode}	c_0
$22 \cdot 10^{-6}$	0.14	$0.2 \cdot 10^{27}$	0.4	1.9	0.42

Table 4.12: Configuration for EGDM simulations of α-NPD according to Mensfoort et al.

devices as Bouhassoune et al. with $L = 100$ and 200. For such device lengths the voltage has to be smaller too, in order to not overheat the device. The recalculated current-voltage characteristics, computed with our simulation program are shown in Figure 4.8. In this example the voltages per experiment, cf. Definition 4.5.1, are distinct, see Table 4.13. The measurement weights are fixed to one as before and the bounds to the lengths and temperatures are given by

$$\begin{aligned}
80 \leq L \leq 300,\\
180 \leq T \leq 350.
\end{aligned}$$

The bounds to the voltages are chosen length dependent.

$$\begin{aligned}
&\text{exp. } 1 \text{ - } 6 \qquad 1.1 \leq V_{\text{app}} \leq 10,\\
&\text{exp. } 7 \text{ - } 12 \qquad 1.1 \leq V_{\text{app}} \leq 20.
\end{aligned}$$

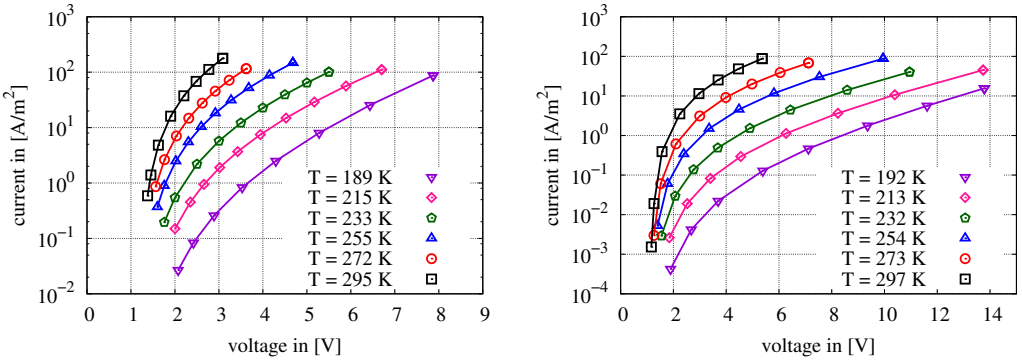

Figure 4.8: α-NPD current-voltage characteristics for Mensfoort parameters computed with the EGDM for 100 nm (left-hand side) and 200 nm (right-hand side).

	length L	temperature T	voltages V_{app}
exp. 1	100	189	2, 2.4, 2.9, 3.5, 4.3, 5.3, 6.4, 7.9
exp. 2	100	215	2, 2.4, 2.7, 3, 3.4, 4, 4.5, 5.2, 5.9, 6.7
exp. 3	100	233	1.8, 2, 2.5, 3, 3.5, 4, 4.5,5,5.5
exp. 4	100	255	1.6,1.8,2,2.3, 2.6,2.9, 3.3, 3.7, 4.1, 4.7
exp. 5	100	272	1.6, 1.8, 2, 2.3, 2.6, 2.9, 3.2, 3.6
exp. 6	100	295	1.4, 1.5, 1.6, 1.9, 2.2,2.5,2.8,3
exp. 7	200	192	1.9, 2.7, 3.7, 5.4, 7.1, 9.4, 11.6, 13.8
exp. 8	200	213	1.8, 2.5, 3.4, 4.6, 6.2, 8.2, 10.4, 13.7
exp. 9	200	232	1.5, 2, 2.8, 3.7, 4.9, 6.4, 8.6, 10.9
exp. 10	200	254	1.4, 1.8, 2.4, 3.4, 4.5, 5.8, 7.5, 9.9
exp. 11	200	273	1.3, 1.5, 2.1, 3, 4, 5, 6, 7.1
exp. 12	200	297	1.2, 1.3, 1.6, 2.2, 3, 3.7, 4.5, 5.4

Table 4.13: Setup for the optimum experimental design with EGDM and Mensfoort parameters.

Again we constrain the device thicknesses to stay equal, where they have been equal at the beginning of the optimization. For the resulting lengths, we assume that they are near 100 nm and 200 nm, respectively, so that the voltage bounds are appropriate for the optimum experimental design solution as well. In Table 4.14 the results of the optimization are displayed. Note, that we have again the same number of

	length L	temperature T	voltages V_{app}
exp. 1	98.9	182.5	3.4, 4.6, 4.7, 4.9, 5, 5.3, 5.5, 10
exp. 2	98.9	180	1.1,2, 3.6,4, 4.2,4.3,4.5,6,10
exp. 3	98.9	232.8	1.8,2,3.7,4.1,4.4,4.6,4.9,5.4,9.8
exp. 4	98.9	255.3	1.9,2,3.4,4,4.3,4.4,4.5,4.6,4.8,8.6
exp. 5	98.9	273.2	1.5, 4, 4.7, 4.8, 4.9
exp. 6	98.9	298.2	5.3, 5.4 5.5, 5.6, 5.8
exp. 7	200.3	180	1.1, 2.0, 4.9, 7.3, 10.5, 14.9, 20
exp. 8	200.3	213.5	1.1, 4.9, 5.8, 6, 9.4, 10.7, 13.3, 20
exp. 9	200.3	231.1	1.1, 2, 2.2, 3.1, 6.5, 10, 10.4, 13.9
exp. 10	200.3	252.3	1.1,1.4,1.5,3.5,5.5,5.8,8.2,11.5
exp. 11	200.3	272.5	1.2,1.9,3.9,4.3,5,5.4,6.6,7.8
exp. 12	200.3	299.4	1.1, 2,3.6,4.6, 5.2, 5.8, 6.5

Table 4.14: Optimum experimental design results for α-NPD with Mensfoort parameters and EGDM.

measurements as in the beginning. Table 4.15 shows a comparison of the relative confidence intervals for this case. In Figure 4.9 selected two dimensional projections of the six dimensional 95%-confidence ellipsoid are displayed. The parameter values are moved to the origin.

	before	after	before & after
A-criterion	0.0060	0.0029	0.0017
θ_1/p_1	0.5923	0.4204	0.3227
θ_2/p_2	0.0403	0.0266	0.0206
θ_3/p_3	0.3066	0.1964	0.1581
θ_4/p_4	0.0198	0.0112	0.0095
θ_5/p_5	0.1084	0.0570	0.0471
θ_6/p_6	0.0151	0.0080	0.0065

Table 4.15: Relative radii of the confidence intervals before and after the optimization, computed by (3.13) for the parameters (4.9) for the EGDM.

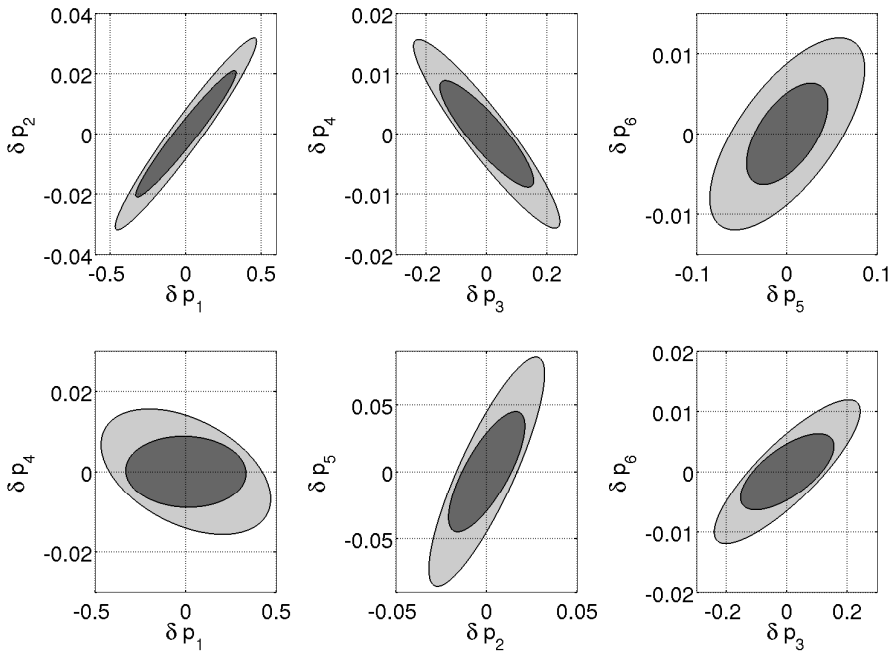

Figure 4.9: Selected projections of the six dimensional ellipsoid of the linearized 95%-confidence regions before (light part) and after (dark part) the optimization. Computed with EGDM for Mensfoort parameters for the α-NPD, cf. Table 4.12, scaled to one.

ECDM

The parameters for the ECDM are given in Table 4.16. The device lengths are again

μ_0	σ	N_t	E_{cathode}	E_{anode}	c_0
$0.5 \cdot 10^{-6}$	0.1	$3.7 \cdot 10^{27}$	0.4	1.9	0.34

Table 4.16: Configuration for ECDM simulations of α-NPD according to Mensfoort et al.

$L = 100$ and 200. The recalculated current-voltage characteristics, computed with our simulation program, are shown in Figure 4.10. The same voltages as for the

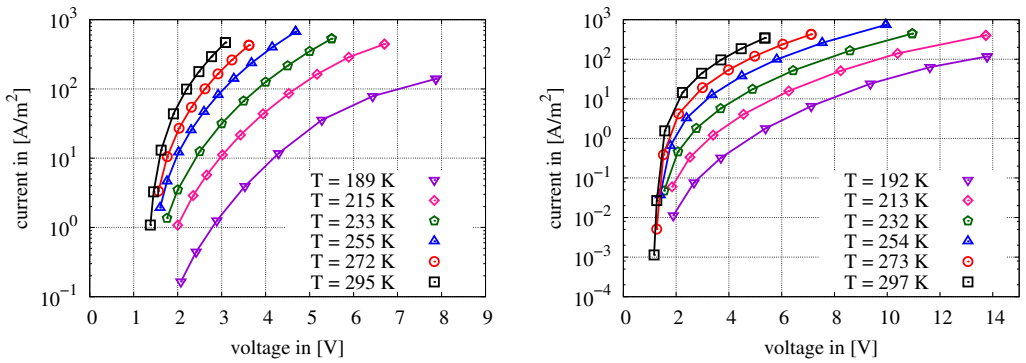

Figure 4.10: α-NPD current-voltage characteristics for Mensfoort parameters computed with the ECDM for 100 nm (left-hand side) and 200 nm (right-hand side).

EGDM are applied, see Table 4.13. As before we choose bounds to the lengths and temperatures

$$80 \leq L \leq 300,$$
$$180 \leq T \leq 350,$$

and also for the voltages

$$\text{exp. } 1 \text{ - } 6 \qquad 1.1 \leq V_{\text{app}} \leq 10,$$
$$\text{exp. } 7 \text{ - } 12 \qquad 1.1 \leq V_{\text{app}} \leq 20.$$

The results of the optimization are displayed in Table 4.17. In Table 4.18 the comparison of the relative confidence intervals is shown for this case and the projections

are displayed in Figure 4.11.

	length L	temperature T	voltages V_{app}
exp. 1	98.9	180	1.7 (3 ×), 6.7, 6.8 (3 ×), 7.5
exp. 2	98.9	218.4	1.7 (2 ×), 3.2, 3.4 (4 ×), 5, 10 (2 ×)
exp. 3	98.9	231.8	1.7 (2 ×), 3.4 (4 ×), 5.3, 5.7, 10
exp. 4	98.9	255	1.6,1.8,2,2.3, 2.6,2.9, 3.3, 3.7, 4.1, 4.7
exp. 5	98.9	272	1.6, 1.8, 2, 2.3, 2.6, 2.9, 3.2, 3.6
exp. 6	98.9	295	1.4, 1.5, 1.6, 1.9, 2.2, 2.5, 2.8, 3
exp. 7	200	192	1.9, 2.7, 3.7, 5.4, 7.1, 9.4, 11.6, 13.8
exp. 8	200	213	1.8, 2.5, 3.4, 4.6, 6.3, 8.2, 10.4, 13.7
exp. 9	200	232	1.5, 2, 2.8, 3.7, 4.9, 6.4, 8.6, 11
exp. 10	200	254	1.4, 1.8, 2.4, 3.4, 4.5, 5.8, 7.5, 9.9
exp. 11	200	273	1.3, 1.5, 2.1, 3, 4, 5, 6, 7.1
exp. 12	200	297	1.2, 1.3, 1.6, 2.2, 3, 3.7, 4.5, 5.4

Table 4.17: Optimum experimental design results for α-NPD with Mensfoort parameters and ECDM.

	before	after	before & after
A-criterion	0.0067	0.0027	0.0017
θ_1/p_1	0.5153	0.3247	0.2614
θ_2/p_2	0.1183	0.0609	0.0532
θ_3/p_3	0.4246	0.2995	0.2284
θ_4/p_4	0.1434	0.0698	0.0625
θ_5/p_5	0.1612	0.0814	0.0716
θ_6/p_6	0.0293	0.0158	0.0135

Table 4.18: Relative radii of the confidence intervals before and after the optimization, computed by (3.13) for the parameters (4.9) for the ECDM.

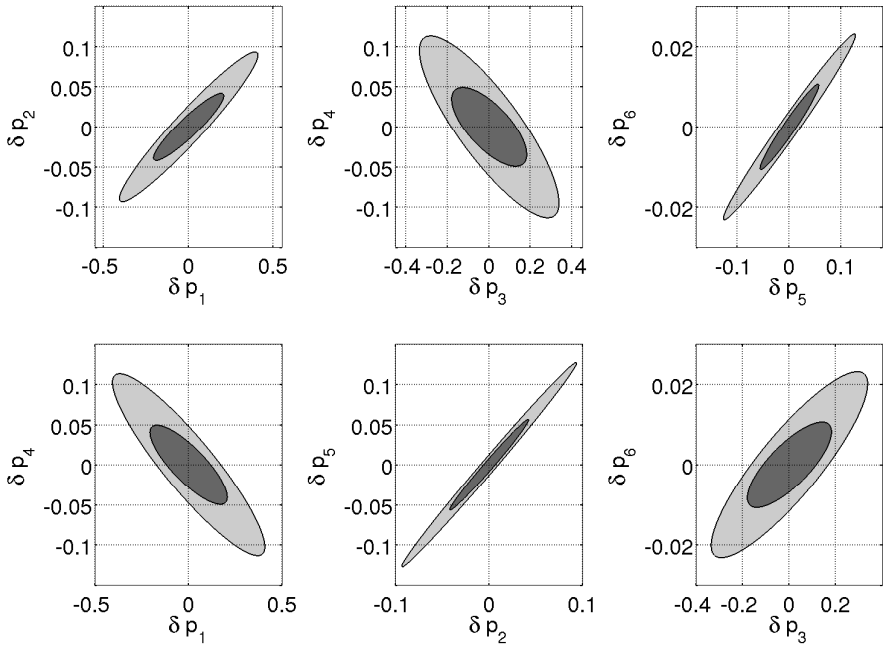

Figure 4.11: Projections of the six dimensional ellipsoid of the linearized 95%-confidence regions before (light part) and after (dark part) the optimization. Computed with ECDM for Mensfoort parameters for the α-NPD, cf. Table 4.16, scaled to one.

4.6 Parameter dependence of the nonlinear optimum experimental design problem

In our case of nonlinear optimum experimental design, the objective not only depends on the control parameters q but also on the parameters p. The parameters are uncertain, which was our main assumption in the first place. As Körkel discussed in his thesis [59], there are the two approaches:

- Consider a robustified objective.
- Make a sequential ansatz.

4.6.1 Robustified optimum experimental design objective

The idea is to exploit a pre-known distribution of the parameters. With an initial value for the mean p_0 and for the variance-covariance matrix C_0 the confidence region is given by

$$\{p \in \mathbb{R}^{N_p} : \|p - p_0\|^2_{C_0^{-1}} \leq \gamma(\alpha)^2\},$$

cf. (3.12). The robust objective is given by the consideration of a *worst-case-design*

$$\min_{q \in \mathbb{R}^{N_q}} \max_{\|p-p_0\|_{C_0^{-1}} \leq \gamma} \phi(\lambda(p), u(p), p). \tag{4.10}$$

This problem is semi-infinite, which makes it hard to solve, cf. the survey article of Hettich et al. [49]. One rather regards a linearization of the function ϕ around the point p_0

$$\phi(\lambda(p), u(p), p) \approx \phi(\lambda(p_0), u(p_0), p_0) + \frac{d}{dp}\phi(\lambda(p_0), u(p_0), p_0)(p - p_0).$$

This linearization leads to the problem

$$\min_{q \in \mathbb{R}^{N_q}} \phi(\lambda(p_0), u(p_0), p_0) + \gamma \left\| \frac{d}{dp}\phi(\lambda(p_0), u(p_0), p_0) \right\|_{C_0},$$

independent of p, see Körkel [59] for further details. The downside is that one has to compute an additional derivative order w.r.t. the parameters p of the objective, which can be a huge effort.

4.6.2 Sequential optimum experimental design

An alternative of the robustified objective is to consider a sequential ansatz, where optimum experimental design, measurement generation, and parameter estimation are performed alternately, cf. Figure 4.12. For sequential optimum experimental design

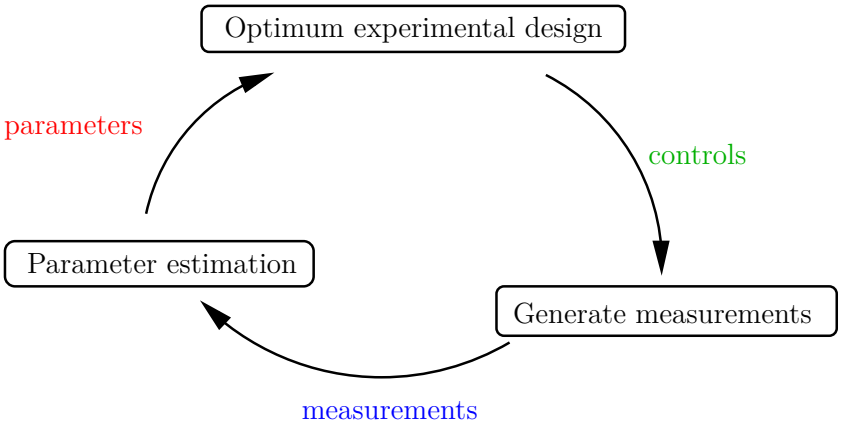

Figure 4.12: Schematic sequential optimum experimental design.

the steps are given in Algorithm 4 in more detail. The termination condition can

Algorithm 4 Algorithm of the sequential optimum experimental design.

1: Start with an initial parameter guess p^0 and set $k = 0$.
2: **while** a termination condition is not satisfied **do**
3: With optimum experimental design plan M_{k+1} additional experiments corresponding to control parameters q^{k+1} while taking into account the previous $M_0 + \cdots + M_{k-1}$ experiments, if available.
4: Generate new measurement values from M_{k+1} new experiments.
5: Perform a parameter estimation with all measurement values. This yields a new iterate p^{k+1}.
6: $k \leftarrow k + 1$
7: **end while**

depend on the available budget and the quality of the parameter estimation. For convergence results we refer to Chaudhuri et al. [24].

Sequential approach for NRS-PPV with EGDM

We observe that our problems are intrinsically robust against parameter perturbations. For the example of NRS-PPV with the EGDM we show that a sequential ansatz reduces the uncertainty of the parameters already after a few iterations down to a satisfactory quantity. We start with the same configuration, i.e. parameters, control parameters, etc., as in the EGDM part of Section 4.5.1, i.e. we consider eight experiments with 30 measurements per experiment. At the beginning we plan eight new experiments with optimum experimental design taking the eight "old" experiments into account. After that we generate new, artificial measurement values for the real parameters, perturbed with a random number according to the assumed distribution. Then we perform a parameter estimation with the additional measurement values to get a new estimate for the parameters and start over again. We run two cycles to get the A-criterion reduced to roughly 2% of its value. The intermediate deviations of the parameters and the value for the A-criterion are shown in Table 4.19. The first column corresponds to a simulation, i.e. computation of the variance-covariance matrix, with the initial guess of the parameters and the initial experimental setup. We see that the variations

	Sim	OED	PE	OED	PE
A-criterion	0.05839	0.00363	0.00313	0.00083	0.00098
θ_1/p_1	1.35008	0.32726	0.32478	0.16271	0.17322
θ_2/p_2	0.12108	0.02415	0.02399	0.00862	0.00980
θ_3/p_3	0.61041	0.17244	0.17543	0.09785	0.10504
θ_4/p_4	0.07849	0.02354	0.02376	0.00756	0.00739

Table 4.19: Relative radii of confidence intervals computed at the beginning and after optimum experimental design (OED) and parameter estimation (PE) resp.

of the parameters caused by a parameter estimation neither worse the confidence intervals nor the A-criterion significantly. This means that the control parameters found by optimum experimental design are robust against parameter uncertainties.

5 Conclusion

We found an efficient robust numerical simulation method for Gaussian disorder modeled organic semiconductors, consisting of an extended Gummel method with linearized continuity equation and corrected stabilization term in Poisson's equation, a contraction based damping strategy and the full step Newton method. The method yields simulation results for a wide range of parameters, control parameters, and boundary values. In few instances the method converges, where commercial software failed to converge.

Optimum experimental design was successfully applied by computing exact derivatives with automatic differentiation and solving tangential and adjoint equations, which has never been done before for Gaussian disorder modeled organic semiconductor devices. The parameter uncertainty of the EGDM applied to NRS-PPV was reduced by a factor of 100 in terms of the A-criterion.

Within the scope of this work we developed a simulation software, in which the above mentioned method is realized as well as the derivative computation of implicitly given derivatives of the solution w.r.t. the parameters, control parameters and both. A previous version of the software was implemented in *MATLAB* as a prototype. This was handed out to the industry partner, where it is successfully used for the simulation of organic semiconductors and the estimation of Gaussian disorder mobility parameters.

For simulating and optimizing higher dimensional problems, our 2D simulation study can be enhanced with a coupling of *deal.ii* and *VPLAN*. For larger problems iterative solvers have to be applied, which require preconditioning. To find adequate preconditioners for the subproblems of Gummel's method is a future challenge.

In this thesis only electron transport layer models were considered. For simulating full organic light emitting devices (OLEDs) a multi-layer model is required with both electron and hole transport layers. Also recombination terms and trap densities have effects on the current flow. Enhancing the models with such extensions and apply optimum experimental design following our pattern can be tasks for future work.

Acknowledgements

At this point I would like to thank my advisor Prof. Dr. Dres. h.c. Bock for giving me the opportunity to do my PhD in his Simulation & Optimization group at the Faculty of Mathematics and Computer Sciences and the Interdisciplinary Center for Scientific Computing (IWR) of the Heidelberg University. He put confidence in me to work for the project PARAPLUE funded by the Federal Ministry of Education and Research (BMBF) under grant 03MS649A. Many thanks go to the people who helped applying for the fund, in particular Dr. Mario Mommer. Furthermore I acknowledge funding from the BASF SE Ludwigshafen.

Special thanks go to my mentor Dr. Stefan Körkel who advised me at many points during my PhD including numerous meetings and strategic planning. He was never tired debating on principles. For many, very fruitful discussions I would like to thank all members of the BASF junior research group. Andreas Schmidt always had a "moment" to argue about topics related to PDE constrained optimization. Dennis Janka could often help me out with SQP problems and optimum experimental design interpretation. Many thanks go to my office mates Sebastian Walter and Manuel Kudruss, too. They always shared their time to talk about small and big questions. I also want to thank the entire Simulation & Optimization group for the "Doktorandenrunde" and always having an open door for me. For several key discussions with Dr. Mario Mommer I am grateful.

I am indebted to Christian Goll, Dennis Janka, Dr. Sebastian Walter, and Dr. Matthias Makowski for valuable comments on a first draft of this thesis. Furthermore I would like to thank Dr. Thomas Carraro for talking through several topics of this work with me.

I also like to thank the members of the group of Dr. Anna Schreieck from the BASF, namely Dr. Alexander Badinski, Dr. Robert Lee, and Sven Stodtmann. They showed me, that things are handled in a slightly different way in industry compared to the university. Mustapha Al Helwi from the InnovationLab Heidelberg takes credit for giving me insight in the physics of organic light emitting devices.

I warmly thank Theresia for her love and steering me into the right direction now and then. Last but not least I would like to thank my parents for their unconditional and never-ending support.

List of Figures

List of Tables

Bibliography

[1] M. Ainsworth and J. Oden. *A Posteriori Error Estimation in Finite Element Analysis*. Pure and Applied Mathematics: A Wiley Series of Texts, Monographs and Tracts. Wiley, 2000.

[2] H. Amann and J. Escher. *Analysis II*. Analysis. Birkhäuser Basel, 2006.

[3] U. Ascher, P. Markowich, C. Schmeiser, H. Steinrück, and R. Weiss. Conditioning of the steady state semiconductor device problem. *SIAM Journal on Applied Mathematics*, 49(1):165–185, 1989.

[4] N. W. Ashcroft and N. D. Mermin. *Solid State Physics*. Holt, Rinehart and Winston, New York, 1988.

[5] I. Babuška and T. Strouboulis. *The Finite Element Method and Its Reliability*. Numerical mathematics and scientific computation. Clarendon Press, 2001.

[6] W. Bangerth, R. Hartmann, and G. Kanschat. deal.II — a general purpose object oriented finite element library. *ACM Trans. Math. Softw.*, 33(4), 2007.

[7] R. E. Bank, W. Coughran, Jr., and L. C. Cowsar. The finite volume scharfetter-gummel method for steady convection diffusion equations. *Computing and Visualization in Science*, 1(3):123–136, 1998.

[8] I. Bauer, H. Bock, S. Körkel, and J. Schlöder. Numerical methods for optimum experimental design in DAE systems. *J. Comput. Appl. Math.*, 120(1-2):1–15, 2000.

[9] R. Becker and R. Rannacher. A feed-back approach to error control in finite element methods: Basic analysis and examples. *East West Journal of numerical mathematics*, 4:237–264, 1996.

[10] R. Becker and R. Rannacher. An optimal control approach to a posteriori error estimation in finite element methods. *Acta Numerica 2001*, 10:1–102, 2001.

[11] B. M. Bell. CppAD: a package for C++ algorithmic differentiation. *Computational Infrastructure for Operations Research*, 2012.

[12] C. Bischof, A. Carle, G. Corliss, A. Griewank, and P. Hovland. ADIFOR generating derivative codes from fortran programs. *Scientific Programming*, 1:11–29, 1992.

[13] C. Bischof, A. Carle, P. Hovland, P. Khademi, and A. Mauer. Adifor 2.0 user's guide (revision d). Technical report, Mathematics and Computer Science Division Technical Memorandum no. 192 and Center for Research on Parallel Computation, 1998.

[14] C. Bischof, P. Khademi, and A. Mauer. The ADIFOR 2.0 system for the automatic differentiation of Fortran 77 programs. Technical Report CRPC–TR94491, Center for Research on Parallel Computation,Rice University, Houston, TX, 1994.

[15] H. Bock. *Randwertproblemmethoden zur Parameteridentifizierung in Systemen nichtlinearer Differentialgleichungen*, volume 183 of *Bonner Mathematische Schriften*. Universität Bonn, Bonn, 1987.

[16] H. Bock, E. Kostina, and O. Kostyukova. Conjugate Gradient Methods for Computing Covariance Matrices for Constrained Parameter Estimation Problems. *SIAM Journal on Matrix Analysis and Application*, 29:626, 2007.

[17] H. Bock, E. Kostina, and J. Schlöder. On the Role of Natural Level Functions to Achieve Global Convergence for Damped Newton Methods. In M. Powell and S. Scholtes, editors, *System Modelling and Optimization. Methods, Theory and Applications*, pages 51–74. Kluwer, 2000.

[18] J. Bonham and D. Jarvis. A new approach to space-charge-limited conduction theory. *Aust. J. Chem.*, 30:705, 1977.

[19] J. Bonham and D. Jarvis. Theory of space-charge-limited current with one blocking electrode. *Aust. J. Chem.*, 31:2103, 1978.

[20] M. Bouhassoune, S. van Mensfoort, P. Bobbert, and R. Coehoorn. Carrier-density and field-dependent charge-carrier mobility in organic semiconductors with correlated Gaussian disorder. *Organic Electronics*, 10(3):437 – 445, 2009.

[21] D. Braess. *Finite Elemente, Theorie, schneller Löser und Anwendungen in der Elastizitätstheorie*. Springer, Berlin – Heidelberg – New York, 4., erw. und "uberarb. edition, 1992.

[22] F. Brezzi, L. Marini, S. Micheletti, P. Pietra, R. Sacco, and S. Wang. Discretization of semiconductor device problems (i). In W. Schilders and E. ter Maten, editors, *Numerical Methods in Electromagnetics*, volume 13 of *Handbook of Numerical Analysis*, pages 317 – 441. Elsevier, 2005.

[23] H. Bässler. Charge Transport in Disordered Organic Photoconductors a Monte Carlo Simulation Study. *physica status solidi (b)*, 175(1):15–56, 1993.

[24] P. Chaudhuri and P. A. Mykland. Nonlinear experiments: Optimal design and inference based on likelihood. *Journal of the American Statistical Association*, 88(422):pp. 538–546, 1993.

[25] B. Christianson. Reverse accumulation and attractive fixed points. *Optimization Methods and Software*, 3(4):311–326, 1994.

[26] T. A. Davis. Algorithm 832: Umfpack v4.3—an unsymmetric-pattern multifrontal method. *ACM Trans. Math. Softw.*, 30(2):196–199, June 2004.

[27] J. deMello. Highly convergent simulations of transport dynamics in organic light-emitting diodes. *Journal of Computational Physics*, 181(2):564 – 576, 2002.

[28] P. Deuflhard. *Newton Methods for Nonlinear Problems: Affine Invariance and Adaptive Algorithms*. Springer Series in Computational Mathematics. U.S. Government Printing Office, 2004.

[29] P. Deuflhard, F. Bornemann, and A. Hohmann. *Numerische Mathematik*. Number Bd. 1 in De Gruyter Lehrbuch. De Gruyter, 2002.

[30] P. Deuflhard and M. Weiser. *Numerische Mathematik: Adaptive Lösung partieller Differentialgleichungen. 3*. De Gruyter Lehrbuch Series. De Gruyter, 2011.

[31] J. I. Díaz, G. Galiano, and A. Jüngel. On a quasilinear degenerate system arising in semiconductors theory. part i: Existence and uniqueness of solutions. *Nonlinear Analysis: Real World Applications*, 2(3):305 – 336, 2001.

[32] A. Einstein and M. von Smoluchowski. *Untersuchungen über die Theorie der Brownschen Bewegung (1905): (1906-1915)*. Ostwalds Klassiker der exakten Wissenschaften / Ostwalds Klassiker der exakten Wissenschaften. Verlag Harri Deutsch, 1997.

[33] P. R. Emtage and J. J. O'Dwyer. Richardson-schottky effect in insulators. *Phys. Rev. Lett.*, 16:356–358, Feb 1966.

[34] K. Eriksson. Introduction to adaptive methods for differential equations, 1995.

[35] Fluxim AG, Dorfstrasse 7, CH-8835 Feusisberg, Switzerland. *setfos 3.2 - User Manual*, 2010.

[36] H. Gajewski and K. Gröger. *Semiconductor equations for variable mobilities based on Boltzmann statistics or Fermi-Dirac statistics*. Karl-Weierstraß-Institut für Mathematik Berlin, Ost: Preprint. Karl-Weierstrass-Inst. für Mathematik, 1988.

[37] H. Gajewski and K. Gärtner. On the iterative solution of van roosbroeck's equations. *ZAMM - Journal of Applied Mathematics and Mechanics / Zeitschrift für Angewandte Mathematik und Mechanik*, 72(1):19–28, 1992.

[38] C. Geiger and C. Kanzow. *Theorie und Numerik Restringiererter Optimierungsaugaben.* Springer-lehrbuch Masterclass. Springer, 2002.

[39] C. Gerhardt. *Analysis I.* Int. Press of Boston, Bosten, 2002.

[40] C. Gerhardt. *Analysis II.* Analysis. International Press, 2006.

[41] D. Gilbarg and N. Trudinger. *Elliptic Partial Differential Equations of Second Order.* Classics in Mathematics. Springer-Verlag GmbH, 2001.

[42] P. E. Gill, W. Murray, Michael, and M. A. Saunders. Snopt: An sqp algorithm for large-scale constrained optimization, 1997.

[43] P. E. Gill, W. Murray, and M. A. Saunders. User's guide for snopt version 7: Software for large-scale nonlinear programming.

[44] A. Griewank. *Evaluating Derivatives.* Frontiers in applied mathematics. SIAM, Philadelphia, 2000.

[45] A. Griewank, D. Juedes, H. Mitev, J. Utke, O. Vogel, and A. Walther. ADOL-C: A package for the automatic differentiation of algorithms written in C/C++. Technical report, Technical University of Dresden, Institute of Scientific Computing and Institute of Geometry, 1999. Updated version of the paper published in *ACM Trans. Math. Software* 22:131–167, 1996.

[46] C. Grossmann, H. Roos, and M. Stynes. *Numerical Treatment of Partial Differential Equations.* Universitext. Springer, 2007.

[47] H. K. Gummel. *IEEE Trans. Electron Devices*, 11:455, 1964.

[48] L. Hascoët and V. Pascual. TAPENADE 2.1 user's guide. Rapport technique 300, INRIA, Sophia Antipolis, 2004.

[49] R. Hettich and K. O. Kortanek. Semi-infinite programming: Theory, methods, and applications. *SIAM Review*, 35(3):pp. 380–429, 1993.

[50] M. Hinze, R. Pinnau, and M. Ulbrich. *Optimization with PDE Constraints.* Mathematical Modelling: Theory and Applications. Springer, 2008.

[51] I. N. Hulea, H. B. Brom, A. J. Houtepen, D. Vanmaekelbergh, J. J. Kelly, and

E. A. Meulenkamp. Wide energy-window view on the density of states and hole mobility in poly(*p*-phenylene vinylene). *Phys. Rev. Lett.*, 93:166601, Oct 2004.

[52] J. W. Jerome. Consistency of semiconductor modeling: An existence/stability analysis for the stationary van roosbroeck system. *SIAM Journal on Applied Mathematics*, 45(4):pp. 565–590, 1985.

[53] J. W. Jerome and B. Brosowski. Evolution systems in semiconductor device modeling: A cyclic uncoupled line analysis for the gummel map. *Mathematical Methods in the Applied Sciences*, 9(1):455–492, 1987.

[54] X. Jiang. Numerical simulations of semiconductor devices by streamline-diffusion methods. Technical report, 1995.

[55] D. W. Kelly, J. P. De S. R. Gago, O. C. Zienkiewicz, and I. Babuska. A posteriori error analysis and adaptive processes in the finite element method: Part i-error analysis. *International Journal for Numerical Methods in Engineering*, 19(11):1593–1619, 1983.

[56] T. Kerkhoven. A proof of convergence of Gummel's algorithm for realistic device geometries. 23(6):1121–1137, Dec. 1986.

[57] C. Kittel. *Introduction to Solid State Physics*. John Wiley & Sons, Inc., New York, 6th edition, 1986.

[58] E. Knapp, R. Häusermann, H. U. Schwarzenbach, and B. Ruhstaller. Numerical simulation of charge transport in disordered organic semiconductor devices. *Journal of Applied Physics*, 108(5):–, 2010.

[59] S. Körkel. *Numerische Methoden für Optimale Versuchsplanungsprobleme bei nichtlinearen DAE-Modellen*. PhD thesis, Universität Heidelberg, Heidelberg, 2002.

[60] T. Lohmann, H. Bock, and J. Schlöder. Numerical methods for parameter estimation and optimal experimental design in chemical reaction systems. *Industrial and Engineering Chemistry Research*, 31:54–57, 1992.

[61] P. Markowich and C. Ringhofer. A singularly perturbed boundary value problem modelling a semiconductor device. *SIAM Journal on Applied Mathematics*, 44(2):231–256, 1984.

[62] P. Markowich, C. Ringhofer, and C. Schmeiser. *Semiconductor equations*. Springer-Verlag, 1990.

[63] P. Markowich, C. Ringhofer, S. Selberherr, and M. Lentini. A singular perturbation approach for the analysis of the fundamental semiconductor equations. *Electron Devices, IEEE Transactions on*, 30(9):1165–1180, 1983.

[64] P. A. Markowich, C. A. Ringhofer, and C. Schmeiser. An asymptotic analysis of one-dimensional models of semiconductor devices. 37(1):1–24, 1986.

[65] P. A. Markowich and M. A. Zlámal. Inverse-average-type finite element discretizations of selfadjoint second-order elliptic problems. *Math. Comp.*, 51:431–449, 1988.

[66] D. Meidner and B. Vexler. Adaptive space-time finite element methods for parabolic optimization problems. *SIAM Journal on Control and Optimization*, 46(1):116–142, 2007.

[67] A. Miller and E. Abrahams. Impurity conduction at low concentrations. *Phys. Rev.*, 120:745–755, Nov 1960.

[68] M. Mock. On the convergence of gummel's numerical algorithm. *Solid-State Electronics*, 15(1):1 – 4, 1972.

[69] M. Mock. An initial value problem from semiconductor device theory. *SIAM Journal on Mathematical Analysis*, 5(4):597–612, 1974.

[70] M. Mock. *Analysis of mathematical models of semiconductor devices*. Advances in numerical computation series. Boole Press, 1983.

[71] J. Nocedal and S. Wright. *Numerical Optimization*. Springer Verlag, Berlin Heidelberg New York, 2nd edition, 2006. ISBN 0-387-30303-0 (hardcover).

[72] M. Obrecht. A new stable method for linearization of discretized basic semiconductor equations. *Solid-State Electronics*, 36(4):643 – 648, 1993.

[73] G. Paasch and S. Scheinert. Charge carrier density of organics with Gaussian density of states: Analytical approximation for the Gauss-Fermi integral. *Journal of Applied Physics*, 107(10):–, 2010.

[74] P. Painter and M. Coleman. *Essentials of Polymer Science and Engineering*. DEStech Publications, Incorporated, 2008.

[75] W. F. Pasveer, J. Cottaar, C. Tanase, R. Coehoorn, P. W. M. B. P. A. Bobbert, D. M. de Leeuw, and M. A. J. Michels. *Phys. Rev. Lett.*, 94(206601), 2005.

[76] C. Pflumm, C. Gartner, and U. Lemmer. A numerical scheme to model current

and voltage excitation of organic light-emitting diodes. *Quantum Electronics, IEEE Journal of*, 44(8):790–798, Aug 2008.

[77] Y. Preezant and N. Tessler. Self-consistent analysis of the contact phenomena in low-mobility semiconductors. *Journal of Applied Physics*, 93(4):2059–2064, 2003.

[78] F. Pukelsheim. *Optimal Design of Experiments*. Classics in Applied Mathematics. Society for Industrial and Applied Mathematics, 2006.

[79] Y. Roichman and N. Tessler. Generalized einstein relation for disordered semiconductors—implications for device performance. *Applied Physics Letters*, 80(11):1948–1950, 2002.

[80] D. L. Scharfetter and H. K. Gummel. *IEEE Trans. Electron Devices*, 16:64, 1969.

[81] M. Schmich and B. Vexler. Adaptivity with dynamic meshes for space-time finite element discretizations of parabolic equations. *SIAM Journal on Scientific Computing*, 30(1):369–393, 2008.

[82] A. Schmidt. Automatisches Differenzieren bei Differentialgleichungsmodellen der Systembiologie. Diploma thesis, Universität Heidelberg, 2008.

[83] J. Scott and G. G. Malliaras. Charge injection and recombination at the metal—organic interface. *Chemical Physics Letters*, 299(2):115 – 119, 1999.

[84] G. A. F. Seber and C. J. Wild. *Nonlinear Regression*. John Wiley & Sons, Inc., 1989.

[85] S. Selberherr. *Analysis and simulation of semiconductor devices / Siegfried Selberherr*. Wien, Austria ; New York : Springer-Verlag, 1984. Includes bibliographies and indexes.

[86] S. Stodtmann, R. M. Lee, C. K. F. Weiler, and A. Badinski. Numerical simulation of organic semiconductor devices with high carrier densities. *Journal of applied physics*, 2012. submited.

[87] J. J. M. van der Holst, M. A. Uijttewaal, B. Ramachandhran, R. Coehoorn, P. A. Bobbert, G. A. de Wijs, and R. A. de Groot. Modeling and analysis of the three-dimensional current density in sandwich-type single-carrier devices of disordered organic semiconductors. *Phys. Rev. B*, 79:085203, Feb 2009.

[88] S. L. M. van Mensfoort and R. Coehoorn. *Phys. Rev. B*, 78(085207), 2008.

[89] S. L. M. Van Mensfoort, V. Shabro, R. De Vries, R. A. J. Janssen, and R. Coehoorn. Hole transport in the organic small molecule material α-npd: evidence for

the presence of correlated disorder. *Journal of Applied Physics*, 107(11):113710–113710–8, 2010.

[90] W. van Roosbroeck. *Bell System Tech*, 29:560, 1950.

[91] S. F. Walter. *Structured Higher-Order Algorithmic Differentiation in the Forward and Reverse Mode with Application in Optimum Experimental Design*. PhD thesis, Humboldt-University at Berlin, 2011.

[92] S. F. Walter and L. Lehmann. Algorithmic differentiation in python with algopy. *J. Comput. Science*, 4(5):334–344, 2013.

[93] C. K. F. Weiler and S. Körkel. Optimum experimental design for extended gaussian disorder modeled organic semiconductor devices. *Journal of Applied Physics*, 113(9):–, 2013.

[94] B. Wu. Existence of weak solutions to a degenerate stead-state semiconductor equations. *Acta Mathematica Scientia*, 31(3):960 – 968, 2011.

[95] A. Wächter and L. T. Biegler. On the implementation of an interior-point filter line-search algorithm for large-scale nonlinear programming. *Mathematical Programming*, 106(1):25–57, 2006.

[96] Z. G. Yu, D. L. Smith, A. Saxena, R. L. Martin, and A. R. Bishop. Molecular geometry fluctuation model for the mobility of conjugated polymers. *Phys. Rev. Lett.*, 84:721–724, Jan 2000.

[97] Y. Zhao, Y. Fan, X. Mu, H. Gao, J. Wang, J. Zhang, W. Yang, L. Chi, and Y. Wang. Self-assembly of luminescent twisted fibers based on achiral quinacridone derivatives. *Nano Research*, 2(6):493–499, 2009.